NANOACOUSTIC EFFECTS IN TYPE-II SUPERCONDUCTORS AND DECOHERENCE OF TWO-STATE SYSTEMS

By

Jaroslav Albert

A dissertation submitted to the Graduate Faculty in Physics in partial fulfillment of the requirements for the degree of

DOCTOR OF PHILOSOPHY

at

THE CITY UNIVERSITY OF NEW YORK

2009

This manuscript has been read and accepted for the Graduate Faculty in Physics in satisfaction of the dissertation requirement for the degree of Doctor of Philosophy.

Date — Dist. Professor Eugene M. Chudnovsky
Chair of Examining Committee

Date — Professor Steven Greenbaum
Executive Officer

Professor L. Krusin-Elbaum

Professor D. A. Garanin

Professor J. I. Gersten

Professor J. Tu
Supervisory Committee

THE CITY UNIVERSITY OF NEW YORK

Abstract

NANOACOUSTIC EFFECTS IN TYPE-II SUPERCONDUCTORS AND DECOHERENCE OF TWO-STATE SYSTEMS

by

Jaroslav Albert

Advisor: Eugene M. Chudnovsky, Distinguished Professor of Physics

In this thesis we focus on two areas of research: nanoacoustic effects in superconductors, and decoherence of two-state systems due to radiation of acoustic phonons. In the first part of this thesis we propose two new nanoacoustic effects: induction of voltage by mechanical stress, and nucleation of a superconducting vortex by an acoustic standing wave. Both of these effects take place in type-II superconductors. In the second part we study relaxation processes via acoustic phonons of a particle in a double-well potential and of a flux qubit.

Part 1: Mechanical stress causes motion of dislocations in solids. In a type-II superconductor a moving dislocation generates a pattern of current that exerts a force on the surrounding vortex lattice capable of depinning it. We show that the concentration and the speed of dislocations needed to produce depinning currents are within practical range. When external magnetic field and transport current are present, this effect generates voltage across the superconductor. In this manner, a type-II superconductor can serve as an electrical sensor of the mechanical stress. Nucleation of vortices in a superconductor below the first critical field can be assisted by transverse sound in the GHz frequency range. We work out from energy considerations that, in the presence of a sound wave, vortices enter and exit the superconductor at the frequency of the sound. The computed threshold parameters of the sound are

shown to be within experimental reach.

Part 2: We propose a method of computing phonon-induced relaxation of two-state systems that is based on symmetry arguments. This allows one to express the rates in terms of independently measurable parameters. For translationally and rotationally invariant systems the conservation of linear and angular momenta must be taken into account when formulating the interaction Hamiltonian. For a particle (e.g., electron or proton) in a rigid double-well potential embedded in a solid the rate is proportional to the seventh power of temperature. For a flux qubit the two-phonon relaxation is important only if the size of the qubit is much smaller than the phonon wavelength. Due to symmetry the two-phonon rate of both systems is proportional to the square of the bias. This allows for additional control of the relaxation rate.

Acknowledgements

I would like to express my gratitude to my advisor and mentor Professor Eugene Chudnovsky for his unceasing involvement and diligence in guiding me through my graduate studies. His intellectual prowess and expertise in a wide range of fields has sharpened my understanding of physics and endowed me with a new appreciation for the intricacies of science. I must also acknowledge his complete availability for discussions which he always welcomed with open arms and mind.

I thank Professor Christopher Gerry who was my advisor and mentor during my undergraduate education and who continues to inspire me to this day. His confidence in my abilities has reinforced my pursuit of physics. It has been a pleasure to learn from him.

I thank Professor Dmitry Garanin for all the discussions enriched by his subtly humorous character. His joy of doing physics is contagious and I thank him for imbuing me with it.

I must mention Carlos Calero with whom I shared many of my ideas. His careful thinking and observation helped me refine my understanding of physics. Many thanks.

Also, I want to thank Adil Benmoussa for helping me grow intellectually.

Finally, I want to express my gratitude to the other members of the committee, Professor Lia Krusin-Elbaum, Professor Joel Gersten, and Professor Jiufeng Tu.

To my mother Mária Albertová

Table of Contents

List of Figures

Part I

Nanoacoustic Effects in Type-II Superconductors

0.1 Introduction

The field of nanoacoustics explores the effects of dynamical displacements of ions - elastic deformations - in solids. The absence of any electrical resistance makes superconductors a fascinating class of solid state systems that respond more dramatically and, in many cases, very differently to the moving ions within them as compared to normal (non-superconducting) metals. In the past, the elastic deformations, i. e. ultrasound, in superconductors have been employed as a tool for probing theoretically and experimentally the superconducting properties. For instance, the gap in the energy spectrum and the penetration depth have been determined from ultrasonic attenuation. In type-II superconductors transverse ultrasound has been employed in the study of elastic as well as transport properties of the flux lattice. The possibility of using the moving flux lattice as a source of sonic coherent radiation, and the contribution of elastic deformations to the inertial mass to the Abrikosov vortex have also been the subject of scrutiny. The first part of this thesis explores new effects in type-II superconductors due to dynamical elastic deformations.

In Chapter 1 we summarize the most essential features of superconductivity that will be invoked in our study of nanoacoustics. We focus mainly on the phenomenological London and Ginzburg-Landau theories. In the second chapter we present new effects generated by elastic deformations that are in the experimentally feasible domain. First, we investigate the electromagnetic properties of moving dislocations and their influence on the flux lattice. We propose a method for detecting rapidly moving dislocations by measuring voltage across the superconductor due to the interaction of the flux lattice with the moving dislocations. This effect can be considered as an example of a piezoelectric effect in a metal. In our second study we investigate the

possibility of nucleation of a vortex in a superconducting slab by a standing sound wave. A standing wave creates local rotations of the crystal lattice which in the rotating frame appears as a fictitious magnetic field. This scenario can be viewed as a local London effect. In the ultrasound frequency range the fictitious field can exceed the first critical field in which case vortices should nucleate in the bulk of the superconductor.

Chapter 1

The phenomenon of superconductivity

In this chapter we present some of the basic facts and theories of the remarkable phenomenon of superconductivity. This will serve the purpose of giving a historical overview on the subject while presenting the tools used by the authors in their contribution to the field. Although, the section on the BCS theory is not essential to the work done by the authors, it deserves mentioning for the sake of completeness and elegance of presentation.

1.1 Phenomenological Theory

1.1.1 The Superconducting state

The discovery of superconductivity goes back to the year 1911 when Kamerlingh Onnes [1] observed the disappearance of electrical resistance in mercury (and later in other metals) below a critical temperature T_c of a few Kelvin. The complete absence of resistance was confirmed after performing experiments with persistent currents in a superconducting ring. The lifetime of the currents was established by nuclear resonance experiments to be of order 10^5 years. This practically perfect

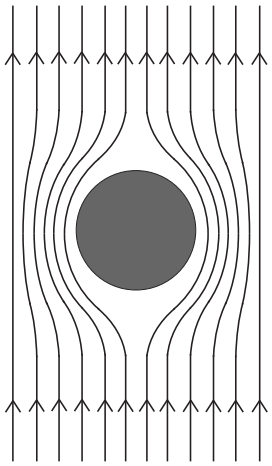

Figure 1.1: Meissner effect - on crossing from the normal to superconducting phase the magnetic field is expelled from the bulk of the sample.

conductivity became the first signature of superconductivity. Another striking effect arising in superconducting materials is the Meissner effect first observed by Meissner and Ochsenfeld [2] in 1933. They found that a magnetic field is expelled from a bulk superconductor when the sample was subjected to the external magnetic field. This might seem like an obvious consequence of perfect conductivity which would indeed keep the magnetic flux out of the sample provided the initial flux was zero. However, the Meissner effect showed that magnetic flux became expelled from the sample when the temperature decreased below T_c. A perfect conductivity would tend to trap the flux in the superconductor and therefore could not provide an explanation of this effect. The existence of Meissner effect suggested that superconductivity involves a thermodynamic phase transition and that superconducting state would be destroyed above a critical temperature-dependent external magnetic field $H_c(T)$. The relation between the change of free energy per unit volume and $H_c(T)$ was found to be (see i. e. [3])

$$f_n(T) - f_s(T) = \frac{H_c(T)^2}{8\pi} \tag{1.1}$$

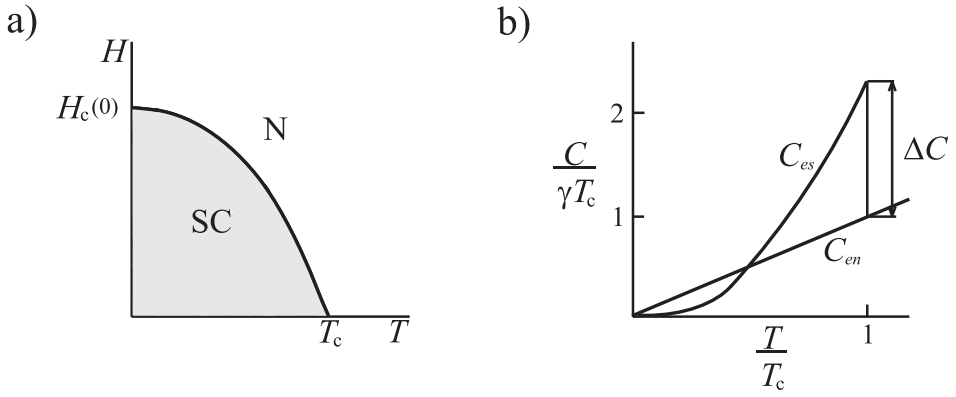

Figure 1.2: (a) A phase diagram relating the external magnetic field to temperature. (b) The specific heat has a discontinuity at T_c due to an energy gap Δ.

where f_n and f_s are the Helmholtz free energies per unit volume in the normal and superconducting states at $H = 0$. The temperature dependence of H_c is plotted in Fig. 1.2 a. It was found empirically that the curve can be fitted quite well by the approximate expression

$$H_c(T) \approx H_c(0)[1 - (T/T_c)^2] \tag{1.2}$$

The specific heat of superconductors was found to have a discontinuity at the critical temperature which is a characteristic of first order phase transitions Fig. 1.2 b. The relation between the normal and superconducting specific heat was found from experiments to be $(c_s - c_n)/c_n = 1.43$ while the temperature dependence of c_s far below T_c yielded an exponential dependence $\exp(-\Delta/k_B T)$. This thermal behavior is typical of a system with an energy gap Δ.

1.1.2 Londons' Equations and the Theory of Pippard

The first theoretical description of the electrodynamics of superconductors was proposed by the brothers F. and H. London [4]. The London equations

$$\mathbf{E} = \Lambda \dot{\mathbf{J}}_s \tag{1.3}$$

$$\mathbf{B} = -c\Lambda \nabla \times \mathbf{J}_s. \tag{1.4}$$

provide the relationships between the electric field $\mathbf{E}$, magnetic field $\mathbf{B}$, and the superconducting current $\mathbf{J}$. The phenomenological parameter Λ was defined as $\Lambda = (4\pi\lambda^2)/c^2$, where

$$\lambda = \left(\frac{mc^2}{4\pi n_s e^2}\right)^{1/2} \tag{1.5}$$

is called the London penetration depth. A good summary of Londons' arguments can be found in [5]. Equation 1.4 can be combined with Maxwell's equation

$$\nabla \times \mathbf{B} = \frac{4\pi}{c}\mathbf{J} \tag{1.6}$$

to give an equation for the magnetic field

$$\nabla \times \nabla \times \mathbf{B} + \frac{1}{\lambda^2}\mathbf{B} = 0 \tag{1.7}$$

For a sample occupying the half-infinite space $x > 0$ in an external field $H\mathbf{e}_z$ the solution to Eq. (1.7) is particularly simple:

$$\mathbf{B}(x) = He^{-x/\lambda}\mathbf{e}_z. \tag{1.8}$$

From this solution one can see that λ is indeed the penetration depth.

The value λ was found experimentally to be almost always larger than predicted by Londons' theory. Pippard explained this discrepancy by introducing a nonlocal generalization of London's equations in which the current at a particular point in space depends on $\mathbf{A}$ over a volume of radius ξ_0:

$$\mathbf{J}_s = -\frac{3}{4\pi\xi_0\Lambda c}\int \frac{\mathbf{R}[\mathbf{R}\cdot\mathbf{A}(\mathbf{r}')]}{R^4}e^{-R/\xi}d\mathbf{r}', \tag{1.9}$$

where $\mathbf{R} = \mathbf{r} - \mathbf{r}'$. The length ξ, called the coherence length, is related to ξ_0, the width of the superconducting electron wavefunction, through the scattering distance l: $\xi^{-1} = \xi_0^{-1} + l^{-1}$. While Pippard obtained this result based on the analogy with

nonlocal Ohm's law a more rigorous derivation with the help of Green's functions can be found in [5]. Pippard used the argument that if a system of quasiparticles has a gap Δ at the fermi level the minimum change of momentum on going from $\epsilon_F - \Delta$ to $\epsilon_F + \Delta$ is $\delta p = 2\Delta/v_F$, where v_F is the fermi velocity. From the uncertainty principle $\delta x \delta p \sim \hbar$ one obtains $\delta x = \xi_0 \sim \hbar v_F/(2\Delta)$. This gives the length over which the wavefunction of the superconducting electrons change appreciably. Since the vector potential changes on the length scale of order λ one must use Pippard's theory unless $\lambda \gg \xi_0$.

1.1.3 Phenomenological Ginzburg-Landau theory of superconductivity

The theories of London and Pippard combined with energy considerations provided the first predictions of electrodynamic behavior of superconductors. However, the theory was restricted only to cases where the density of superconducting electrons was constant throughout all space. Calculations involving spatial variations such as energy in a magnetic domain wall or spacial dependence near a superconductor-normal metal interphase could only be described qualitatively. The phenomenological theory that incorporated spacial variations was first proposed by Ginzburg and Landau (GL theory) [6] in 1950. They introduced a complex order parameter $\psi(\mathbf{r})$ whose square modulus $|\psi(\mathbf{r})|^2$ represented the local density of superconducting electrons $n_s(\mathbf{r})$. Ginsburg and Landau then expanded the free energy in powers of $|\psi(\mathbf{r})|$ and its derivatives $|\nabla\psi(\mathbf{r})|$ in the temperature region $T \approx T_c$ where $\psi(\mathbf{r})$ is very small and varies on the length scale of order $\xi \gg \xi_0$. Variation of this free energy with respect to ψ^* yilded two coupled differential equations for ψ and the vector potential $\mathbf{A}$. Initially, GL theory did not receive much attention as there was no microscopic theory

that could support it. However, once Bardeen, Cooper, and Schrifer developed a microscopic theory (BCS theory) [7], Gor'kov [8] who generalized the BCS theory to include spacial variations with the help of Green's functions showed that GL expansion is indeed valid in the limit $T \approx T_c$. The GL theory not only allowed quantitative treatment of superconducting systems with spatial variations but made it possible to predict new fascinating manifestations of quantum mechanics on the macroscopic scale.

The GL free energy per unit volume up to the forth order on $|\psi(\mathbf{r})|$ has the form

$$f_s = f_0 + \alpha|\psi|^2 + \frac{\beta}{2}|\psi|^4 + \frac{1}{2m^*}\left|\left(\frac{\hbar}{i}\nabla - \frac{e^*}{c}\mathbf{A}\right)\psi\right|^2 + \frac{|\nabla\times\mathbf{A}|^2}{8\pi}. \tag{1.10}$$

The coefficients α and β are function's of temperature, and m^* and e^* are the effective mass and charge. The starred quantities were originally assigned their bare values m and e. However, experiments yielded values closer to $e^* \approx 2e$ and $m^* \approx 2m$. This suggested that the superconducting charges come in pairs. In real metals these values could be altered by up to an order of magnitude due to the Fermi surface. In the absence of vector potential and spatial variations the free energy functional in Eq. (1.10) is minimized if $|\psi_\infty|^2 = -\alpha/\beta$. Clearly, the theory can only yield a nonzero ψ only if α is negative. On the other hand β must be positive otherwise $|\psi|$ would tend to increase to large values for which the theory is not valid. Minimizing the free energy in Eq. (1.10) with respect to ψ^* yields GL differential equations:

$$\alpha\psi + \beta|\psi|^2\psi + \frac{1}{2m^*}\left(\frac{\hbar}{i}\nabla - \frac{e^*}{c}\mathbf{A}\right)^2\psi = 0, \tag{1.11}$$

$$\nabla\times(\nabla\times\mathbf{A}) = -\frac{2\pi e^*\hbar i}{m^*c}(\psi^*\nabla\psi - \psi\nabla\psi^*) - \frac{4\pi e*^2}{m^*c^2}\psi^*\psi\mathbf{A} \tag{1.12}$$

or

$$\mathbf{J} = \frac{e^*}{m^*}|\psi|^2\left(\hbar\nabla\varphi - \frac{e^*}{c}\mathbf{A}\right), \tag{1.13}$$

where in the last equation we used the fact that the complex function ψ can be written in terms of its magnitude $|\psi|$ and phase φ, $\psi = |\psi|e^{\varphi}$, and that the left hand side of Eq. (1.12) is proportional to electric current according to the Maxwell's equation $\nabla \times \mathbf{B} = (4\pi/c)\mathbf{J}$. The right hand side of Eq. (1.12) is therefore proportional to the quantum mechanical current carrying particles of charge e^* and mass m^*. These equations must be solved simultaneously for ψ and $\mathbf{A}$.

Since Londons' theory had been around long before Ginzburg and Landau proposed theirs it is useful to look at the similarities between these two approaches. In particular, a homogeneous superconductor should be described on equal footing by both theories. Setting $|\psi| = |\psi_\infty|$, Eq. (1.13) becomes

$$\mathbf{J} = -(\Lambda_{eff}c)^{-1}\mathbf{Q} \tag{1.14}$$

with

$$\Lambda_{eff} = \frac{4\pi\lambda_{eff}^2}{c^2} \qquad \lambda_{eff} = \left(\frac{m^*c^2}{4\pi e^{*2}|\psi_\infty|^2}\right)^{1/2}, \qquad \mathbf{Q} = \mathbf{A} - \frac{\hbar e^*}{c}\nabla\varphi, \tag{1.15}$$

where $\mathbf{Q}$ is a gauge invariant vector potential. All physical quantities obtained from Eq. (1.14) must be independent of the particular gauge choice, that is if $\varphi \to \varphi + \phi$, then $\mathbf{A} \to \mathbf{A} + (c\hbar/e^*)\nabla\phi$. The London's gauge corresponds to $\nabla\varphi = 0$. Taking the effective quantities $e^* = 2e$ and $m^* = 2m$, reduces the effective parameters in Eq. (1.15) to $\lambda_{eff} = \lambda$ and $\Lambda_{eff} = \Lambda$. Hence, for a homogeneous superconductor the GL theory reduces to that of the Londons'.

Let us divide Eq. (1.11) by $\alpha|\psi_\infty|^2$ and define $f = \psi/\psi_\infty$. Assuming there are no fields, equation Eq. (1.11) in one dimension simplifies to

$$\xi^2(T)\frac{d^2f}{dx^2} + f - f^3 = 0, \qquad \xi^2(T) = \frac{\hbar^2}{2m^*|\alpha(T)|} \tag{1.16}$$

and we can take f to be real. If a homogeneous superconductor is perturbed by a small amount $g(x) \ll 1$, such that $f(x) = 1 + g(x)$, then a solution to Eq. (1.16) is approximately

$$g(x) \sim e^{-\sqrt{2}x/\xi}. \tag{1.17}$$

This shows that any deviation from a homogeneous solution will decay in a characteristic length $\xi(T)$. One is tempted to draw a connection between $\xi(T)$ and ξ_0 since they both give estimate of the length scale at which either the cooper pairs or the order parameter decay. Indeed, we can establish a connection between $\xi(T)$ and ξ_0 provided we know the relationships among $\alpha(T)$, $\beta(T)$, and $H_c(T)$. Beginning with the thermodynamic relation (1.1) we find

$$f_n(T) - f_s(T) = \frac{H_c(T)^2}{8\pi} = \frac{-\alpha}{2\beta}, \tag{1.18}$$

where as mentioned previously $f_n(T)$ and $f_s(T)$ are the free energies in the absence of external fields and gradients. Combining Eq. (1.18) with $|\psi_\infty|^2 = -\alpha/\beta$ yields

$$|\psi_\infty|^2 = \frac{mc^2}{8\pi\lambda_{eff}^2}, \quad \alpha(T) = -\frac{2e^2}{mc^2}H_c^2(T)\lambda_{eff}^2, \quad \beta(T) = \frac{16\pi e^4}{m^2c^4}H_c^2(T)\lambda_{eff}^4 \tag{1.19}$$

According to the BCS theory, which will be discussed in the last section of this chapter, the critical field $H_c(0)$ is related to the energy gap $\Delta(0)$ through the equation $H_c^2(0) = 4\pi N(0)\Delta^2(0)$ with $N(0)$ being the density of states. Combining this result with $\xi_0 = \hbar v_F/\pi\Delta(0)$ yields

$$\frac{\xi(T)}{\xi_0} = \frac{\pi}{2\sqrt{3}}\frac{H_c(0)}{H_c(T)}\frac{\lambda(0)}{\lambda_{eff}(T)}. \tag{1.20}$$

This equation shows that at zero temperature the coherence length is of the order of ξ_0. On the other hand, at $T \approx T_c$ the behavior of $\xi(T)$ in pure and dirty superconductors

respectively, is give by

$$\xi(T) = 0.74\frac{\xi_0}{[1-T/T_c]^{1/2}} \text{ pure} \tag{1.21}$$

$$\xi(T) = 0.855\frac{(\xi_0 l)^{1/2}}{[1-T/T_c]^{1/2}} \text{ dirty} \tag{1.22}$$

In conclusion it should be emphasized that GL theory was derived in the temperature range $T \approx T_c$ for which the order parameter ψ is small. Therefore one should not expect the GL theory to give correct results at temperatures well below T_c. Yet, the GL theory has proven to yield surprisingly good results even at low temperatures going all the way down to zero.

1.1.4 Flux quantization

Consider an infinite homogeneous superconducting sample in a magnetic field H with a hole born through it as shown in Fig. 1.3. To keep the field out of the bulk and at the same time satisfy the boundary conditions at the surface, Meissner currents must flow around the hole according to the Londons' equations. Let us encircle the hole by a closed loop shown in Fig. 1.3. The total magnetic flux threading through the loop is then given by the integral

$$\Phi = \int \mathbf{B}\cdot d\mathbf{s} = \int \nabla\times\mathbf{A}\cdot d\mathbf{s} = \oint \mathbf{A}\cdot d\mathbf{r} \tag{1.23}$$

where the last integral on the right follows from Stoke's theorem. With the help of Eq. (1.13) the flux Φ can be written as

$$\Phi = \oint \frac{c\hbar}{e^*}\nabla\varphi\cdot d\mathbf{r} - \frac{4\pi\lambda^2|\psi_\infty|^2}{c}\oint \frac{\mathbf{J}\cdot d\mathbf{r}}{|\psi|^2}. \tag{1.24}$$

If we make the loop large enough, so that it extends to regions where all fields and currents are zero, the second term in Eq. (1.24) drops out. If one goes around the

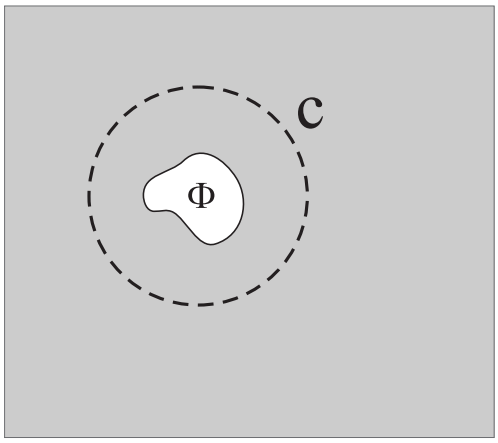

Figure 1.3: A superconductor with a hole. The magnetic flux threading through the loop C can only take discrete values of the flux quantum Φ_0.

loop n times, for $e^* = 2e$, the flux becomes

$$\Phi = \Phi_0 n, \qquad n = 1, 2, 3, ... \tag{1.25}$$

where $\Phi_0 = \frac{hc}{2e}$ is called the flux quantum. This shows that the magnetic field can penetrate a superconductor only in discrete quantities.

1.2 Applications of the Ginzburg-Landau theory

1.2.1 Surface energy and domain walls

In the Meissner phase the magnetic field is expelled from the entire bulk of the sample. This situation, however, is not energetically favorable for all geometries. For instance, a long superconducting slab of thickness $d \ll \lambda$ embedded in a magnetic field oriented along the normal to the slab, will develop superconducting and normal domains (see Fig. 1.4). In the normal region the magnetic flux fully penetrates the sample while the superconducting region develops Meissner currents that expel it. This state of a superconductor is called the mixed state. The domain wall energy may be written in terms of a parameter δ, which has the dimension of length, as $\gamma = H_c^2 \delta/(8\pi)$.

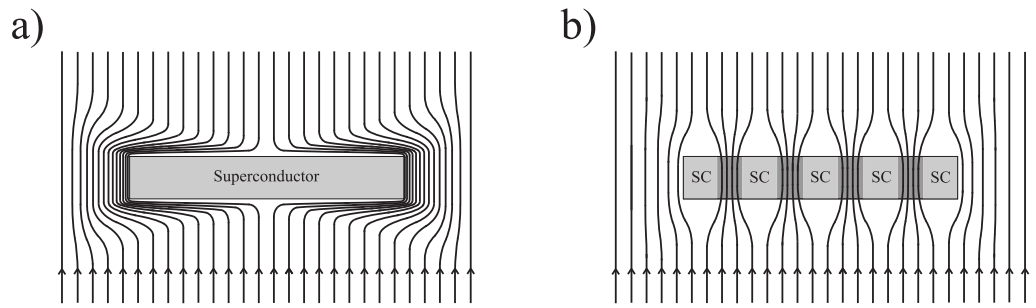

Figure 1.4: Total expulsion of magnetic filed is not always energetically favorable. The magnetic filed lines shown in (a) become very dense as they flow around the sample. (b) A partial penetration allows for lesser field density throughout the region surrounding the superconductor.

The behavior of ψ and $\mathbf{A}$ near the edge of a superconducting sample depends on a particular boundary conditions. For a superconductor-insulator (or vacuum) the most natural choice is

$$\left(\frac{\hbar}{i}\nabla - \frac{e^*}{c}\mathbf{A}\right)\psi \cdot \mathbf{n} = 0, \tag{1.26}$$

where $\mathbf{n}$ is a unit vector normal to the boundary. This condition ensures that no current passes through the boundary. For a metal-superconductor a more appropriate boundary condition is of the form [9]

$$\left(\frac{\hbar}{i}\nabla - \frac{e^*}{c}\mathbf{A}\right)\psi \cdot \mathbf{n} = \frac{i\hbar}{b}\psi. \tag{1.27}$$

The real constant b depends on the nature of the material and is a measure of how much ψ penetrates into the normal region. In this approximation it is assumed that ψ decreases linearly inside the normal metal. Combining the GL free energy with Eq. (1.11) yields [10]:

$$\delta = \int_{-\infty}^{\infty}\left[\left(1 - \frac{B}{H_c}\right)^2 - \left(\frac{\psi}{\psi_\infty}\right)^4\right]dx \tag{1.28}$$

Analytical solutions are only obtainable in two limiting cases:

$$\delta = \frac{4\sqrt{2}\xi}{3}, \qquad \kappa \ll 1 \tag{1.29}$$

$$\delta = \frac{-8(\sqrt{2}-1)\lambda}{3}, \qquad \kappa \gg 1, \tag{1.30}$$

where $\kappa = \lambda/\xi$. These results illustrate that the domain wall energy is positive when $\xi \gg \lambda$ and negative for $\xi \ll \lambda$. A positive energy tends to minimize the area of the normal-superconductor interface. Therefore a sample in a mixed state with $\xi \gg \lambda$ will have finite domains. On the other hand, if the interface energy is negative the sample breaks up into smallest possible domains in order to maximize the area of the interface. Since the order parameter cannot change over distances smaller that ξ the smallest area of the normal domain must be of order ξ^2. Numerical results showed that the crossover between these two types of behavior occurs at $\kappa = 1/\sqrt{2}$. Materials with $\kappa < 1/\sqrt{2}$ are called type-I superconductors while those with $\kappa > 1/\sqrt{2}$ are labeled as type-II superconductors.

1.2.2 Quantized vortices

The study of type-II superconductors was ushered in by Abrikosov with his ground breaking paper [11] in which he solved the linearized GL equations near the phase transition, $H \lesssim H_{c2}$. Abrikosov's solution showed that the normal domains curl up into cylindrical filaments carrying a quantum of flux $\Phi = hc/(2e)$ that form a periodic lattice (flux lattice). The maximum external magnetic field that could support superconductivity turned out to be $H_{c2} = \sqrt{2}\kappa H_c$. From this result one can see that for $\kappa = 1/\sqrt{2}$ the maximum external field becomes the thermodynamic critical field H_c. Hence, type-II superconductors allow a greater external magnetic field in their bulk than those of type-I. The linearized GL equations do not tell us however which particular vortex configuration is energetically most favorable. This shortcoming is a consequence of two factors: the nonlinear term $|\psi|^2\psi$ is ignored in Eq. (1.11), and the vector potential $\mathbf{A}$ is approximated by $H_{c2}x\mathbf{e}_y$. This can be corrected by adding $\mathbf{A}_1 = (0, (H_{c2} - H)x, 0) + \delta\mathbf{A}$ to $\mathbf{A}$, where $\delta\mathbf{A}$ arises from the

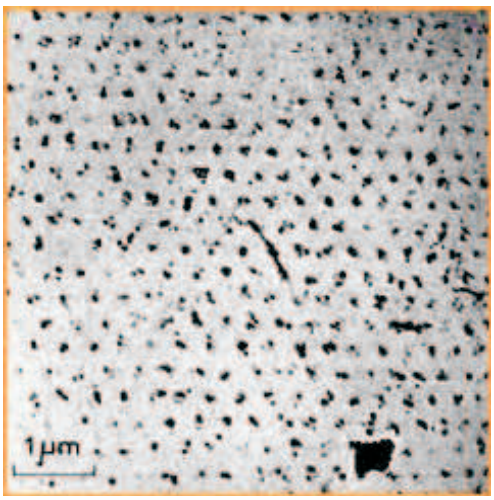

Figure 1.5: Triangular vortex lattice

currents of the vortex lattice. When these deviations are accounted for one can resort to perturbative solutions to ψ and $\mathbf{A}$ that lead to

$$\langle|\psi|^2\rangle = \frac{2\kappa^2|\psi_\infty|^2}{(2\kappa^2-1)\beta_A}\left(1-\frac{H}{H_{c2}}\right), \tag{1.31}$$

where $\langle|\psi|^2\rangle = S^{-1}\int|\psi|^2 dxdy$ is the average of $|\psi|^2$ over the area S occupied by the vortex array, and $\beta_A = \langle|\psi|^4\rangle/\langle|\psi|^2\rangle$ is called the Abrikosov parameter. The total Gibb's free energy in terms of β_A then follows ([12] and references therein):

$$\mathcal{F} = \frac{B^2}{8\pi} - \frac{(H_{c2}-B)^2}{8\pi[1+(2\kappa^2-1)\beta_A]}. \tag{1.32}$$

For a square lattice $\beta_A = 1.18$ while for a hexagonal lattice $\beta_A = 1.16$. Hence, the hexagonal lattice corresponds to the minimum of the free energy.

Another solution to the GL equations comes from the gauge choice for the phase $\varphi = \theta$, with θ being the angle with respect to the x-axis. The vector potential is then $\mathbf{A}(\mathbf{r}) = A(r)\hat{\theta}$. In the limit $r \to 0$, $|\psi|$ starts out linearly and then saturates to a plateau as $r \to \infty$. A good approximation to $|\psi|$ for the entire range is

$$|\psi| \approx |\psi_\infty| \tanh\left(\frac{\nu r}{\xi}\right) \tag{1.33}$$

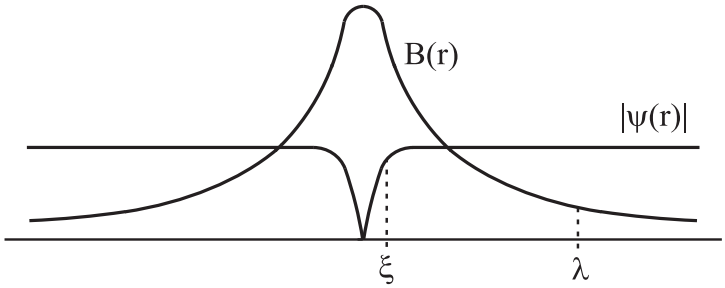

Figure 1.6: Behavior of $|\psi|$ and B as functions of r for $\kappa = 8$.

where ν is a constant ~ 1. Notice that $|\psi|$ approaches unity in the distance ξ from the vortex center. Thus, ξ defines the radius of the vortex core. The behavior of $|\psi|$ and B is sketched in Fig. 1.6

The magnetic field of the vortex is most easily obtained in the limit $\kappa \gg 1$. In this case the dimension of the vortex core is much smaller that the distance over which the magnetic field varies. This permits us to use the second London equation $\mathbf{B} + 4\pi\lambda^2/c\nabla \times \mathbf{J}_s = 0$. To take into account the vortex core we must replace the zero on the right hand side with $\Phi_0\delta(r)\mathbf{e}_z$. This ensures that the flux is quantized when we integrate both sides over the entire xy-plane. The modified London equation then becomes

$$\mathbf{B} + \frac{4\pi\lambda^2}{c}\nabla \times \mathbf{J}_s = \Phi_0\delta(r)\mathbf{e}_z. \tag{1.34}$$

The solution for the magnetic field outside of the core is then

$$\mathbf{B}(r) = \frac{\Phi_0}{2\pi\lambda^2}K_0\left(\frac{r}{\lambda}\right)\mathbf{e}_z, \tag{1.35}$$

where K_0 is a zero order modified bessel function. Over the core the magnetic field is approximately constant and equal to its value at $r = \xi$.

A vortex will enter the superconductor only if its presents lowers the free energy. Since the vortex carries magnetic flux and thus induces magnetization the appropriate

thermodynamic function to consider is the Gibbs free energy. At the phase transition the Gibbs function must be the same regardless of whether or not the vortex has entered the sample. This condition can be expressed symbolically as

$$F_s = F_s + \epsilon_1 L - \frac{H_{c1} \int B}{4\pi}, \tag{1.36}$$

where ϵ_1 is the vortex energy per unit line and H_{c1} is the critical field. The integral over the magnetic field gives $\Phi_0 L$, and so the condition for a nucleation of a vortex may be written as

$$H_{c1} = \frac{4\pi\epsilon_1}{\Phi_0}. \tag{1.37}$$

The vortex line energy is simply due to the kinetic energy of the circulating currents and the magnetic energy:

$$\epsilon_1 = \frac{1}{8\pi} \int (B^2 + \lambda^2 |\nabla \times \mathbf{B}|^2) d^2 r. \tag{1.38}$$

Since the vortex core is very small its contribution to the energy is negligible and can be excluded from the integration. Transforming the second term with the help of standard vector identities and using Eq. (1.34) yields a line integral over the core:

$$\epsilon_1 = \frac{\lambda^2}{8\pi} \oint [\mathbf{B} \times (\nabla \times \mathbf{B})] \cdot d\mathbf{s}. \tag{1.39}$$

Inserting Eq. (1.35) into Eq. (1.39) and taking into account that $K_0(1/\kappa) \approx \ln \kappa$ for $\kappa \gg 1$ yields

$$\epsilon_1 \approx \left(\frac{\Phi_0}{4\pi\lambda} \right)^2 \ln \kappa = \pi \xi^2 \frac{H_c^2}{8\pi} 4 \ln \kappa, \tag{1.40}$$

where in the last step we used the definition of ξ and α given by Eqs. (1.16) and (1.19) to obtain a more physically transparent expression. Remembering that $f_n - f_s = H_c^2/8\pi$, Eq. (1.40) says that the energy per unit line of the vortex is proportional

to the change in free energy within a disk of area $\pi\xi^2$. Finally, from Eq. (1.37) and (1.40) we obtain the first critical filed

$$H_{c1} = \frac{H_c}{\sqrt{2}} \ln \kappa. \tag{1.41}$$

Comparing this result to $H_{c2} = \sqrt{2}\kappa H_c$ we can see that up to the term $\ln \kappa$, H_c is approximately the geometric mean of H_{c1} and H_{c2}.

1.2.3 Vortex-vortex interaction and surface effects

The first critical field H_{c1} was derived in the previous section based on minimization of the free energy. We found that when a magnetic field exceeds H_{c1} a vortex enters the superconductor accompanied by a phase transition which reduces the gibb's free energy. That implies that the system could reduce its free energy even further by admitting more vortices. This is in fact what happens in any real system. It should be pointed out that the energy of two vortices is smaller than energy of one vortex with two flux quanta. Inspecting Eq. (1.40) one can see that the energy of n vortices is additive, $\varepsilon = n\epsilon_1$ while a single vortex of flux quantum $\Phi_0 n$ has energy $n^2\epsilon_1$.

Consider a situation where the vortices are separated by distances greater than λ. Then the magnetic field and the order parameter ψ of each vortex are distorted only slightly, and so, superposition can be used. For two vortices with their cores located at points $\mathbf{r}_1$ and $\mathbf{r}_2$ the magnetic field can be written as

$$\mathbf{B}(\mathbf{r}) = \mathbf{B}_v(|\mathbf{r} - \mathbf{r}_1|) + \mathbf{B}_v(|\mathbf{r} - \mathbf{r}_2|), \tag{1.42}$$

where $\mathbf{B}_v$ is given by Eq. (1.35). Using the notation B_{v1} and B_{v2} to represent the fields of the individual vortices and inserting Eq. (1.42) into Eq. (1.39) renders the

result

$$\epsilon = \frac{\Phi_0}{8\pi}[B_{v1}(\mathbf{r}_1) + B_{v2}(\mathbf{r}_2) + B_{v1}(\mathbf{r}_2) + B_{v2}(\mathbf{r}_1)] = 2\left[\frac{\Phi_0}{8\pi}B_{v1}(\mathbf{r}_1)\right] + \frac{\Phi_0}{4\pi}B_{v1}(\mathbf{r}_2). \quad (1.43)$$

The first term in the last expression is twice the line energy of one flux while the second is the interaction energy per line between the two vortices. Hence, the interaction energy between vortices per unit line is

$$\epsilon_{12} = \frac{\Phi_0^2}{8\pi^2\lambda^2}K_0\left(\frac{r_{12}}{\lambda}\right), \quad (1.44)$$

where r_{12} is the separation distance between the vortex centers. Because ϵ_{12} is positive the free energy of a superconductor grows with increasing flux density. For this reason, the number of vortices in a superconductor is not arbitrary but is determined by the balance between the negative work done by the external field $-HB/(4\pi)V$ (V=AL) and the positive interaction energy $\sum_{i>j} L\epsilon_{ij}$.

Thus far, we have been considering vortices in large samples whose surface was far away to have any noticeable effects on them. It may seem reasonable so suspect that vortices nucleate in the bulk of a sample without feeling the presence of the sample surface. However, early experiments, [13] suggest that a surface may be influencing the magnetic behavior of type-II superconductors. An example of this is the observation of a hysteresis in the magnetization curve in low fields. One explanation came from Bean and Livingston [14] who argued that the vortex enters the sample through the surface where it encounters an energy barrier. The barrier arises from two opposing effects, namely the attractive interaction of a vortex with its image on the outside of the surface, and the repulsive vortex interaction with the external field that penetrates a distance λ into the sample. The first contribution is a consequence of boundary conditions on the current, that is, no current at the boundary can flow

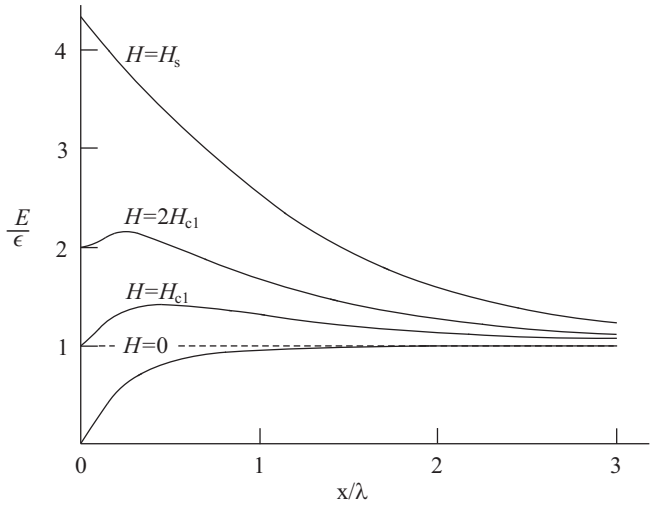

Figure 1.7: Dependence of the line energy E of the flux thread on x, distance from the surface, for various applied fields. Results presented are for $\lambda = 10\xi$.

in the direction normal to the surface. This condition is easily satisfied by placing an image vortex on the outside of the surface. If, for instance, the currents of the vortex flow counterclockwise then those of the image flow clockwise and the net current at the boundary vanishes. The two contributions to the energy can be calculated by inserting the magnetic field of the form $\mathbf{B}_v + \mathbf{B}_i + \mathbf{B}_M$ into Eq. (1.39), so that

$$\epsilon = \epsilon_1 + \frac{\lambda^2}{8\pi} \oint \mathbf{B}_i \times (\nabla \times \mathbf{B}_v) \cdot d\mathbf{s} + \frac{\lambda^2}{8\pi} \oint \mathbf{B}_M \times (\nabla \times \mathbf{B}_v) \cdot d\mathbf{s}, \tag{1.45}$$

where $\mathbf{B}_v$ is the field of the vortex and, $\mathbf{B}_M$ and $\mathbf{B}_i$ are the Meissner field and the field of the image, respectively. In Eq. (1.45) we retained only the leading terms which leads to a good approximation as long as the distance from the vortex to the surface is greater than the coherence length. The first term is the line energy of the vortex, the second and the third terms give the image-vortex energy and the energy coming from the interaction of the Meissner field with the vortex, respectively. Inserting the solutions of $\mathbf{B}_v$ and $\mathbf{B}_M$, given by Eqs. (1.35) and (1.8), the total energy of the vortex

near the surface reads

$$\epsilon = \epsilon_1 - \left(\frac{\Phi_0}{4\pi\lambda}\right)^2 K_0\left(\frac{2x}{\lambda}\right) + \frac{\Phi_0}{4\pi} H e^{-x/\lambda}, \tag{1.46}$$

where x is the distance from the vortex to the surface. Fig. 1.7 shows various potentials as a function of x for different values of the external field H. For $H < H_{c1}$ any vortex within the superconductor will be expelled. Upon crossing from $H < H_{c1}$ to $H > H_{c1}$ a potential barrier is formed which disappears at some new critical field H_s. One question that arises is how can a vortex overcome this barrier at $H = H_{c1}$? One answer is that the surface of any sample contains imperfections which may lower the potential barrier.

1.3 BCS Theory of Superconductivity

1.3.1 The effective interaction

In the same year when Abrikosov discovered the periodic solution to the linearized GL equations the microscopic theory of superconductivity was born [7]. Its arrival was not sudden. Many of the ingredients that make up the theory had already been around, but it was Bardeen, Cooper, and Schriffer who dovetailed them. The essential feature of the theory is based on the idea that electrons at the Fermi level experience attractive interaction. While the origin of this attraction is not important for the validity of the theory it was initially thought to arise due to electron-phonon interaction. This idea precedes the BCS theory by at least seven years. In 1950 Fröhlich [15] suggested that the electron-lattice interaction might play a role in explaining superconductivity. He derived, by applying a unitary transformation, an effective electron-electron interaction hamiltonian that did indeed became attractive for certain phonon frequencies. Fröhlich's idea was later confirmed experimentally by

the discovery of the isotope effect [16]. The earliest attempts to calculate the effective electron-electron potential mediated by elastic deformations were given by Bardeen and Pines [17]. For the jellium model the calculation yields

$$V(\mathbf{q},\omega) = \frac{4\pi e^2}{q^2 + k_s^2}\left(1 + \frac{\omega_{\mathbf{q}}^2}{\omega^2 - \omega_{\mathbf{q}}^2}\right), \tag{1.47}$$

with ω and k_s are fitting parameters and $\omega_{\mathbf{q}}$ is the frequency of a phonon. Clearly, the overall sign of the potential can become negative when $\omega < \omega_{\mathbf{q}}$. However, a singularity occurs when $\omega = \omega_{\mathbf{q}}$ which implies that the spectrum is not valid for all frequencies. A more elegant approach to obtaining the interaction hamiltonian came from Safonov [18] who used the one step unitary transformation. More recently Wagner [19, 20] introduced so called continuous unitary transformation which relies on solving a set of coupled differential equations known as flow equations. The simplest solution to the flow equations for the interaction potential is given by

$$V_{\mathbf{kq}} = V_{\mathbf{q}}^c - \frac{M_{\mathbf{q}}^2 \omega_{\mathbf{q}}}{\omega_{\mathbf{q}}^2 + (\varepsilon_{\mathbf{k+q}} - \varepsilon_{\mathbf{k}})^2} \tag{1.48}$$

The first term is just the Coulomb potential while the second is due to phonon exchange. Unlike the jellium model this result always gives a negative contribution to the Coulomb potential and is finite for all frequencies.

1.3.2 Energy gap

Cooper [21] investigated the consequence of attractive electronic potential by considering a simplified model where only two electrons are interacting above the Fermi level and the effect of all other electrons is felt only through the Pauli exclusion principle. He discovered that the electrons form a bound state regardless of how weak the strength of the interaction. The energy of the (Cooper) pair in the limit $N(0)V \ll 1$

gives approximately

$$E \approx 2E_F - 2\hbar\omega_c e^{-2/N(0)V}, \tag{1.49}$$

where ω_c is a cut-off phonon frequency, $N(0)$ is the density of states at the Fermi level, and V is the interaction potential taken to be a constant. The fact that Eq. (1.49) is not analytic at $V = 0$ means that this result cannot be obtained by standard perturbation methods.

The general problem of many electrons at the Fermi level interacting via an attractive potential became tractable after BCS suggested a trial wavefunction:

$$|\Psi\rangle = \prod_{\mathbf{k}} (u_{\mathbf{k}} + v_{\mathbf{k}} c^+_{\mathbf{k}\uparrow} c^+_{-\mathbf{k}\downarrow})|0\rangle \tag{1.50}$$

where u_k and v_k are some complex functions of $|\mathbf{k}|$ that satisfy the relation $|u_{\mathbf{k}}|^2 + |v_{\mathbf{k}}|^2 = 1$. These functions must be chosen in such a way as to minimize the pairing (reduced) hamiltonian introduced by BCS which reads

$$\mathcal{H}_{red} = \sum_{\mathbf{k}\sigma} \varepsilon_{\mathbf{k}} c^+_{\mathbf{k}\sigma} c_{\mathbf{k}\sigma} + \sum_{\mathbf{kl}} V_{\mathbf{kl}} c^+_{\mathbf{k}\uparrow} c^+_{-\mathbf{k}\downarrow} c_{-\mathbf{l}\downarrow} c_{\mathbf{l}\uparrow}, \tag{1.51}$$

where the potential $V_{\mathbf{kl}}$ is negative. The BCS wavefunction Eq. (1.50) does not conserve the total number of particles and therefore, the quantity to be minimized is

$$\mathcal{G} = \langle \mathcal{H}_{red} - \mu N \rangle \tag{1.52}$$

This functional is the thermodynamic potential with μ being the chemical potential and $N = \sum_{\mathbf{k}\sigma} c^+_{\mathbf{k}\sigma} c_{\mathbf{k}\sigma}$ the number operator. Extremizing $\mathcal{G}$ produces the condition

$$\Delta_{\mathbf{k}} = -\frac{1}{2} \sum_{\mathbf{l}} \frac{\Delta_{\mathbf{l}}}{(\Delta^2_{\mathbf{l}} + \xi^2_{\mathbf{l}})} V_{\mathbf{kl}}, \qquad \Delta_{\mathbf{k}} = -\sum_{\mathbf{l}} V_{\mathbf{kl}} u_{\mathbf{l}}\, v_{\mathbf{l}}, \qquad \xi_{\mathbf{k}} = \varepsilon_{\mathbf{k}} - \mu. \tag{1.53}$$

A reasonable approximation is to replace $V_{\mathbf{kl}}$ with a constant $-V$ for $|\xi_{\mathbf{k}}|, |\xi_{\mathbf{l}}| < \hbar\omega_D$ and zero for $|\xi_{\mathbf{k}}|, |\xi_{\mathbf{l}}| > \hbar\omega_D$, where ω_D is the Debye frequency. The solution to $\Delta_{\mathbf{k}}$

then becomes straightforward:

$$\Delta \approx 2\hbar\omega_D e^{-1/N(0)V}. \tag{1.54}$$

The solutions to $u_{\mathbf{k}}$ and $v_{\mathbf{k}}$ follow from the second condition in Eq. (1.53) and from the requirement that $u_{\mathbf{k}}^2 + v_{\mathbf{k}}^2 = 1$:

$$u_{\mathbf{k}} = \frac{1}{\sqrt{2}}\left[1 - \frac{\xi_k}{(\Delta^2 + \xi_{\mathbf{k}}^2)^{1/2}}\right]^{1/2} \tag{1.55}$$

$$v_{\mathbf{k}} = \frac{1}{\sqrt{2}}\left[1 + \frac{\xi_k}{(\Delta^2 + \xi_{\mathbf{k}}^2)^{1/2}}\right]^{1/2} \tag{1.56}$$

The energy difference between the superconducting and normal state yields

$$\langle E_s - E_n \rangle = -\frac{1}{2}N(0)\Delta^2(0) \tag{1.57}$$

This is simply the condensation energy which must be equal to $H_c^2(0)/(8\pi)$. From this relation one can calculate the T-H phase diagram provided $\Delta(T)$ is known for all temperatures from 0 to T_c.

1.3.3 Inhomogeneous superconductivity and the Bogoliubov-deGennes equations

All of the above results were obtained based on the assumption that the superconductor is homogeneous. This is reflected in the fact that the hamiltonian in Eq. (1.51) admits only pair interaction between particles of quantum numbers, $\mathbf{k}$ and $-\mathbf{k}$. In order to include in the BCS theory spatial variations one must relax this restriction. A convenient way to write the superconducting hamiltonian is in terms of the field operators $\Psi_\alpha(\mathbf{r})$ and $\Psi_\alpha^+(\mathbf{r})$ so that

$$\begin{aligned} \mathcal{H}_{BCS} &= \int d^3r \Psi_\alpha^+(\mathbf{r}) \left[\frac{1}{2m}\left(-i\hbar\nabla - \frac{e}{c}\mathbf{A}\right)^2 - \mu\right] \Psi_\alpha(\mathbf{r}) \\ &- \frac{g}{2}\int d^3r \Psi_\beta^+(\mathbf{r})\Psi_\alpha^+(\mathbf{r})\Psi_\alpha(\mathbf{r})\Psi_\beta(\mathbf{r}), \end{aligned} \tag{1.58}$$

where the repeated indices α and β are summed over and the positive constant g measures the strength of the attractive interaction. This hamiltonian is too complicated to diagonalize and one must resort to mean field methods. In a normal phase the interaction term in Eq. (1.58) can be simplified with the Hartree-Fock approximation which in the language of field theory corresponds to

$$V_{HF} \equiv -g \int d^3r \{\langle \Psi_\alpha^+(\mathbf{r})\Psi_\alpha(\mathbf{r})\rangle \Psi_\beta^+(\mathbf{r})\Psi_\beta(\mathbf{r}) - \langle \Psi_\alpha^+(\mathbf{r})\Psi_\beta(\mathbf{r})\rangle \Psi_\beta^+(\mathbf{r})\Psi_\alpha(\mathbf{r})\}. \quad (1.59)$$

When a system is in a superconducting state we must add a new feature to the Hartree-Fock term, namely the mean interaction between Cooper pairs:

$$V_{CP} \equiv -\frac{g}{2} \int d^3r \{\langle \Psi_\alpha^+(\mathbf{r})\Psi_\beta^+(\mathbf{r})\rangle \Psi_\beta(\mathbf{r})\Psi_\alpha(\mathbf{r}) + \langle \Psi_\beta(\mathbf{r})\Psi_\alpha(\mathbf{r})\rangle \Psi_\alpha^+(\mathbf{r})\Psi_\beta^+(\mathbf{r})\}. \quad (1.60)$$

Making the definition $\Delta(\mathbf{r}) \equiv -g\langle \Psi_\uparrow(\mathbf{r})\Psi_\downarrow(\mathbf{r})\rangle = g\langle \Psi_\downarrow(\mathbf{r})\Psi_\uparrow(\mathbf{r})\rangle$ the effective mean field hamiltonian becomes

$$\begin{aligned} \mathcal{H}_{eff} &= \int d^3r \Psi_\alpha^+(\mathbf{r}) \left[\frac{1}{2m}\left(-i\hbar\nabla - \frac{e}{c}\mathbf{A}\right)^2 - \mu + U(\mathbf{r})\right] \Psi_\alpha(\mathbf{r}) \\ &- \int d^3r \Delta^*(\mathbf{r})\Psi_\uparrow(\mathbf{r})\Psi_\downarrow(\mathbf{r}) + \int d^3r \Delta(\mathbf{r})\Psi_\downarrow^+(\mathbf{r})\Psi_\uparrow^+(\mathbf{r}). \end{aligned} \quad (1.61)$$

The function $U(\mathbf{r})$ contains the Hartree-Fock potential as well as any other external potential that may enter the system including impurities. This hamiltonian is easily diagonalized by a linear transformation of the field operators

$$\begin{aligned} \Psi_\uparrow^+(\mathbf{r}) &= \sum_{\mathbf{k}} [\gamma_{\mathbf{k}\uparrow}^+ u_{\mathbf{k}}^*(\mathbf{r}) - \gamma_{\mathbf{k}\downarrow} v_{\mathbf{k}}(\mathbf{r})] \qquad \Psi_\downarrow^+(\mathbf{r}) = \sum_{\mathbf{k}} [\gamma_{\mathbf{k}\downarrow}^+ u_{\mathbf{k}}^*(\mathbf{r}) + \gamma_{\mathbf{k}\uparrow} v_{\mathbf{k}}(\mathbf{r})] \\ \Psi_\uparrow(\mathbf{r}) &= \sum_{\mathbf{k}} [\gamma_{\mathbf{k}\uparrow} u_{\mathbf{k}}(\mathbf{r}) - \gamma_{\mathbf{k}\downarrow}^+ v_{\mathbf{k}}^*(\mathbf{r})] \qquad \Psi_\downarrow(\mathbf{r}) = \sum_{\mathbf{k}} [\gamma_{\mathbf{k}\downarrow} u_{\mathbf{k}}(\mathbf{r}) + \gamma_{\mathbf{k}\uparrow}^+ v_{\mathbf{k}}^*(\mathbf{r})] \end{aligned} \quad (1.62)$$

where $u_{\mathbf{k}}$ and $v_{\mathbf{k}}$ are the single particle wavefunctions for an electron and a hole, respectively. The new operators $\gamma_{\mathbf{k}\alpha}$ and $\gamma_{\mathbf{k}\beta}^+$ change the number of quasiparticles by ± 1.

They satisfy the fermion anti-commutation rules $\{\gamma_{\mathbf{k}\alpha}, \gamma^+_{\mathbf{k}'\beta}\} = \delta_{\mathbf{k}\mathbf{k}'}\delta_{\alpha\beta}$. Substitution of Eq. (1.62) into the effective hamiltonian of Eq. (1.61) yields

$$\mathcal{H}_{eff} = E_0 + \sum_{\mathbf{k}} \epsilon_{\mathbf{k}}[\gamma^+_{\mathbf{k}\uparrow}\gamma_{\mathbf{k}\uparrow} + \gamma^+_{\mathbf{k}\downarrow}\gamma_{\mathbf{k}\downarrow}] \tag{1.63}$$

where E_0 is the ground state energy and $\epsilon_{\mathbf{k}}$ is an eigenenergy of the system of Bogoliubov equations

$$\begin{pmatrix} \mathcal{H}_e & \Delta(\mathbf{r}) \\ \Delta^*(\mathbf{r}) & -\mathcal{H}_e \end{pmatrix} \begin{pmatrix} u_{\mathbf{k}}(\mathbf{r}) \\ v_{\mathbf{k}}(\mathbf{r}) \end{pmatrix} = \epsilon_{\mathbf{k}} \begin{pmatrix} u_{\mathbf{k}}(\mathbf{r}) \\ v_{\mathbf{k}}(\mathbf{r}) \end{pmatrix} \tag{1.64}$$

The operator $\mathcal{H}_e$ is the single electron hamiltonian. Inserting the field operators defined in Eq. (1.62) into the definition of $\Delta(\mathbf{r})$ we obtain

$$\Delta(\mathbf{r}) = g\sum_{\mathbf{k}}[1 - 2f(\epsilon_{\mathbf{k}})]u_{\mathbf{k}}(\mathbf{r})v^*_{\mathbf{k}}(\mathbf{r}), \tag{1.65}$$

where $f(\epsilon_{\mathbf{k}})$ is the Fermi function. One can also write the quantum mechanical current in terms of the functions $u_{\mathbf{k}}(\mathbf{r})$, $v_{\mathbf{k}}(\mathbf{r})$ and their complex conjugates as

$$\begin{aligned} \mathbf{J} &= \frac{c}{4\pi}\nabla \times [\nabla \times \mathbf{A}(\mathbf{r})] \\ &= -\frac{2e\hbar i}{m}\sum_{\mathbf{k}}[f(\epsilon_{\mathbf{k}})(u^*_{\mathbf{k}}\nabla u_{\mathbf{k}} - v^*_{\mathbf{k}}\nabla v_{\mathbf{k}}) + (1 - f(\epsilon_{\mathbf{k}}))(v_{\mathbf{k}}\nabla v^*_{\mathbf{k}} - u_{\mathbf{k}}\nabla u^*_{\mathbf{k}})] \\ &\quad -\frac{2e^2}{mc}[f(\epsilon_{\mathbf{k}})u^*_{\mathbf{k}}u_{\mathbf{k}} + (1 - f(\epsilon_{\mathbf{k}}))v^*_{\mathbf{k}}v_{\mathbf{k}}]\mathbf{A}(\mathbf{r}). \end{aligned} \tag{1.66}$$

For particular boundary conditions equations (1.64), (1.65), and (1.66) can in principle be solved for the functions $u_{\mathbf{k}}$, $v_{\mathbf{k}}$, Δ, and $\mathbf{A}$, although, exact analytic solutions for arbitrary temperature $T < T_c$ and external field $H(T)$ have never been implemented. However, at temperatures $T \approx T_c$ Δ approaches zero continously and can therefore be treated as a perturbation. A detailed analysis of the Bogoliubov equations is presented in the book by deGennes [9].

Chapter 2

Interaction of vortices with crystal deformations

2.1 Pinning of vortices by defects

Any realistic solid contains defects or imperfections - deviations form a perfect lattice or periodic structure. A defect can have a short range extent occupying only the space from one to a few atoms, or it can have an extended structure that pervades the entire solid. The first, referred to as point defects, include interstitial atoms, impurities, and vacancies, the latter are the screw and edge dislocations. An edge dislocation is formed by inserting an extra plain of atoms inside a solid. A screw dislocation is characterized by a plane of atoms in a solid that are shifted by one lattice spacing relative to its neighboring atoms. In both cases the atoms in the solid become shifted from their equilibrium positions. We defer a more detailed discussion of dislocations to section 2.3.1. Point defects in crystals contribute to such phenomena as electrical conductivity, photoconductivity, heat diffusion, color, etc. Plastic behavior of solids on the other hand can be almost exclusively explained by the dynamics of dislocations.

2.1.1 Pinning by point defects

In superconductors, defects play quite a different role. In 1953 Pippard introduced the coherence length that was related to the scattering length l as mentioned in section (1.1.2). Indeed, the two limiting cases in which the concentration of impurities goes to either zero or infinity give quite different results. For instance, the gap function defined in section (1.3.3) which can be expressed by the integral relation [9] $\Delta(\mathbf{r}) = \int d\mathbf{r}^{'} K(\mathbf{r}, \mathbf{r}^{'})\Delta(\mathbf{r}^{'})$ depends on the scattering length l. In in the case of a pure metal the range of the kernel $K(\mathbf{r}, \mathbf{r}^{'})$ is of the order $\xi_0 = 0.18\hbar v_F/(k_B T)$ while in the dirty limit it varies significantly over the length $\sqrt{\xi_0 l}$.

The effects of impurities on the gap function can also be studied in the context of GL theory. The most interesting scenario is when the vortices enter a superconductor. If impurities were absent the vortices would form a flux lattice. The presence of impurities introduces a random potential which interacts with the order parameter ψ. The vortices then become attracted to the defects and tend to center their normal cores at the site of the impurity. At low fields $H \approx H_{c1}$ the interaction between vortices is exponentially small, and so, the core of each vortex becomes aligned with a nearby defect without much cost in vortex-vortex interaction energy. Since the displacement of flux lines in the limit $H \gtrsim H_{c1}$ can exceed the coherence length ξ by a factor ~ 10 or more, the flux lattice becomes completely disordered. This is known as the vortex glass. In the opposite limit $H \lesssim H_{c2}$ the situation is complicated by the high stiffness of the flux lattice. One would therefore expect the lattice structure to remain approximately periodic with only small displacements from the equilibrium positions. However, careful analysis of this problem revealed that while short range order is preserved within a characteristic volume V_c, the flux lattice becomes disordered over

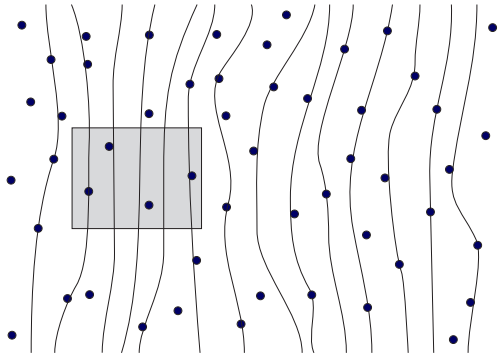

Figure 2.1: Flux is pinned by randomly distributed point defects. In the shaded region the flux lines are distorted by distances of order ξ or less.

distances $\gtrsim V_c^{1/3}$. The region within V_c was given the name vortex bundle. The first attempts to study this problem were carried out by Larkin and Ovchinnikov [22, 23], and later refined by Feigl'man *et. al* [24] and Natterman [25]. According to Larkin's theory, the impurities create a random potential which enters the GL free energy Eq. (1.10) through the coefficient α and the inverse effective mass m^{*-1}, such that $\alpha = \alpha_0 + \alpha_1(\mathbf{r})$ and $m^{*-1} = m_0^{-1} + m_1^{-1}(\mathbf{r})$. The random functions α_1 and m_1 have zero expectations, but nonzero correlations: $\langle \alpha_1 \rangle = 0$, $\langle m_1^{-1} \rangle = 0$, $\langle \alpha_1(0)\alpha_1(\mathbf{r}) \rangle = \varphi(r)$, $\langle m_1^{-1}(0) m_1^{-1}(\mathbf{r}) \rangle = \chi(r)$. One can assume the correlation functions to be Gaussian:

$$\varphi(r) = \frac{a}{(2\pi)^{1/2} L^3} e^{-r^2/2L^2}, \qquad \chi(r) = \frac{b}{(2\pi)^{1/2} L^3} e^{-r^2/2L^2}, \tag{2.1}$$

where a, b, and L are phenomenological parameters that characterize the strength and length scale of the inhomogeneities. The change in the free energy of a distorted flux lattice can also be written in terms of the displacement vector field $\mathbf{u}(\mathbf{r}) = \mathbf{r} - \mathbf{r}_0$ with $\mathbf{r}_0$ being the lattice vector:

$$\delta \mathcal{F} = \frac{1}{2} \int \left[(C_{11} - C_{66})(\nabla \mathbf{u})^2 + C_{66} (\nabla_\alpha u_\beta)^2 + C_{44} \left(\frac{\partial u_\alpha}{\partial z} \right)^2 \right] d^3 r. \tag{2.2}$$

The coefficients C_{11}, C_{44}, and C_{66} are the elastic moduli of the vortex lattice [26]. For a small vortex displacement the work done on a vortex by moving it a distance $\mathbf{u}$ from

its equilibrium position is $U = \int \mathbf{u}\cdot\mathbf{f}$, where $\mathbf{f}$ is the force due to impurities. When U is added to Eq. (2.2) and minimized with respect to $\mathbf{u}$ the equation in fourier space that connect $\mathbf{u_k}$ with $\mathbf{f_k}$ reads

$$(C_{11} - C_{66})(k\, u_{\mathbf{k}})k_\alpha + (C_{66}k_\beta^2 + C_{44}k_z^2)u_{\mathbf{k}\alpha} + f_{\mathbf{k}\alpha} = 0. \tag{2.3}$$

The quantity of interest is the average deviation of the relative displacement among vortices given by $\langle[\mathbf{u}(\mathbf{r}) - \mathbf{u}(0)]^2\rangle$. From Gaussian statistics we get $\langle f_{\mathbf{k}\alpha} f_{\mathbf{k}'\beta}\rangle = (2\pi)^3\delta_{\alpha\beta}\delta(\mathbf{k} - \mathbf{k}')W$ which leads to

$$\langle[\mathbf{u}(\mathbf{r}) - \mathbf{u}(0)]^2\rangle = \frac{W}{4\pi C_{44}}[(r_\perp^2 C_{44} + r_\parallel^2 C_{11})^{1/2}C_{11}^{-3/2} + (r_\perp^2 C_{44} + r_\parallel^2 C_{66})^{1/2}C_{66}^{-3/2}], \tag{2.4}$$

where $r_\parallel$ is the component of $\mathbf{r}$ parallel to the magnetic field and $r_\parallel$ is the perpendicular component. The coefficient W determines the width of the Gaussian distribution. From this formula we see that the relative displacement between any two vortices increases linearly with their separation distance. The volume of the vortex bundle according to Larkin's theory is $V_c = R_c^2 L_c$ where $R_c \approx C_{44}^{1/2}C_{66}^{3/2}\xi^2/W$ and $L_c \approx C_{44}C_{66}^2\xi^2/W$.

Decorations experiments revealed that, despite point defects, the vortex lattice looks surprisingly periodic. The reason this is so was given by Chudnovsky [27, 27] who argued that the flux lattice appears perfectly periodic because its orientational order is maintained over distances much greater than the lengths R_c and L_c. In another work [29] Chudnovsky extended Larkin's theory to take hopping defects into account and showed that the vortex lattice crosses from a glass to a crystal state as a function of the rate of hopping.

2.1.2 Pinning by dislocations

Random distribution of point defects is a source of weak pinning because a flux line can only thread through a finite number of defects. This situation is substantially different in the presence of dislocations. Because a dislocation is an extended object it can pin an entire flux line. For this reason dislocations provide strong pinning of superconducting vortices. The interaction of a single vortex in layered superconductors with a spiral defect (screw dislocation) parallel to the external magnetic field **H** was first studied theoretically by Ivlev and Thompson [30]. They found that when the vortex is centered at the core of the spiral defect exotic currents are induced along the axis parallel to **H**. In their follow up paper [31] Ivlev and Thompson computed the strength of the attractive potential between a vortex and a spiral defect as a function of the separation distance between the two objects. Similar result was obtained in a later paper by Chudnovsky [32] where the interaction of a vortex with a screw dislocation entered the problem through an effective inverse mass tensor m_{ij}^{-1}.

2.1.3 Applications of pinning and the transport current

Understanding vortex pinning can be of great value, not only for fundamental physics, but for applications to building modern devices. One of the biggest obstacles to be overcome is the problem of sending large external current through a superconducting wire. Thus far, superconducting solenoids capable of inducing a magnetic field of 100,000 Gauss have been designed. Although, this envelope is constantly being pushed the difficulties in producing strong currents in superconducting solenoids still remain and are rooted in the fact that the magnetic field induced by the current threads through the wire and generates a vortex lattice. The magnetic field of a vortex exerts

a Lorentz force per unit volume on the cooper pairs that move through it according to the formula

$$\mathbf{F} = -\frac{1}{c}\,\mathbf{J} \times \mathbf{B}. \tag{2.5}$$

By Newton's third law the cooper pairs exert an equal and opposite force on the vortex. The total force per unit length of the line exerted on a vortex by the external current is obtained by integrating Eq. (2.5) over the plane to which the magnetic field is normal:

$$\mathbf{f} = \frac{\Phi_0}{c}\,\mathbf{J} \times \mathbf{e}_z. \tag{2.6}$$

Thus, unless a vortex is pinned by a defect or is held in place by some other means it will start to drift in the direction transverse to the current. Due to the Faraday's law a moving vortex in turn induces an electric field given by

$$\mathbf{E} = \mathbf{B} \times \frac{\mathbf{v}}{c}, \tag{2.7}$$

where $\mathbf{v}$ is the velocity of the vortex. The electric field $\mathbf{E}$ is parallel to $\mathbf{J}$ and therefore acts as a resistive voltage. Dissipation of power occurs in the normal core of the vortex as it moves through the superconductor. To obtain the relationship between the electric field and the current in the spirit of Ohm's law we can assume that the driving force in Eq. (2.6) is equal to $\eta\mathbf{v}$. Combining Eqs. (2.6) and (2.7) yields

$$E = \rho J, \qquad \rho = \left(\frac{B\Phi_0}{\eta c^2}\right). \tag{2.8}$$

Various mechanisms of dissipation from a moving vortex have been proposed. The simplest model is that by Bardeen and Stephen [33] in which the vortex core is approximated by a cylinder of radius $a \sim \xi$. Outside the core the problem is treated by London equations whereas within the core one assumes ordinary Ohm's resistance.

This simplified model produced an estimate for the conductivity $\eta = BH_{c2}\sigma_n/c^2$ where σ_n is the conductivity of the normal state. An improvement to this model came from Caroli and Maki [34] who used the Bogoliubov-deGennes equations, Eqs. (1.64) to study the excitation spectrum inside a vortex. Although the order parameter $\Delta(\mathbf{r})$ goes to zero there the vortex core contains low-lying excitations which are roughly equal to the excitations in a cylinder of radius ξ. This calculation provided a supporting evidence for the validity of the Bardeen-Stephen model.

Regardless of the defect concentration, the flux lattice can always be set into motion by strong enough transport current. The threshold current above which the flux flow occurs is called the critical current j_c.

2.2 Some effects of sound in superconductors

When a sound wave enters a solid, the ions of the crystal lattice become mobile thus generating electromagnetic fields that interact with other charges inside the solid. In ordinary metals the screening of the electromagnetic fields by conduction electrons produces dissipation of energy due to Ohm's resistance. For this reason normal metals cannot support any macroscopic net currents without significant energy losses. Superconducting electrons, however, experience no resistance and can therefore sustain currents without any dissipation. In type-II superconductors the situation is more complicated due to the presence of normal cores inside vortices. In this section we discuss some works done in the past on the effects of sound in superconductors.

2.2.1 Ultrasonic attenuation

One of the first applications of sound waves in superconductors was to measure the energy gap Δ and the penetration length λ. Because the presence of an energy gap in superconductors excludes absorbtion of waves with frequency less than Δ/h, one can expect a drop in the attenuation of the sound upon crossing from normal to superconducting state. For both, longitudinal and transverse waves a rapid drop in the attenuation at the critical temperature was indeed observed. In particular, the attenuation drop for transverse waves was measured to be more that 50% in the temperature range of 0.01K below T_c [36, 35]. In the low frequency limit, that is $f = (\omega/2\pi) \lesssim 10^9$Hz, the ratio of superconducting to normal material transition rate between the energy levels E and $E + \hbar\omega$ has a simple form [10]

$$\frac{\alpha_s}{\alpha_n} = \frac{2}{1 + e^{\Delta/k_B T}}. \tag{2.9}$$

From this expression and with data on α_s/α_n obtained from experiment one can extract the value of $\Delta(T)$. In crystals, measuring the attenuation rate of sound propagating in different directions allows one to measure the anisotropy of $\Delta_{\mathbf{k}}$ [37]. Due to screening of superconducting currents the transverse sound waves complicate the calculation and measurement of ultrasonic attenuation. However, this complication can be used to measure the penetration depth λ [38].

2.2.2 Interaction of vortices with ultrasound

Shear waves in type-II superconductors generate a wide range of phenomena. Over the period of several decades since the discovery of Abrikosov vortices much investigation has been done in the study of the interaction of shear waves with flux lines. Because sound waves are dynamical in nature the usual approach of minimizing the

GL free energy is not applicable except in cases where the frequency of sound f is much smaller than the relaxation time of the cooper pairs and the dimensions of the superconducting sample are small, so that it can easily reach thermodynamic equilibrium. The criteria for this approximation will be discussed in section 2.4.

The transport and electromagnetic properties of type-II superconductors in the presence of external field are largely determined by the dynamical behavior of vortices. As mentioned in section 2.1.3, when vortices become mobile the near gapless normal core acts as a resistor which dissipates power of the source that is driving the vortex motion, i.e. the transport current. However, at low temperatures, this situation is complicated by vortex pinning which prevents the flux lattice from moving. On the other hand a sound wave would perturb the pinning centers from their static positions making the vortex cores oscillate as they follow their pinning sites. This method was first proposed by Pankert [39] and extended to the low-temperature regime by Domíngez *et al* [40, 41].

A moving flux lattice is subject to several forces including Lorentz, viscous, ,hydrodynamic or Magnus force, and the inertial force. The Lorentz force which comes from the transport current and the viscous force due to the low-lying states in the vortex core were discussed previously in section 2.1.3. Another contribution to the Lorentz force comes from the oscillating motion of the ions. The Magnus force arises from hydrodynamical effects and is equal to $\alpha_M \dot{\mathbf{u}} \times \mathbf{n}$ where $\mathbf{n}$ is the unit vector along the external magnetic field and $\dot{\mathbf{u}}$ is the vortex velocity field. The coefficient of proportionality α_M was estimated by Noziéres and Vinen [42]: $\alpha_M = \pi\hbar n_s(B/\Phi_0)$, where n_s is the density of the superconducting electrons. The inertial term first estimated by Suhl [43] contributes $M_v\dot{\mathbf{u}}^2/2$ to the kinetic energy of the vortex where the

coefficient M_v is interpreted as the vortex mass. Another contribution to the mass of the vortex was shown by Chudnovsky and Kuklov [44] to arise from the reaction force of the ions to the electric field induced by the moving vortex. They obtained the vortex mass per unit length $M_l = m^2c^2/(64\pi\alpha^2\mu\lambda^4)\ln\kappa$, where $\alpha = e^2/\hbar c \approx 137$ is the fine structure constant and μ is the shear modulus of elasticity. A comprehensive study of the vortex dynamics induced by ultrasound where all these forces are included is presented in a paper by Domingez *et al* [45](also see Sonin [46]). Recently, Chudnovsky and Bulaevskii [47] proposed a way to generate coherent radiation of sound by a moving flux lattice. They argued that a vortex moving with supersonic speed must produce Cherenkov-type radiation of sound waves. The periodicity of the flux lattice combines coherently the sound generated by each vortex, giving, as a net effect, a strong coherent radiation of sound waves.

2.2.3 Coupling elastic deformations to the superfluid

Within continuous elastic theory, local deformations are described by the displacement vector field, $\mathbf{u}(\mathbf{r}, t)$, such that $u \ll k_s^{-1}$, where $k_s = 2\pi/\lambda_s$ is the wave vector and λ_s is the wavelength or characteristic length of the deformation. The equations of motions for $\mathbf{u}$ can be derived by minimizing the elastic energy of the solid which can be written as

$$E_s = \int d^3r \frac{1}{2}(\rho_0 \dot{\mathbf{u}}^2 - \lambda_{iklm} u_{ik} u_{lm}) \tag{2.10}$$

in which ρ_0 is the combined mass density of ions and normal electrons, λ_{iklm} is the tensor of elastic coefficients and $u_{ik} = \frac{1}{2}(\partial_i u_k + \partial_k u_i)$ is the strain tensor. The general equation of motion then reads [48]

$$\rho_0 \ddot{u}_i - \lambda_{iklm} \frac{\partial^2 u_m}{\partial x_k \partial x_l} = 0. \tag{2.11}$$

This equation is completely general and applies to a solid of any crystal structure. Solution of Eq. (2.11) will have three different velocities which will depend on the crystal structure. The wavevector $\mathbf{k}$ of the sound wave will not be in general oriented along the propagation direction or perpendicular to the polarization of the sound wave. These complications due to the crystal structure make analytical studies of problems in solids involving sound waves difficult to carry out. To simplify our analysis we will direct our attention to isotropic materials and ignore any complications arising from the crystal structure. The equation of motion, Eq. (2.11), then reduces to a much simpler form:

$$\rho\frac{\partial^2\mathbf{u}}{\partial t^2} = \mu\nabla^2\mathbf{u} + (\mu+\lambda)\nabla(\nabla\cdot\mathbf{u}), \tag{2.12}$$

where μ and λ are the Lamé coefficients. They are related to the Young's modulus E and Poisson's ratio σ through

$$E = \frac{9K\mu}{3K+\mu}, \qquad \sigma = \frac{3K-2\mu}{2(3K+2\mu)}, \qquad K = \lambda + \frac{2}{3}\mu. \tag{2.13}$$

This simplification allows us to decouple the components of $\mathbf{u}$ along and perpendicular to $\mathbf{k}$. Hence, one can write the solution of $\mathbf{u}$ in two parts:

$$\mathbf{u} = \mathbf{u}_l + \mathbf{u}_t, \tag{2.14}$$

where $\mathbf{u}_l$ and $\mathbf{u}_t$ stand for the longitudinal and transverse displacement vector fields, respectively. In the long wave limit, the first term of Eq. (2.14) produces local changes in volume while the second creates shear deformations of the crystal lattice, such that

$$\nabla\times\mathbf{u}_l = 0, \qquad \nabla\cdot\mathbf{u}_t = 0. \tag{2.15}$$

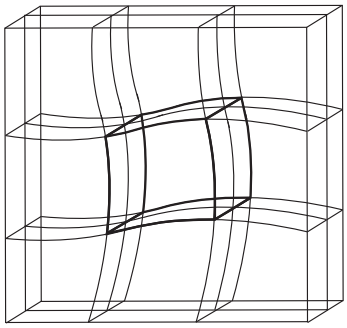

Figure 2.2: A local rotation of the crystal matrix produced by a sound wave.

The transverse shear waves do not affect the density of the ionic lattice but result in a local rotation at an angular velocity (see Fig. 2.2)

$$\mathbf{\Omega}(\mathbf{r},t)=\frac{1}{2}\nabla\times\dot{\mathbf{u}}\,. \tag{2.16}$$

In what follows we will only consider the effects of transverse sound on superconductors and ignore any effects generated by the longitudinal deformations. It should be pointed out that this kind of simplification is not as restrictive as may seem. Although, sound waves in crystals always contain both transverse and longitudinal components we may take into account only the transverse part and disregard the longitudinal component provided its effects do not modify the analysis under scrutiny.

When a time dependent deformation enters a superconductor the Cooper pairs respond to the local electromagnetic fields induced by moving ion cores. Using the two-fluid model we can write the net current as

$$\mathbf{J}=n_s e\mathbf{v}_s+n_n e\mathbf{v}_n-(n_s+n_n)e\dot{\mathbf{u}}, \tag{2.17}$$

where n_s and $\mathbf{v}_s$ are the density and velocity of the superconducting electrons, while n_n and $\mathbf{v}_n$ denote the density and velocity of the normal electrons. The last term in Eq. (2.17) is the electric current of the moving ions in accordance with the neutrality

of charge in a solid. If we regroup the terms in Eq. (2.17) with the same densities such that $\mathbf{J} = n_s e(\mathbf{v}_s - \dot{\mathbf{u}}) + n_n e(\mathbf{v}_n - \dot{\mathbf{u}})$, it becomes clear that the total current is equivalent to the transport of charges by both the superconducting and normal fluid relative to the moving ions. At finite temperatures the motion of normal electrons relative to the ions is impeded by scattering on impurities and thermal phonons. Consequently, the net normal current contributes only negligibly in comparison with the frictionless flow of superconducting electrons. For this reason, it is safe to retain only the superconducting current in Eq. (2.17). Writing the simplified net current in terms of the vector potential $\mathbf{Q}$ with the help of Maxwell's equation (1.6), equation (1.7) becomes

$$\lambda^2 \nabla \times (\nabla \times \mathbf{Q}) + \mathbf{Q} = -\frac{mc}{e}\dot{\mathbf{u}}. \tag{2.18}$$

This equation describes the response of the vector potential in the presence of moving ions. Note that the source driving the ion motion , i.e. sound wave, moving dislocation, etc., is irrelevant as long as the relative displacement of the ions is within the limit of the theory of elasticity mentioned above.

2.3 Voltage from mechanical stress in type-II superconductors: Depinning of the flux lattice by moving dislocations

It is well known that when an elastic material is subjected to large enough external stress dislocations begin to move at a high velocity and build up in a small region of the solid. This causes a crack in the crystal which grows until the material breaks. For this reason, a timely detection of high elastic stress is of practical importance. In a transparent material detection of motion of dislocations can be achieved by optical

methods. In this section we present a method [49] by which one can detect elastic stress in a type-II superconductor embedded in external magnetic field $H_{c1} < H < H_{c2}$ in the presence of a transport current $J < J_c$. We show that under these conditions external stress induces voltage across the superconductor which can be easily detected. This is an example of a piezoelectric effect in a metal.

2.3.1 Stationary dislocations

Dislocations are topological defects in a crystal. Two types of dislocations occur in crystals: Edge dislocation and screw dislocation. In a screw dislocation atoms shift relative to one another by one lattice spacing along a particular plane, Fig. (2.3a). An edge dislocation is formed by inserting an extra plane of atoms into the crystal Fig. (2.3b). In both cases the dislocations create stress and strain in the solid. An area with radius of the order of few lattice spacings around the dislocation line defines a dislocation core. One can use continuous theory of elasticity to study many aspects of dislocations provided the length over which the displacement vector $\mathbf{u}$ changes significantly is much larger than the lattice spacing a. This condition is satisfied outside of the dislocation core. Although, dislocation lines may be curved, in this section we only focus on straight dislocations in order to illustrate our ideas more succinctly. Generalization to curved dislocations is straightforward and will be studied elsewhere.

A dislocation can be defined as an increment to the displacement vector $\mathbf{u}$ on going around a closed loop L encircling the dislocation core. From Fig. (2.3) it is clear that no matter how large the loop, the increment will always be the same. Mathematically

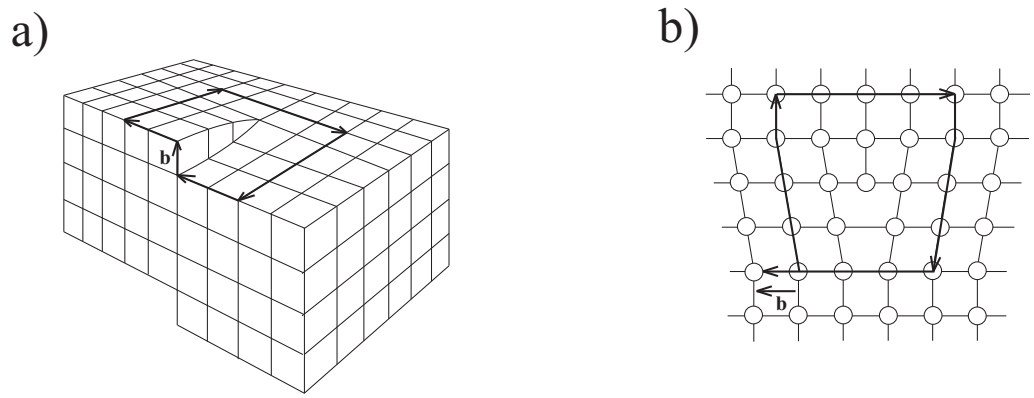

Figure 2.3: A screw dislocation - the crystal plain is shifted in the direction of the Burger's vector as shown in (a). An edge dislocation (b) is formed by inserting a plain of atoms in the crystal. In both cases the strain tensor acquires a Burger's vector after each closed contour.

this can be expressed as

$$\oint_L du_i = \oint_L \frac{\partial u_i}{\partial x_k}\, d\, x_k = -b_i \tag{2.19}$$

where b_i is called the Burger's vector. According to this condition the displacement vector $\mathbf{u}$ is a multi-valued function of the azimuthal angle ϕ. Eq. (2.19) can be converted to a differential form by transforming the contour integration to an integration over the surface bounded by L. Thus,

$$\oint_L \frac{\partial u_i}{\partial x_k}\, d\, x_k = \int_S \varepsilon_{ilm} \frac{\partial^2 u_m}{\partial x_k \partial x_l} ds_i, \tag{2.20}$$

with ε_{ilm} being the antisymmetric tensor. The Burger vector b_k can be written in integral over the surface as

$$b_k = \int_s n_i b_k \delta^{(2)}(\mathbf{r}) ds_i, \tag{2.21}$$

where $\delta^{(2)}(\mathbf{r})$ is a two-dimensional delta function and $\mathbf{r}$ is the radius vector that originates from and is perpendicular to the dislocation line. Therefore, the differential equation for a dislocation becomes

$$\varepsilon_{ilm} \frac{\partial^2 u_m}{\partial x_k \partial x_l} = -n_i b_k \delta^{(2)}(\mathbf{r}). \tag{2.22}$$

Combining the condition of equilibrium, Eq. (2.12) for $\dot{\mathbf{u}} = 0$, with Eq. (2.22) and making some strait forward manipulations yields

$$\nabla^2 \mathbf{u} + \frac{1}{1-2\sigma} \nabla(\nabla \cdot \mathbf{u}) = \mathbf{n} \times \mathbf{b} \delta^{(2)}(\mathbf{r}). \tag{2.23}$$

This equation is completely general and applies to straight as well as curved dislocations.

Let us now solve Eq. (2.23) for the two types of dislocations mentioned above. First, we begin with a screw dislocation whose line stretches along the z-axis, so that $b_x = b_y = 0$, $b_z = b$ and $\mathbf{n} = \mathbf{e}_z$, which means $\mathbf{n} \times \mathbf{b} = 0$. Since in the first order on the strain tensor a screw dislocation does not change the local volume the second term on the left hand side of Eq. (2.23) drops out. This reduces Eq. (2.23) to

$$\nabla^2 u_z = 0. \tag{2.24}$$

The solution to u_z in cylindrical coordinates which also satisfies Eq. (2.19) then yields

$$u_z = \frac{b\theta}{2\pi} \tag{2.25}$$

For en edge dislocation with the z-axis along the dislocation line and Burger's vector $b_x = b$, $b_y = b_z = 0$, Eq. (2.23) becomes

$$\nabla^2 \mathbf{u} + \frac{1}{1-2\sigma} \nabla(\nabla \cdot \mathbf{u}) = -b \delta^{(2)}(\mathbf{r}) \mathbf{e}_y. \tag{2.26}$$

In cartesian coordinates the result is

$$u_x = \frac{b}{2\pi} \left[\tan^{-1} \frac{y}{x} + \frac{1}{2(1-\sigma)} \frac{xy}{x^2+y^2} \right], \tag{2.27}$$

$$u_y = -\frac{b}{2\pi} \left[\frac{1-2\sigma}{2(1-\sigma)} \log \sqrt{x^2+y^2} + \frac{1}{2(1-\sigma)} \frac{x^2}{x^2+y^2} \right] \tag{2.28}$$

2.3.2 Moving dislocations

Dislocations can be set to motion by subjecting the sample to external stress. When the stress becomes large the velocity of dislocations can be as high as the speed of sound. The dynamics of moving dislocations have been intensively studied in the past both theoretically [50, 51] and experimentally [52]. Within continuous linear theory of elasticity the dislocation speed is limited by the shear wave velocity c_t [53]. When the anharmonicity of the crystal is taken into account the speed of dislocations has been shown to be intersonic (between c_t and the speed of longitudinal sound c_l) and in some cases even supersonic [54, 55, 56], that is above c_l. For the purpose of this chapter, however, it will suffice to consider linear elasticity.

Let's consider a screw dislocation parallel to the z-axis, $u_i = (0, 0, u_z)$, moving with velocity v. Writing Eq. (2.12) in the cartesian coordinates for a screw dislocation, we obtain the well known equation for a transverse shear wave

$$\left(\frac{\partial^2}{\partial x^2} + \frac{\partial^2}{\partial y^2}\right) u_z = \frac{1}{c_t^2}\frac{\partial^2 u_z}{\partial t^2}, \tag{2.29}$$

where $c_t = (\mu/\rho)^{1/2}$ is the speed of the shear wave. A convenient way to solve this equation is by making a Lorentz like coordinate transformation

$$x^{'} = \frac{x - vt}{(1 - v^2/c_t^2)^{1/2}}, \quad y^{'} = y, \quad z^{'} = z, \quad t^{'} = \frac{t - vx/c_t^2}{(1 - v^2/c_t^2)^{1/2}}. \tag{2.30}$$

This transformation leaves Eq. (2.29) unchanged. However, in the moving frame the displacement vector **u** surrounding the dislocation must appear to be constant in time, and so, Eq. (2.29) reduces to

$$\left(\frac{\partial^2}{\partial x'^2} + \frac{\partial^2}{\partial y'^2}\right) u_z = 0. \tag{2.31}$$

This equation is identical in structure to Eq. (2.24) for a stationary screw dislocation. Thus, the solution is

$$u_z(x,y,t) = \frac{b}{2\pi}\tan^{-1}\frac{y^{'}}{x^{'}} = \frac{b}{2\pi}\tan^{-1}\frac{\gamma y}{x-vt}, \tag{2.32}$$

where

$$\gamma = \left(1-\frac{v^2}{c_t^2}\right)^{1/2} \tag{2.33}$$

is the effective relativistic factor. Clearly for a sensible solution v must not exceed c_t. As in relativistic mechanics the screw dislocation becomes contracted in the direction of its velocity. This can be seen by looking at the shape of a contour around the dislocation along which u_z =constant. For a stationary dislocation this would be a circle. For a moving dislocation the circle is contracted to an ellipse with eccentricity that increases as v approaches c_t.

We now turn attention to the edge dislocation parallel to the z-axis and moving in the x-direction. The displacement field $u_i = (u_x, u_y, 0)$ will have both the transverse and longitudinal components, and therefore Eq. (2.12) can be written in a simplified form

$$\rho\frac{\partial^2\mathbf{u}}{\partial t^2} = -\mu(\nabla\times\mathbf{G}) + (\lambda+2\mu)\nabla H, \tag{2.34}$$

where

$$\mathbf{G} = \nabla\times\mathbf{u}, \qquad H = \nabla\cdot\mathbf{u}. \tag{2.35}$$

Taking the curl and divergence of Eq. (2.34) give us separate equations for $\mathbf{G}$ and H:

$$\rho\frac{\partial^2 G_z}{\partial t^2} = \mu\left(\frac{\partial^2}{\partial x^2}+\frac{\partial^2}{\partial y^2}\right)G_z, \qquad \rho\frac{\partial^2 H}{\partial t^2} = (\lambda+2\mu)\left(\frac{\partial^2}{\partial x^2}+\frac{\partial^2}{\partial y^2}\right)H. \tag{2.36}$$

Transformation to the moving frame gives

$$\nabla_t^2 G = 0, \qquad \nabla_l^2 H = 0, \tag{2.37}$$

where

$$\nabla_t^2 = \left(\frac{\partial^2}{\partial x_t^2} + \frac{\partial^2}{\partial y^2}\right) \qquad \nabla_l^2 = \left(\frac{\partial^2}{\partial x_l^2} + \frac{\partial^2}{\partial y^2}\right)$$
$$x_t = \frac{x - vt}{\gamma_t} \qquad x_l = \frac{x - vt}{\gamma_l}$$
$$\gamma_t = \left(1 - \frac{v^2}{c_t^2}\right)^{1/2} \qquad \gamma_l = \left(1 - \frac{v^2}{c_l^2}\right)^{1/2}. \tag{2.38}$$

and c_t and c_l are the transverse and longitudinal speeds of sound. The solution to G_z and H with the boundary conditions $G_z, H \to 0$ as $r \to \infty$ are [53]

$$G_z(x,y,t) = \frac{b(1+\gamma_t^2)}{2\pi\gamma_t^2}\frac{x_t}{r_t^2} \qquad H(x,y,t) = \frac{bc_t^2}{\pi\gamma_l c_l^2}\frac{x_t}{r_l^2}, \tag{2.39}$$

$$r_t^2 = x_t^2 + y^2 \qquad r_l^2 = x_l^2 + y^2. \tag{2.40}$$

For the purposes of the next section we do not need to solve these equations for the displacement field as we will only be interested in the vector function $\nabla \times \dot{\mathbf{u}}$.

2.3.3 Current generated by moving dislocations

We now want to solve the problem of finding the magnetic fields and currents produced by moving dislocations. First, let us consider a screw dislocation parallel to the z-axis. Taking a time derivative of Eq. (2.32) yields the velocity field of the ions:

$$\dot{\mathbf{u}}(\mathbf{r},t) = v\gamma\frac{bp}{2\pi}\frac{y}{[y^2 + \gamma^2(x-vt)^2]}\mathbf{e}_z\,, \tag{2.41}$$

To simplify mathematics, in what follows we will consider the case of $v^2 \ll c_t^2$. Estimates based upon this approximation will be valid up to $v \sim 0.3c_t$. In this case

$$\dot{\mathbf{u}}(\mathbf{r},t=0) = v\frac{bp}{2\pi}\frac{\sin\theta}{r}\mathbf{e}_z\,, \tag{2.42}$$

where θ is the angle in cylindrical coordinates. Substituting Eq. (2.42) into Eq. (2.18)yields

$$\lambda^2\nabla\times(\nabla\times\mathbf{Q}) + \mathbf{Q} = -\frac{mcv}{e}\frac{bp}{2\pi}\frac{\sin\theta}{r}\mathbf{e}_z. \tag{2.43}$$

It is convenient to introduce the dimensionless parameter $\beta = (bp/2\pi\lambda)$ and dimensionless distance from the dislocation $\rho = r/\lambda$. Substituting Eq. (2.41) into Eq. (2.18) we obtain

$$\rho^2 \frac{\partial^2 Q_z}{\partial^2 \rho} + \frac{\partial^2 Q_z}{\partial^2 \theta} + \rho \frac{\partial Q_z}{\partial \rho} - \rho^2 Q_z = \frac{mcv}{e} \beta \rho \sin\theta. \tag{2.44}$$

If we choose a solution of the form $Q_z(\rho, \theta) = (mcv/e) f(\rho) \sin\theta$ then Eq. (2.44) becomes an ordinary differential equation for $f(\rho)$:

$$\rho^2 f''(\rho) + \rho f'(\rho) - (1 + \rho^2) f(\rho) = \beta\rho. \tag{2.45}$$

The general solution of this equation that goes to zero as $\rho \to \infty$ is

$$f(\rho) = \beta \left[C K_1(\rho) - \frac{1}{\rho} \right], \tag{2.46}$$

where $K_1(\rho)$ is a modified Bessel function and C is a constant of integration that can be obtained from the requirement that $\mathbf{Q}$ is finite everywhere. Since $K_1(\rho) \to 1/\rho$ as $\rho \to 0$, this gives $C = 1$. The expression for the supercurrent reads

$$\mathbf{j} = -\frac{c}{4\pi\lambda^2} \left[\frac{mc}{e} \dot{\mathbf{u}} + \mathbf{Q} \right] = -\frac{mc^2 v}{4\pi e \lambda^2} \beta K_1(\rho) \sin\theta \mathbf{e}_z. \tag{2.47}$$

Because the angle θ is defined with respect to the x-axis, $\mathbf{j}$ vanishes in the plane spanned by the Burgers vector $\mathbf{b}$ and the dislocation velocity $\mathbf{v}$. In the yz-plane the current flows along a closed loop. It generates a dipole-like magnetic field,

$$\mathbf{B} = \nabla \times \mathbf{Q} = -\frac{mcv}{e\lambda\rho} \left[f(\rho) \cos\theta \, \mathbf{e}_r - \rho f'(\rho) \sin\theta \, \mathbf{e}_\theta \right]. \tag{2.48}$$

For edge dislocation the angular frequency $\mathbf{\Omega}$ is obtained by taking a time derivative of $G_z(x, y, t)/2$ which at $t = 0$ yields

$$\frac{1}{2} \dot{G}_z(x, y, 0) = \frac{1}{2} (\nabla \times \dot{\mathbf{u}})_z = \frac{bv}{2\pi} \frac{\cos 2\theta}{r^2}. \tag{2.49}$$

Upon taking a curl of Eq. (2.18) and substituting Eq. (2.49) for the right hand side we end up with an equation for the magnetic field

$$\nabla^2 B_z - \frac{B_z}{\lambda^2} = \frac{2mcv\beta}{e\lambda}\frac{\cos 2\theta}{r^2}. \tag{2.50}$$

As before, we can try a solution of the form $B_z = 2mcv/(e\lambda)g(\rho)\cos 2\theta$ which reduces Eq. (2.50) to

$$\rho^2 g''(\rho) + \rho g'(\rho) - (4+\rho^2)g(\rho) = \beta. \tag{2.51}$$

A simple solution for which B_z approaches zero when $r \to \infty$ is

$$g(\rho) = \frac{2mc}{e\lambda}\left[CK_2(\rho) - \frac{1}{\rho^2}\right]. \tag{2.52}$$

The magnetic field for edge dislocation moving at the speed v is then

$$\mathbf{B} = \frac{2mc}{e\lambda}\beta\left[CK_2(\rho) - \frac{1}{\rho^2}\right]\cos 2\theta \mathbf{e}_z, \tag{2.53}$$

and the electric current is

$$\mathbf{J} = -\frac{2mc^2}{4\pi e\lambda^2}\beta\left[\frac{g(\rho)}{\rho}\sin 2\theta \mathbf{e}_r + g'(\rho)\cos 2\theta \mathbf{e}_\theta\right] \tag{2.54}$$

2.3.4 Motion of the flux lattice

In section 2.1.3 we discussed vortex pinning by dislocations oriented parallel to the flux lines. Because the flux line runs along the entire line of the dislocation the vortex pinning is very strong. At low temperature, when a large external stress is applied, dislocations accelerate to high velocities ($v \sim c_t$) while point defects remain relatively immobile. It is therefore reasonable to expect that the flux lattice will be dragged by dislocations in the direction of their motion. This situation is not generic however because it only exists when linear dislocations are parallel to the flux lines. Only in

this case the normal core of a vortex line can be effectively pinned by the dislocation. If the dislocation is at an angle with the flux line then the pinning is more or less equivalent to the pinning by a point defect, which is much weaker than the pinning of the flux line by the entire length of the dislocation.

We want to examine a more general situation in which dislocations are not necessarily parallel to the flux lines. The effect we are going to discuss is not due to pinning of normal cores of flux lines by the dislocations. Rather, we look at a situation in which the screw dislocations are perpendicular to the flux lines. As we calculated in the previous section, the current generated by a screw dislocation flows in a direction parallel to the dislocation line and therefore perpendicular to the flux line. In this geometry vortices feel a transverse force fluctuating in space due to the local current generated by a moving dislocation. The equicurrent lines from an array of moving parallel dislocations are shown in Fig. (2.4). As the velocity of dislocations increases the equicurrent loops expand. In the presence of the transport current, j_t, normal to a flux line, the line becomes locally mobile if the combined force exerted on it by j_t and the current j_d due to moving dislocations exceeds the depinning threshold. To compute this effect one should notice that the direction and amplitude of j_d fluctuates in space and time due to random distribution of dislocations. For an ensemble of parallel dislocations moving at the same speed v the depinning threshold should be roughly determined by the condition

$$\langle j_d^2 \rangle^{1/2} \sin\vartheta = j_c - j_t \,, \tag{2.55}$$

where $j_c > j_t$ is the critical current in the absence of moving dislocations and ϑ is the angle that dislocations make with the flux lines. The latter enters Eq. (2.55)

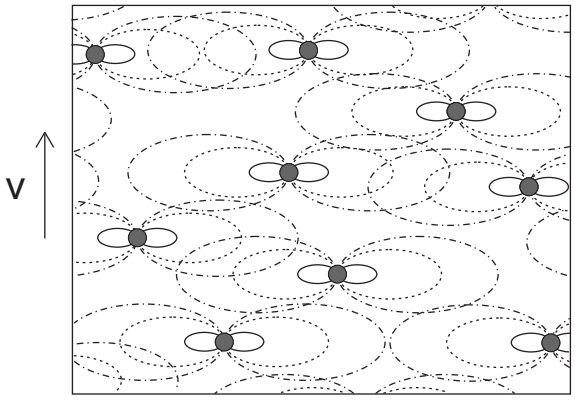

Figure 2.4: Equicurrent lines for an array of moving parallel screw dislocations that are normal to the picture.

because only the component of $\mathbf{j}_d$ normal to the flux line exerts a force on the line. The amplitude of the fluctuating current that appears in Eq. (2.55) can be computed as

$$\langle j_d^2 \rangle = n_d \int d^2 r \mathbf{j}^2(\mathbf{r}) \,, \tag{2.56}$$

where n_d is a 2D concentration of dislocations and $\mathbf{j}(\mathbf{r})$ is given by Eq. (2.47). At the lower limit this integral should be cutoff by the size of the dislocation core, $r \sim b$. This gives

$$\langle j_d^2 \rangle = n_d \left(\frac{mc^2 vb}{8\pi^2 e\lambda^2} \right)^2 \pi \ln \frac{\lambda}{b} \,. \tag{2.57}$$

Substituting this result in Eq. (2.55), one obtains the critical (depinning) concentration of dislocations as function of their velocity:

$$\sqrt{n_d} = \frac{\bar{j}_c}{\lambda} \left(1 - \frac{j_t}{j_c} \right) \frac{c_t}{v} \,, \tag{2.58}$$

where we have introduced a dimensionless critical current

$$\bar{j}_c = \left[\frac{64\pi^3}{\ln(\lambda/b)} \right]^{1/2} \frac{e\lambda^3}{mc^2 c_t b \sin\vartheta} \, j_c \,. \tag{2.59}$$

For typical values of the parameters: $\lambda \sim 10^{-5}$cm, $b \sim 2 \times 10^{-8}$cm, $c_t \sim 2 \times 10^5$ cm/s, and $\vartheta = 90^\circ$, the parameter $\bar{j}_c$ is of order unity at $j_c \sim 10^5$ A/cm^2.

According to Ref. [51] the speed of a screw dislocation very rapidly approaches the speed of sound on increasing the elastic stress. Taking $v \sim 0.1c_t$ and $j_t \sim 0.9j_c$ we obtain a reasonable value of the critical concentration of dislocations: $n_d \sim 1/\lambda^2$. Even smaller concentration of dislocations will be required if the transport current is brought closer to j_c. In experiment this effect will manifest itself as a rapid shift of the critical current towards lower values in the presence of plastic deformation of the material. The resulting depinning of flux lines will generate voltage across the superconductor. Since this voltage originates from the elastic stress, this would be a remarkable example of a strong non-equilibrium piezoelectric effect in a conducting material.

Although our analysis of flux depinning was restricted to screw dislocations only one can see that edge dislocations would produce a similar effect provided they are oriented parallel to the flux lines.

2.4 Nucleation of a vortex by ultrasound

A superconducting cylinder rotated at an angular velocity $\mathbf{\Omega}$ about its symmetry axis develops a magnetic moment $\mathbf{M} = -(mc/2\pi e)\mathbf{\Omega}$, where m and e are bare electron mass and charge, and c is the speed of light. This effect predicted by London [57] has been subsequently tested in experiment and proved with an accuracy to many significant figures. It is a consequence of a more general gyromagnetic effect predicted by Barnett [58]: "A substance which is magnetic must become magnetized by a sort of molecular gyroscopic motion on receiving an angular velocity". The Barnet effect is, in its turn, a consequence of the Larmor theorem [59]: In the rotating frame of reference the action of the rotation on charged particles is equivalent to the action

of the magnetic field $\mathbf{H}_\Omega = \mathbf{\Omega}/\gamma$, where γ is the gyromagnetic ratio. For electron's orbital motion $\gamma = e/(2mc) \approx 0.9\times10^7$ (Gauss)$^{-1}$ s^{-1}. Thus, in practice, the fictitious field in the reference frame of a rotating macroscopic cylinder can hardly exceed a fraction of a milligauss. This would be well below the lower critical field $\mathbf{H}_{c1}$, Eq. (1.41), when the temperature of the superconductor is not too close to T_c. Due to the Meissner effect [2] (considered in the frame of the rotating cylinder) such a field would be expelled from the bulk of the cylinder by a superconducting current induced at the surface. Writing $\mathbf{B} = \mathbf{H}_\Omega + 4\pi\mathbf{M} = 0$ for the total field in the bulk, one obtains the London's magnetic moment, $\mathbf{M} = -\mathbf{H}_\Omega/(4\pi) = -(mc/2\pi e)\mathbf{\Omega}$. Due to the symmetry of the problem it is the same in the rotating and laboratory frames.

In this section we would like to take this problem a little further [60] and look at the consequence of an angular velocity well beyond the experimental limit. In particular, we are interested in the rotational velocity of a magnitude that would generate a fictitious magnetic field that exceeds $\mathbf{H}_{c1}$. If Larmor's theorem still holds, than it must be the case that a superconducting vortex enters the bulk of the cylinder. This would require the angular velocity to be of order 10^9s^{-1}, clearly surpassing the feasible experimental value for a mechanical rotation. While this scenario is merely a thought experiment we will use it as a motivation to study the effect of local rotations generated in a superconductor by high frequency ultrasound. The frequency of ultrasound achievable in experiment with, e.g., surface acoustic waves can easily be in the ballpark of $f \sim 10^{10}\text{s}^{-1}$ [61]. According to Eq. (2.16) a sound of such frequency and amplitude of a few nanometers can provide $\Omega \sim 10^9\text{s}^{-1}$ that can generate fictitious magnetic fields above $\mathbf{H}_{c1}$. For practical purposes, it may be convenient to loosen the restriction on the frequency and amplitude of ultrasound by applying an external

magnetic field $\mathbf{H}$ near, but less than, $\mathbf{H}_{c1}$. We shall see that within one percent of $\mathbf{H}_{c1}$, vortices can be ignited by the ultrasound in the GHz frequency range.

2.4.1 Free energy

For a vortex to enter a superconductor, the Gibbs free energy of the system with a vortex must be less than the system witout a vortex. We compute the change in free energy due to the vortex and determine the condition at which it becomes negative. It should be noted that the system under consideration is dynamical, and therefore is not at a thermodynamical equilibrium. However, we are interested in the free energy of the Cooper pairs which can adjust to the changes of state in a time scale orders of magnitude shorter than the period of the sound. This time scale is proportional to the relaxation time τ of the cooper pairs, i.e. $\tau \sim 10^{-12}$s. As mentioned before, the period of the sound $T = 1/f$ will be always greater than 10^{-10}s. Under these conditions, our system is adiabatic and the thermodynamic equilibrium can be safely established.

In terms of the total current $\mathbf{j}$, the kinetic energy of the superconducting electrons may be expressed in the form

$$KE_e = \int d^3r \frac{n_s m}{2} \left(\frac{1}{n_s e}\mathbf{j} + \dot{\mathbf{u}} \right)^2 . \tag{2.60}$$

Using Maxwell's equation $\nabla \times \mathbf{B} = (4\pi/c)\mathbf{j}$ and combining Eqs. (2.60) and (2.10) the expression for the total Gibbs free energy yields

$$\begin{aligned} G &= \mathcal{F}_0 + \frac{1}{8\pi}\int d^3r \left[\mathbf{B}^2 + \frac{\lambda^2}{f(r)} (\nabla \times \mathbf{B})^2 \right] + \int d^3r \frac{1}{2} \left[\rho\, \dot{\mathbf{u}}^2 - \lambda_{iklm} u_{ik} u_{lm} \right] \\ &+ \frac{1}{4\pi}\int d^3r \frac{mc}{e} \dot{\mathbf{u}} \cdot (\nabla \times \mathbf{B}) - \frac{1}{4\pi}\int d^3r \mathbf{H} \cdot \mathbf{B}, \end{aligned} \tag{2.61}$$

Here, $\mathcal{F}_0$ is the free energy in the absence of currents, fields, and sound, $\lambda^2 =$

$mc^2/4\pi n_s e^2$ is the London penetration depth, and $\rho = \rho_0 + n_s m$ is the total mass density of the superconductor. The last term can be recognized as the interaction of the external magnetic field with the magnetization. It is this term that is responsible for the nucleation of vortices in the absence of sound when $H \geq H_{c1}$.

Before we can calculate the free energy of Eq. (2.61) we must first work out the magnetic field. The equation for the gauge invariant vector potential over all space is

$$\lambda^2 \nabla \times (\nabla \times \mathbf{Q}) + f(r)\mathbf{Q} = -\frac{mc}{e} f(r)\dot{\mathbf{u}}. \tag{2.62}$$

where $f(r) = (|\psi|/|\psi_\infty|)^2$, ψ is the complex order parameter, and $|\psi_\infty| = \sqrt{n_s/2}$ is the order parameter in the absence of gradients and fields. For certainty we consider a transverse standing sound wave having one node at the center of a superconducting slab of thickness d, with the external field applied parallel to the slab, see Fig. (2.5). In this case $\lambda_s = 2d$. Generalization to standing waves with many nodes is straightforward. Since the thickness of the slab d may be of order or less then λ, the vortex in general will not have a cylindrical symmetry due to the boundary condition on the current, $\mathbf{J}_\perp \cdot \mathbf{n} = 0$, where $\mathbf{n}$ is the direction of the surface. We can satisfy this boundary condition by placing image vortices of alternating sign a distance d apart on the outside of the slab. The equation for the magnetic field, in the region $r > \xi$ where $|\psi| = 1$, can then be written in two parts, namely $\mathbf{B} = \mathbf{B}_0 + \mathbf{B}_v$, such that the first term satisfies

$$\lambda^2 \nabla \times (\nabla \times \mathbf{B}_0) + \mathbf{B}_0 = -\frac{2mc}{e}\mathbf{\Omega}, \tag{2.63}$$

while the second is a solution of

$$\lambda^2 \nabla \times (\nabla \times \mathbf{B}_v) + \mathbf{B}_v = \Phi_0 \mathbf{e}_z \sum_{n=-\infty}^{\infty} (-1)^n \delta(\mathbf{r} + nd\mathbf{e}_x), \tag{2.64}$$

where $\Phi_0 = hc/2e$ is the flux quantum of a vortex.

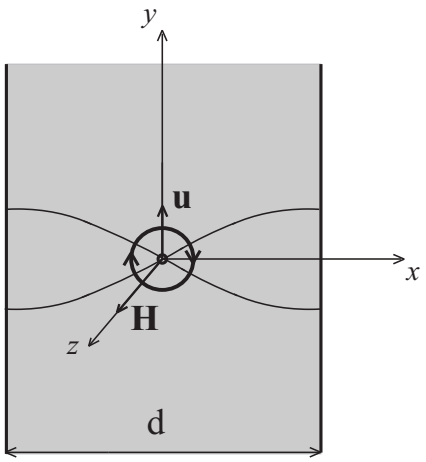

Figure 2.5: Standing wave in a slab with one node at the center. The vortex is generated at the node where Ω is maximum.

Since we are interested in standing sound waves we can choose the displacement vector $\mathbf{u}$ to be

$$\mathbf{u}(\mathbf{r},t) = u_0 \sin(kx)\sin(\omega t)\mathbf{e}_y. \tag{2.65}$$

The quantity $k = \omega/v = 2\pi/\lambda_s = \pi/d$ is the wave number with λ_s and v being the wavelength and the speed of sound respectively. It is easy to see from Eq. (2.16) that Ω is maximum at the nodes. The corresponding solutions to Eqs. (2.63) and (2.64) with the boundary condition $\mathbf{B} = \mathbf{H}$ at $x = \pm d/2$ are

$$\mathbf{B}_0(x) = \mathbf{B}_M + \mathbf{B}_s \tag{2.66}$$

$$\mathbf{B}_v(\mathbf{r}) = \sum_{n=-\infty}^{\infty} (-1)^n \mathbf{b}(\mathbf{r}_n) \tag{2.67}$$

where

$$\mathbf{B}_M = 2\mathbf{H}\frac{\sinh(d/2\lambda)}{\sinh(d/\lambda)}\cosh\left(\frac{x}{\lambda}\right) \tag{2.68}$$

$$\mathbf{B}_s = -\frac{2mc}{e}\frac{\mathbf{\Omega}}{1+k^2\lambda^2} \tag{2.69}$$

$$\mathbf{b}(\mathbf{r}_n) = \frac{\Phi_0}{2\pi\lambda^2}K_0(|\mathbf{r}+nd\mathbf{e}_x|/\lambda)\mathbf{e}_z\,, \tag{2.70}$$

and K_0 is the modified Bessel function. The first term in Eq. (2.66) is the Meissner field while the second is due to the sound.

Let us now integrate by parts the third term in Eq. (2.61) and insert $\mathbf{B} = \mathbf{B}_0 + \mathbf{B}_v$. By doing so we obtain

$$G = G_0 + \Delta E + \frac{1}{4\pi}\int dr^3 \left[\frac{2mc}{e}\mathbf{\Omega} + \mathbf{B}_s\right]\cdot\mathbf{B}_v + \frac{1}{4\pi}\int d^3r \frac{\lambda^2}{f(r)}(\nabla\times\mathbf{B}_v)\cdot(\nabla\times\mathbf{B}_s)$$

where G_0 is the Gibbs free energy without a vortex and

$$\begin{aligned}\Delta E &= \frac{1}{4\pi}\int d^3r \left[\mathbf{B}_M\cdot\mathbf{B}_v + \frac{\lambda^2}{f(r)}(\nabla\times\mathbf{B}_M)\cdot(\nabla\times\mathbf{B}_v)\right] \\ &+ \frac{1}{8\pi}\int d^3r \left[\mathbf{B}_v^2 + \frac{\lambda^2}{f(r)}(\nabla\times\mathbf{B}_v)^2\right] - \frac{1}{4\pi}\int dr^3\mathbf{H}\cdot\mathbf{B}_v \qquad (2.71)\end{aligned}$$

is the vortex energy. One can simplify the volume integrals in Eq. (2.71) by separating the volume over the core from the volume outside of the core. When the latter is integrated by parts, the integrals outside the core cancel and the free energy in Eq. (2.71) with the help of Eq. (2.69) becomes $\Delta\mathcal{F} = \Delta\mathcal{F}_1 + \Delta\mathcal{F}_2 + \Delta\mathcal{F}_3 + \Delta E$, where

$$\Delta\mathcal{F}_1 = \frac{1}{4\pi}\int_c dr^3 \left[\frac{2mc}{e}\mathbf{\Omega} + \mathbf{B}_s\right]\cdot\mathbf{B}_v \qquad (2.72)$$

$$\Delta\mathcal{F}_2 = \frac{\lambda^2}{4\pi}\oint_c \mathbf{B}_v\times(\nabla\times\mathbf{B}_s)\cdot d\mathbf{s} \qquad (2.73)$$

$$\Delta\mathcal{F}_3 = \frac{1}{4\pi}\int_c d^3r\frac{\lambda^2}{f(r)}(\nabla\times\mathbf{B}_v)\cdot(\nabla\times\mathbf{B}_s). \qquad (2.74)$$

The subscript c indicates an integration over the core. Near the vortex core the function $f(r) = (r/a)^2$, where $a \approx \xi$. It is straightforward to check that in the limit $r \to 0$ the exact solution to Eq. (2.18) for the vector potential $\mathbf{A}_s(\mathbf{r})$ is

$$\mathbf{A}_s(\mathbf{r}) = -\frac{2mc}{e}\Omega_0 x\mathbf{e}_y, \qquad (2.75)$$

and the magnetic field $\mathbf{B}_s = \nabla \times \mathbf{A}_s(\mathbf{r})$ generated by the sound at the center of the core yields

$$\mathbf{B}_s(\mathbf{r}) = -\frac{2mc}{e}\Omega_0 \mathbf{e}_z, \tag{2.76}$$

in which

$$\Omega_0 = \frac{1}{2}u_0 k\omega = \frac{\pi}{2}\frac{u_0}{d}\omega. \tag{2.77}$$

It can be shown that near the vortex core, $\nabla \times B_v \propto r$ and $\nabla \times B_s \propto r^3$. The expression under the integral in Eq. (2.74) is therefore proportional to r^3 near the center of the core and to $rK_1(r/\lambda)$ at $r \gtrsim \xi$. Thus, the integral in Eq. (2.74) can be neglected in the limit $k\lambda \ll 1$.

The case of $k\lambda \geq 1$ is rather involved as it requires explicit knowledge of the magnetic fields in the vortex core. For $k\lambda \ll 1$ Eq. (2.69) provides $\mathbf{B}_s \cong -(2mc/e)\mathbf{\Omega}$ in all regions of space, so that $\Delta\mathcal{F} \to 0$. In this case the Meissner field $\mathbf{B}_M$ and the fields due to the images can be neglected. The total interaction energy per unit length of the vortex acquires the simplest form at $\kappa = \lambda/\xi \gg 1$, which is

$$\frac{\Delta\mathcal{F}_2}{L} = -\frac{mc}{2\pi}\Omega_0\Phi_0\left(\frac{k\lambda}{\kappa}\right)^2 \ln\kappa \tag{2.78}$$

where L is the dimension of the slab in the z-direction.

If one excludes small contribution from the vortex core in Eq. (2.71), then the integration by parts yields

$$\frac{\Delta E}{L} = \frac{\lambda^2}{8\pi}\oint \mathbf{B}_v \times (\nabla \times \mathbf{B}_v)\cdot d\mathbf{s} - \frac{1}{4\pi}\int d^3r \mathbf{H}\cdot\mathbf{B}_v. \tag{2.79}$$

This approximation is good if λ and d are large compared to the coherence length ξ.

The vortex energy per unit length of the line then yields

$$\frac{\Delta E}{L} = \frac{\Phi_0^2}{(4\pi\lambda)^2}\ln\kappa - \frac{\Phi_0 H}{4\pi} \tag{2.80}$$

The first term in this expression is the self energy of the vortex, while the second term is the energy of interaction of the flux quantum with the external field. For the purpose of estimation we will use this reduced expression when working out the analytical result.

2.4.2 Condition for nucleation of a vortex

A vortex will enter the superconductor only if its presence minimizes the free energy of the system. By setting the change in the free energy to zero, we can find the critical parameters, i. e. the frequency and the amplitude of the sound, above which the presence of a vortex becomes favorable. Hence, the condition for the nucleation of a vortex $\Delta\mathcal{F}_2 + \Delta E = 0$, yields

$$\frac{2mc}{e}\Omega_0\left(\frac{k\lambda}{\kappa}\right)^2 \ln\kappa = \epsilon H_{c1}\,, \tag{2.81}$$

where

$$\epsilon = 1 - \frac{H}{H_{c1}} \tag{2.82}$$

and $H_{c1} = \beta\Phi_0 \ln\kappa/(4\pi\lambda^2)$ is the first critical field which can be obtained from Eq. (2.80) at $\Delta E = 0$. Substituting Eq. (2.77) into Eq. (2.81), the conditions on the frequency f and amplitude u_0 of the sound needed to nucleate a vortex in the geometry shown in Fig. 2.5 can be written as

$$f = \frac{v}{2d}\,, \qquad u_0 = \frac{\epsilon}{4}\left(\frac{d}{\pi\lambda}\right)^4 \frac{\hbar\kappa^2}{mv}\,. \tag{2.83}$$

While the last formula is valid for $\pi\lambda \ll d$ and $\kappa \gg 1$, it should give the correct answer even for $d \sim \pi\lambda$, $\kappa \gg 1$ and be true by order of magnitude for $\kappa \sim 1$.

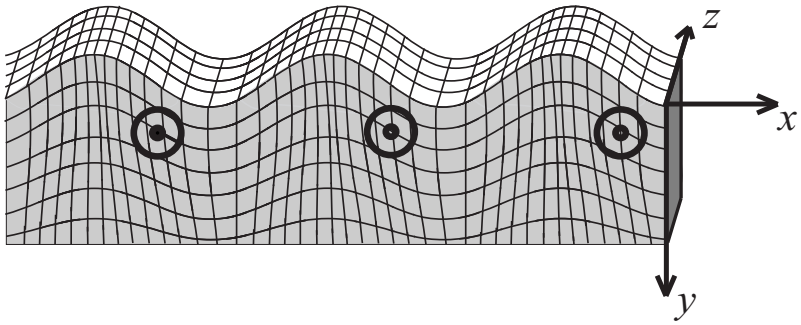

Figure 2.6: Surface acoustic waves can ignite vortices near the surface.

In this case the expression for H_{c1} carries the signature of the surface barrier [62]: $H_{c1} = \beta\Phi_0 ln\kappa/(4\pi\lambda^2)$, where

$$\beta = \frac{1 - 2(\ln\kappa)^{-1}\sum_1^\infty (-1)^n K_0(dn/\lambda)}{1 - 2\sinh(d/2\lambda)[\sinh(d/\lambda)]^{-1}}. \tag{2.84}$$

For the speed of transverse sound $v \sim 3 \times 10^5$cm/s, in a slab of thickness $d \sim \pi\lambda \sim 6 \times 10^{-5}$cm and $\kappa \sim 2$, with H within one percent of H_{c1}, one gets from Eq. (2.83) $f \sim 3$GHz and $u_0 \sim 0.2$nm. These are accessible values of frequency and amplitude of ultrasound.

As $\mathbf{\Omega}$ changes its sign every half a period of the sound, vortices are periodically attracted and repelled by the standing acoustic wave in Fig. 2.5. Periodic entering and expulsion of vortices should result in the elevated attenuation of the ultrasound and in the ac voltage across the slab at the sound frequency. In a different experiment one can assist vortices to enter or exit the superconductor with the help of the surface acoustic waves (SAW): Fig. 2.6. Like in the problem with a slab, local rotation of the crystal produced by the SAW may assist nucleation of the vortex at the field just below H_{c1}.

2.4.3 Numerical analysis

We now present a numerical analysis of the problem which was discussed above and obtain the critical amplitude as a function of frequency when κ and $k\lambda$ are ~ 1 We show that, to a good approximation, the condition derived in Eq. (2.83) is correct. However, we do not investigate numerically the full GL equations, Eqs. (1.11) and (1.12), but instead compute the magnetic field inside the vortex core with the assumption that the function $\sqrt{f} = |\psi|/|\psi_\infty|$ has the same form as Eq. (1.33). This assumption is reasonable since the magnetic field generated by the sound wave does not significantly distort the structure of ψ over the vortex core. We then insert the numerical solution for B_s into the integrals (2.72) and (2.74) and compute the free energy due to the interaction of the vortex with the standing wave. Because we are working with small κ the standard approximations employed previously to work out the energy per unit line of the vortex no longer apply so, we must obtain it numerically as well. In order to avoid the complicated behavior of the magnetic field near the boundary of the sample we adopt a slightly different geometry than the one considered thus far. Fig. 2.7 shows a standing wave in a slab with dimensions d and L both of which are large enough to eliminate any effects of the boundary, namely the image and the Meissner fields. Note that the vortices can now enter the sample through the top and the bottom surface along the y-axis. This allows us to excite higher harmonics and hence consider $k\lambda \gtrsim 1$.

Dividing Eq. (2.18) by $\lambda^2 f$ and taking a curl of both sides renders

$$\nabla \times \left[\frac{1}{f}\nabla \times \mathbf{B}\right] + \frac{\mathbf{B}}{\lambda^2} = \frac{2mc}{e\lambda^2}\mathbf{\Omega}. \tag{2.85}$$

Using standard vector identities we can rewrite this equation in cylindrical coordinates

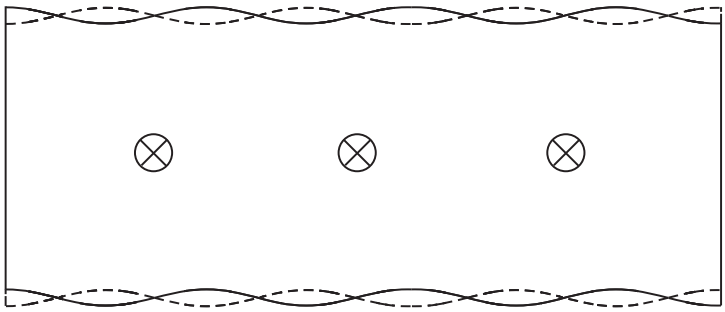

Figure 2.7: Standing waves with seven nodes. The vortices nucleate at the nodes where the energy is minimum.

as

$$\left\{\frac{\partial^2}{\partial r^2}+\frac{1}{r^2}\frac{\partial^2}{\partial\theta^2}-\left[\frac{g(r)}{\lambda}-\frac{1}{r}\right]\frac{\partial}{\partial r}-\frac{f(r)}{\lambda^2}\right\}B(r,\theta)=\frac{2mc}{e\lambda^2}\Omega_0 f(r)\cos(kr\cos\theta), \tag{2.86}$$

where

$$g(r)\equiv 2\nu\kappa\left[\sinh\left(\frac{\nu r}{\xi}\right)\cosh\left(\frac{\nu r}{\xi}\right)\right]^{-1}. \tag{2.87}$$

Notice that in order to compute the free energy given by Eqs. (2.72) (2.74) it is sufficient to know the quantity $F(r)=(4\pi mc\Omega_0/e)^{-1}\int_0^{2\pi}B_s(r,\theta)d\theta$. Integrating Eq. (2.86) with the substitution $\eta=r/\lambda$ yields an equation for $F(\eta)$:

$$\eta^2F''(\eta)+[1-\eta^2g(\eta)]F'(\eta)-\eta^2f(\eta)F(\eta)=\frac{2mc}{e}\Omega_0 f(r)2\pi\eta^2J_0\left(\frac{k\lambda\eta}{\kappa}\right). \tag{2.88}$$

This equation must be supplemented with boundary conditions for $F(\eta)$ and $F'(\eta)$. Since outside of the vortex core the solution of $F(\eta)$ is known, namely $F(\eta)=-J_0(k\eta/\kappa)$, (see Eq. (2.69)), we can set

$$F\left(\frac{1}{\kappa}\right)=-J_0\left(\frac{k\lambda}{\kappa}\right) \tag{2.89}$$

and

$$F'\left(\frac{1}{\kappa}\right)=J_1\left(\frac{k\lambda}{\kappa}\right) \tag{2.90}$$

. The field of the vortex is $\Phi_0/(2\pi\lambda^2)\bar{\mathbf{b}}$, where $\bar{\mathbf{b}}$ satisfies the equation

$$\eta^2\bar{b}''(\eta) + [1-\eta^2 g(\eta)]\bar{b}'(\eta) - \eta^2 f(\eta)\bar{b}(\eta) = 0. \tag{2.91}$$

The solution to $\bar{b}$ and $\bar{b}'$ over the core must connect to the functions $K_0(\eta)$ and $-K_1(\eta)$ at $\eta = 1/\kappa$ respectively. Carrying out the angular integration in Eqs. (2.72), (2.73), and (2.74) with the substitution of F and $\bar{\mathbf{b}}$ yields

$$\Delta\mathcal{F}_1 = \frac{mc\Phi_0}{4\pi e}\Omega_0 \int_0^{1/\kappa} \eta\bar{b}(\eta)\left[J_0(k\lambda\eta) + F(\eta)\right] d\eta \tag{2.92}$$

$$\Delta\mathcal{F}_2 = -\frac{mc\Phi_0}{4\pi e\kappa}\frac{\Omega_0 k\lambda}{1+k^2\lambda^2}\bar{b}(1/\kappa)J_0(k\lambda/\kappa) \tag{2.93}$$

$$\Delta\mathcal{F}_3 = \frac{mc\Phi_0}{4\pi e}\Omega_0 \int_0^{1/\kappa} \eta\,\bar{b}'(\eta)\coth^2(\nu\kappa x)F'(\eta). \tag{2.94}$$

Finally, the interaction energy reads

$$\Delta\mathcal{F} = \frac{\Phi_0 mc}{2\pi e}\Omega_0\left[P_1(k\lambda,\kappa) + P_3(k\lambda,\kappa) - \frac{k\lambda}{1+(k\lambda)^2}K_0\left(\frac{1}{\kappa}\right)J_0\left(\frac{k\lambda}{\kappa}\right)\right], \tag{2.95}$$

in which

$$P_1(k\lambda,\kappa) = \int_0^{1/\kappa} x\bar{b}(x)\left[J_0(k\lambda x) + F(\eta)\right] dx, \tag{2.96}$$

and

$$P_3(k\lambda,\kappa) = \int_0^{1/\kappa} \eta\coth^2(\nu\kappa\eta)\bar{b}'(\eta)F'(\eta)d\eta. \tag{2.97}$$

We now compute the vortex energy expressed in Eq. (2.71) with $\mathbf{B}_M = 0$. Integration by parts yields a simplified expression of the form

$$\Delta E = \frac{1}{8\pi}\int_c d^3r\left[\mathbf{B}_v^2 + \frac{\lambda^2}{f(r)}(\nabla\times\mathbf{B}_v)^2\right] + \frac{\lambda^2}{8\pi}\oint[\mathbf{B_v}\times(\nabla\times\mathbf{B}_v)]\cdot d\mathbf{s} - \frac{1}{4\pi}\int dr^3\mathbf{H}\cdot\mathbf{B}_v, \tag{2.98}$$

or by replacing B_v with $\Phi_0/(2\pi\lambda^2)\bar{\mathbf{b}}(x)$ one obtains

$$\Delta E = \left(\frac{\Phi_0}{4\pi\lambda^2}\right)^2\left[G(\kappa) + K_0(1/\kappa)K_1(1/\kappa)/\kappa\right] - \frac{\Phi_0 H}{4\pi}, \tag{2.99}$$

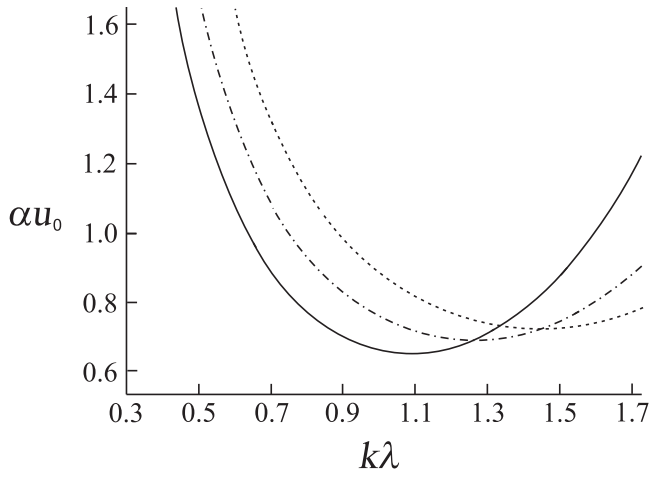

Figure 2.8: Plot of αu_0 versus $k\lambda$, where $\alpha = 4mv/(\hbar\epsilon)$. For $v \sim 2 \times 10^5$cm/s and $\epsilon = 0.05$, $\alpha = 1.6 \times 10^9$. In ascending order the three minima correspond to $\kappa = 0.8$, $\kappa = 0.9$, and $\kappa = 1$.

where

$$G(\kappa) = \int_0^{1/\kappa} x[\bar{b}^2(x) + \coth^2(\nu\kappa x)\bar{b}'^2(x)]dx. \tag{2.100}$$

As before the vortex energy ΔE can be written in terms of the first critical field

$$H_{c1} = \frac{\Phi_0}{4\pi\lambda^2}[G(\kappa) + K_0(1/\kappa)K_1(1/\kappa)/\kappa] \tag{2.101}$$

simply as

$$\Delta E = \frac{\Phi_0}{4\pi} H_{c1}\epsilon. \tag{2.102}$$

The critical amplitude of the sound u_0 at which a vortex will nucleate becomes

$$u_0 = \frac{\hbar\epsilon}{4mv}\left(\frac{1}{k\lambda}\right)^2 S(k\lambda, \kappa), \tag{2.103}$$

where

$$S(k\lambda, \kappa) = \frac{G(\kappa) + K_0(1/\kappa)K_1(1/\kappa)/\kappa}{P_1(k\lambda, \kappa) + P_3(k\lambda, \kappa) - k\lambda[1 + (k\lambda)^2]^{-1}K_0(1/\kappa)J_0(k\lambda/\kappa)}. \tag{2.104}$$

Fig. 2.8 shows a plot of αu_0 versus $k\lambda$ at $\epsilon = 0.05$, where $\alpha = 4mv/(\hbar\epsilon)$. This graph shows that, at $\kappa = 1$, for $k\lambda = 1$ corresponding to the frequency $f \sim 2$GHz the

amplitude of sound that is required to nucleate a vortex is ~ 0.5nm. These values confirm the prediction of Eq. (2.83).

2.5 Conclusion of Part I

We presented a brief summary of works that analyze the consequences of elastic deformations in superconductors and proposed two new effects both of which are experimentally feasible. We have seen that dynamical elastic deformations can have dramatic effects on the electronic state of superconductors. We showed that the flux lattice can be driven by an external current below the critical value J_c with the help of moving screw dislocations. Since external stresses exert forces on dislocations and hence set them into motion, one can say that the voltage which the moving flux produces can be attributed to these external stresses. This *piezoelectric effect* can serve as a warning mechanism of stress loads that can cause material fractures. Although, our calculations were based on linear elasticity, which limits the dislocation velocity to the speed of sound, it is reasonable to assume that the predicted effect should be present when nonlinearity and non-locality are taken into account. Then, we argued, based on adiabatic approximation, that ultrasound in a superconducting slab can generate vortices when the external magnetic field is below the critical field H_{c1}. The vortices enter and exit the superconductor at half the frequency of the ultrasound which manifests as an AC voltage across the sample. Our numerical results demonstrated that the analytical result which was based on low frequency and small κ approximations gives the correct order of magnitude for the critical amplitude and frequency of the ultrasound. A simpler version of this scenario can be done by exciting surface acoustic waves. This would have practical advantages as

the amplitude of surface waves can be as large as several nanometers while reducing the problem of sample heating. The problem of heating is especially important since according to our findings only superconductors with small κ experience the above described effect. Therefore, in order to preserve locality one must work near the critical temperature and be aware of temperature changes due to sample heating.

Part II

Decoherence of Two-state Systems

Chapter 3

Relaxation of two-state systems due to phonons

3.1 Quantum decoherence

Any quantum mechanical system is constantly in contact with the environment that surrounds it. The environment itself, however, is also governed by the laws of quantum mechanics and should be described by the Schrödinger's equation. The difficulty with this picture, while fundamentally correct, is that one cannot impose bounds on the environment. For instance, if we define the environment as molecules of air contained in a box we must consider the interaction of the box with its environment which in turn interacts with its environment, and so on. This is sometimes called *infinite regression*. For this reason, in order to get an accurate picture of any quantum state we would have to solve the Schrödinger's equation for the entire universe. While philosophically intriguing, this approach bears no usefulness in practice. Fortunately, our everyday experience provides a clue to this apparently impossible problem. Why is it that we never see macroscopic objects in superposition of quantum states? For some time it was believed that quantum mechanics does not apply to macroscopic systems and therefore the strange quantum effects do not interfere with everyday life. The famous

Schrödinger's cat thought experiment was devised by Schrödinger to illustrate the absurdity that would have to follow if quantum effects invaded the macroscopic realm. Nowadays, however, as more macroscopic objects are being prepared in superposition states it is becoming convincingly clear that quantum mechanics does apply on all scales. The best known example is the superposition state of the SQUID (Quantum Superposition Interference Device) whose size can be of the order of micrometers. At this point a case can be made that quantum mechanics does not discriminate against the macroscopic. The actual reason we do not see quantum behavior in everyday life is because of decoherence. Decoherence is a process by which the relative amplitudes and phases of a superposition state are altered over some characteristic times τ_1 and τ_2. The latter is known as the relaxation time. This behavior is observed whenever the system of interest is much smaller than the environment in which it is embedded. This implies that the environment can be simply defined as a heat bath (classical or quantum), conforming to the laws of thermodynamics. It should be emphasized, however, that even at zero temperature decoherence of a small quantum system is still present due to fluctuations of the electromagnetic vacuum or, in the case of solid bodies, the zero point oscillations. Thus, every system that is at some point in a superposition state will decay into the ground state in some relaxation time.

In applications, decoherence presents serious problems for devices that rely on the superposition state, i. e., the quantum computer. Although the principles of the quantum computer are entirely different from the conventional one, both machines require bits - components that can perform computations. In the case of quantum computers these bits are called quantum bits or qubits. One important class of systems that can be used as qubits are two-state systems that arise from tunneling

between two degenerate eigenstates, i. e. a particle in a double-well potential, magnetic particle in molecular nanomagnets, etc. In the following sections we will study the relaxation time of two specific systems - particle in a double-well potential and a SQUID embedded in a solid.

3.2 Relaxation of a particle in a double-well potential

Relaxation and decoherence in a two-state system coupled to environment is a fundamental problem of quantum physics. It was intensively studied in the past; see, e.g., the review of Leggett *et al.* [63]. In the last years the interest to this problem has been revived by the effort to build solid state qubits. Recently, symmetry implications have been considered for the problem of a particle in a rigid double-well potential embedded in a solid [64]. It was demonstrated that symmetry arguments allow one to obtain parameter-free lower bound on the relaxation of quantum oscillations in a rigid double well, caused by the elastic environment. One of the arguments is that the double-well potential formed by the local arrangement of atoms in a solid is defined in the coordinate frame of that local atomic environment, not in the laboratory frame. Another argument is that interactions of the tunneling variable with phonons must be invariant with respect to global translations and rotations. When these arguments were taken into account, a simple universal result for the relaxation rate was obtained [64] in terms of measurable constants of the solid, with no unknown interaction constants.

The above mentioned universal result refers to the low temperature limit when the relaxation of a two state system is dominated by the decay of the excited state due to

the emission of one phonon. In this section we extend the method developed in Ref. [64] to the study of direct and Raman two-phonon processes in double-well structures [65, 66, 67, 68, 69, 70]. Such processes can dominate relaxation at higher temperatures [71, 72, 73]. We will show [74, 75] that in the temperature range bounded by the level splitting from below and by the Debye temperature from above, the two-phonon rates for a biased rigid double well is given by a universal expression, very much like the rate of the direct one-phonon process. Both the Raman and the direct rate is proportional to the seventh power of temperature, while the one-phonon rate is linear on temperature. Interestingly, however, at small bias, the Raman rate, unlike the one-phonon rate, is proportional to the square of the bias. Consequently two-phonon processes can be switched on and off by controlling the bias. This universal result, which is a consequence of the parity of quantum states, must have important implications for solid-state qubits at elevated temperatures. Indeed, for an electron in a quantum dot, the rate of a direct one-phonon process is usually small. If the rate of a two-phonon process can be made small as well, this means that one can eliminate phonons as a significant source of relaxation and decoherence of the electron states in solid-state qubits.

3.2.1 The double well as a two state system

The problem of a particle in a double-well potential is almost as old as quantum mechanics. Although, attempts to obtain a nearly exact solution have been carried out, for most practical purposes it suffices to treat the problem in the two-state model. A particle in a double-well potential can tunnel between the two wells which creates a splitting in the ground state energy that is proportional to the overlap of the wavefunctions localized around the potential minima of the left and the right wells.

For large energy barriers, the overlap and hence the energy splitting is much smaller than the energy difference between the ground and the first excited states of each separate well. For this reason, the double-well potential is to a good approximation a two-state system.

Let's consider the above argument in a greater detail. If the two wells are separated by a large distance the particle which is initially placed in say, the left well, does not feel the second well. When the two wells are brought to closer proximity the particle's wavefunction penetrates the barrier without significantly changing its shape. Equivalently, we might place the particle in the right well and expect the same outcome. Therefore, the total wavefunction $|\psi\rangle$ must be a superposition of the eigenstates $|\varphi_1\rangle$ and $|\varphi_2\rangle$ corresponding to the left and the right potential wells respectively:

$$|\psi\rangle = c_1|\varphi_1\rangle + c_2|\varphi_2\rangle, \tag{3.1}$$

such that $|c_1|^2 + |c_2|^2 = 1$, $\langle\varphi_1|\varphi_1\rangle = \langle\varphi_2|\varphi_2\rangle = 1$ and $\langle\varphi_1|\varphi_2\rangle = \langle\varphi_2|\varphi_1\rangle = 0$. The Schrödinger's equation then reads

$$i\hbar \begin{pmatrix} \dot{c}_1|\varphi_1\rangle \\ \dot{c}_2|\varphi_2\rangle \end{pmatrix} = \mathcal{H} \begin{pmatrix} c_1|\varphi_1\rangle \\ c_2|\varphi_2\rangle \end{pmatrix}. \tag{3.2}$$

Multiplying both sides by $\langle\varphi_1|$ and $\langle\varphi_2|$ yields

$$\begin{aligned} i\hbar\dot{c}_1 &= E_1 c_1 + \frac{1}{2}\Delta_0 c_2 \\ i\hbar\dot{c}_2 &= E_2 c_2 + \frac{1}{2}\Delta_0 c_1, \end{aligned} \tag{3.3}$$

where E_1 and E_2 are the ground state energies of the left and the right wells respectively and $\Delta_0 = 2\langle\varphi_1|\mathcal{H}|\varphi_2\rangle$. The factor of 2 was inserted for convenience. Although, the energies E_1 and E_2 are the same for a symmetric potential one can make a generalization by introducing a bias ϵ, so that the minimum of one well is shifted with

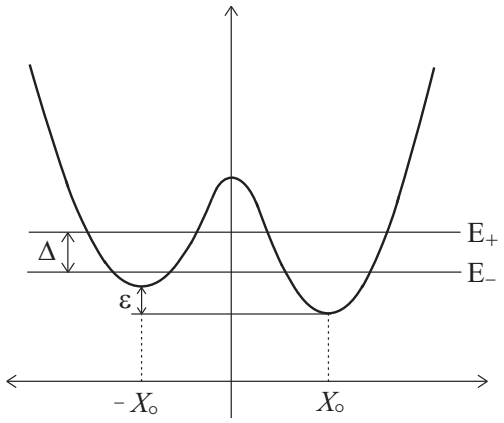

Figure 3.1: A double-well well potential with a bias. The ground state energy of the individual wells become separated by the energy splitting Δ due to tunneling.

respect to the other. If the bias is small compared to Δ_0 our arguments stated above must still hold. The Hamiltonian can than be written as

$$\mathcal{H} = \begin{pmatrix} E_0 + \frac{\epsilon}{2} & \frac{\Delta_0}{2} \\ \frac{\Delta_0}{2} & E_0 - \frac{\epsilon}{2} \end{pmatrix} \tag{3.4}$$

where E_0 is the ground state of the particle located in either one of the wells at zero bias. The eigenvectors that diagonalize this Hamiltonian are

$$\begin{aligned} |\psi_-\rangle &= \frac{1}{\sqrt{2}}(c_1|\varphi_1\rangle + c_2|\varphi_2\rangle) \\ |\psi_+\rangle &= \frac{1}{\sqrt{2}}(c_2|\varphi_1\rangle - c_1|\varphi_2\rangle) \end{aligned} \tag{3.5}$$

with the coefficients

$$c_1 = \sqrt{1 - \varepsilon/\Delta} \qquad c_2 = \sqrt{1 + \varepsilon/\Delta} \qquad \Delta = \sqrt{\Delta_0^2 + \varepsilon^2}. \tag{3.6}$$

The first two eigenenergies are

$$E_g = E_0 + \frac{1}{2}\sqrt{\epsilon^2 + \Delta^2} \qquad E_e = E_0 - \frac{1}{2}\sqrt{\epsilon^2 + \Delta^2}. \tag{3.7}$$

We can solve for the states that correspond to the particle being in the left and the

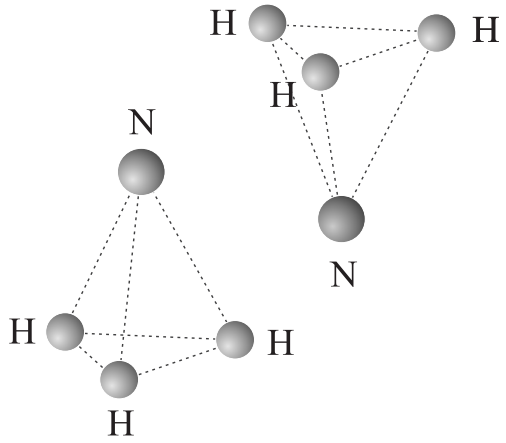

Figure 3.2: Ammonia molecule is an example of a double-well system. Here the Hydrogen plain tunnels across the Nitrogen atom.

right wells form Eq. (3.5):

$$|\varphi_1\rangle = \frac{1}{\sqrt{2}}[c_1|\psi_-\rangle + c_2|\psi_+\rangle]$$
$$|\psi_2\rangle = \frac{1}{\sqrt{2}}[c_2|\psi_-\rangle - c_1|\psi_+\rangle] \tag{3.8}$$

Applying the time evolution operator $e^{-i\mathcal{H}t/\hbar}$ to $|\varphi_1\rangle$ yields

$$|\varphi_1(t)\rangle = \frac{e^{-iE_-t/\hbar}}{\sqrt{2}}[c_1|\psi_-\rangle + c_2e^{-i\Delta t/\hbar}|\psi_+\rangle]. \tag{3.9}$$

For a symmetric double well ($\varepsilon = 0$), the particle initially in the state $|\varphi_1\rangle$ will tunnel after the time $t = \pi\hbar/\Delta$ to the state $|\varphi_2\rangle$ and vise versa. The tunneling will occur with frequency $f = \Delta/h$.

A well-known example of a two-state system is the ammonia molecule. Fig. 3.2 shows the structure of the ammonia molecule with two possible orientations. The letters H and N stand for hydrogen and nitrogen respectively. The two possible orientations have the same energy corresponding to the two minima of the potential. If the wavefunctions of the nitrogen atom at the top position and the one below the hydrogen plane overlap, a coherent tunneling between the two states will occur.

Because the mass of hydrogen is much smaller than that of nitrogen, the hydrogen plane will oscillate in free space around the center of mass situated close to the nitrogen atom. If, however, the ammonia molecule were placed inside a solid and coupled to the crystal matrix, the environment would inevitably co-wiggle with the oscillating molecule and consequently radiate phonons. It has been argued by some that in the scenario just described the entire solid would co-wiggle with the molecule as in the case of Mössbauer effect [76] in which case no phonons would be excited. This proposal can be easily refuted by the following argument. The frequency of tunneling can be of order $f \sim 10^9 \mathrm{s}^{-1}$. Let us take our sample size L to be $\sim$ 1cm and the speed of sound $v_s \sim 10^5 \mathrm{cm/s}$. In the time 10^9s the information that the ammonia molecule has tunneled travels a distance $10^9 v_s \sim 10^{-4}$cm. By the time this information reaches the surface the molecule would have tunneled about $10,000$ times.

3.2.2 Coupling of the particle to phonons

The problem of coupling a quantum system to the crystal matrix is an old and complex one. The difficulty stems from the complicated behavior of the atoms in a crystal. Although, the use of phonons as collective excitations of the crystal lattice present a tremendous simplification the question still remains as to how the phonons interact with the system of interest. A well-known approach is to consider a charged particle, i. e. electron, in a double-well potential embedded in a piezoelectric material. In substance, the longitudinal phonons expand and contract the local environment which in turn induces electric fields that interact with the charged particle. The downside of this approach, however, is that it only works in specific materials. Another approach that has been introduced in the past is to write down the most general form of the

interaction Hamiltonian of the form

$$\mathcal{H}_{int} = b_{ij}x_i u_j + c_{ijk}x_i u_j u_k + \dots , \tag{3.10}$$

with b_{ji} and c_{ijk} being some unknown interaction tensors to be determined from experiment. One obvious disadvantage of this approach is that one cannot obtain theoretical results from this Hamiltonian that can be compared to experiments. More importantly however, Eq. (3.10) is not translationally invariant. This fact can be easily seen by adding an arbitrary vector $\mathbf{a}$ to $\mathbf{u}$. Equivalently, one can view this as translating our coordinate system by $-\mathbf{a}$ which must preserve any Hamiltonian. Clearly, Eq. (3.10) violates this necessary condition. We now present a new approach already mentioned in the previous section which takes into account the translational and rotational symmetries in the limit of long-wave phonons.

In the absence of phonons, the Hamiltonian in the laboratory frame is

$$\mathcal{H}_o = \frac{\mathbf{p}^2}{2m} + V(\mathbf{r}) , \tag{3.11}$$

where $\mathbf{r}$ is the radius vector in the laboratory frame, $\mathbf{p}$ is the momentum, and m is the mass of the particle (e.g. electron). A rigid double well at the position $\mathbf{R}$ will be translated in space by a long-wave phonon described by the displacement field $\mathbf{u}(\mathbf{R})$. The Hamiltonian of the system (including the free phonon field) in the laboratory frame can simply be written as

$$\mathcal{H} = \frac{\mathbf{p}^2}{2m} + V(\mathbf{r} - \mathbf{u}) + \mathcal{H}_{ph} \ . \tag{3.12}$$

Here, $\mathcal{H}_{ph}$ is the Hamiltonian of the free phonon field. Clearly, this form of Hamiltonian preserves the translational symmetry. We intend to obtain a Hamiltonian of the form $\mathcal{H} = \mathcal{H}_o + \mathcal{H}_{ph} + \mathcal{H}_{e-ph}$ where the last term describes the interaction of phonons

with the electron in the double well potential. Using the fact that $\mathbf{u}$ is small, one can expand $V(\mathbf{r}-\mathbf{u})$ in Taylor series to obtain

$$\mathcal{H} = \frac{\mathbf{p}^2}{2m} + V(\mathbf{r}) + \mathcal{H}_{ph} - \frac{\partial V}{\partial r_i}u_i + \frac{1}{2!}\frac{\partial^2 V}{\partial r_i \partial r_j}u_i u_j \ + \ldots \tag{3.13}$$

The first three terms form the interaction-free part of the total Hamiltonian. The rest of the terms containing powers of $\mathbf{u}$ comprise the electron phonon interaction. It is clear that Eq. (3.13) requires detailed knowledge of the potential and its derivatives. One can, however, obtain Eq. (3.12) by performing a unitary transformation on Eq. (3.11) with the help of translation operator $\mathcal{R}= e^{i\mathbf{p}\cdot\mathbf{u}}$, so that

$$\mathcal{H} = e^{-i\mathbf{p}\cdot\mathbf{u}}\ \mathcal{H}_o e^{i\mathbf{p}\cdot\mathbf{u}} + \mathcal{H}_{ph}\,. \tag{3.14}$$

This can be expanded for small $\mathbf{u}$ as

$$\mathcal{H} = \mathcal{H}_o + \mathcal{H}_{ph} \ + i[\mathcal{H}_o\,, p_i]u_i + \frac{i^2}{2}[[\mathcal{H}_o\,, p_i], p_j]u_i u_j + \ldots \ . \tag{3.15}$$

Working out the commutators brings one back to Eq. (3.13). However, the use of Eq. (3.15) that we are going to employ allows one to obtain parameter-free results solely in terms of the energy levels of our effective two-state system without knowledge of the explicit form of $V(\mathbf{r})$.

We consider the case in which the particle, with good accuracy, is localized near $\mathbf{r} = \pm\mathbf{R}_o$, where $\pm\mathbf{R}_o$ are the energy minima of the left or right wells. Without loss of generality we assume that $\pm\mathbf{R}_o = \pm X_o\mathbf{e}_x$. The localization length of the state inside each well is small compared to the distance between the minima of the double-well potential. The bare ground states (when tunneling is neglected) in the left and right wells, that we denote by $|\pm X_o\rangle$, are approximately orthonormal,

$$\langle \pm X_o|\pm X_o\rangle = 1\,, \quad \langle -X_o|X_o\rangle = 0\,. \tag{3.16}$$

As we already discussed in the previous section, the tunneling between the wells leads to the hybridization of the states described by orthonormal wave functions given in Eq. (3.5). Note that the double well also has states, $|\psi_\xi\rangle$, with energies, E_ξ, other then $E_\pm$ corresponding to $|\psi_\pm\rangle$. The energy splitting $\Delta = E_+ - E_-$ is considered small compared to the distance from $E_\pm$ to other E_ξ. As we shall see, in this limit the summation over all states $|\psi_\xi\rangle$ renders result for phonon-induced transitions between $|\psi_\pm\rangle$ that is insensitive to the explicit form of the potential.

Below we shall deal with the matrix elements of operators $p \equiv p_x$, x, and their combinations. Other components of $\mathbf{p}$ and $\mathbf{r}$ are irrelevant. Localization of $|\psi_\pm\rangle$ allows one to compute matrix elements of powers of the operator x with the help of the relation

$$x|\pm X_o\rangle = \pm X_o|\pm X_o\rangle\,. \tag{3.17}$$

This gives

$$\langle\psi_\pm|x|\psi_\pm\rangle = X_o\frac{1}{2}(C_+^2 - C_-^2) = X_o(\varepsilon/\Delta) \tag{3.18}$$

$$\langle\psi_-|x|\psi_+\rangle = X_o C_+ C_- = X_o(\Delta_o\Delta) \tag{3.19}$$

To compute other matrix elements we shall use relations

$$p = m\dot{x} = -im[x, \mathcal{H}_o] \tag{3.20}$$

and

$$px + xp = m(\dot{x}x + x\dot{x}) = m\frac{dx^2}{dt} = -im[x^2, \mathcal{H}_o]\,. \tag{3.21}$$

This gives

$$\langle\psi_\xi|p|\psi_{\xi'}\rangle = im(E_\xi - E_{\xi'})\langle\psi_\xi|x|\psi_{\xi'}\rangle \tag{3.22}$$

$$\langle\psi_\xi|p\,x + xp|\psi_{\xi'}\rangle = im(E_\xi - E_{\xi'})\langle\psi_\xi|x^2|\psi_{\xi'}\rangle \tag{3.23}$$

and thus, $\langle\psi_-|px|\psi_+\rangle = 0$.

As we shall see, perturbation theory for Raman processes requires computation of the sum

$$\Sigma = \sum_{\xi\neq+} \frac{\langle\psi_-|p|\psi_\xi\rangle\langle\psi_\xi|p|\psi_+\rangle}{E_\xi - E_+}\,. \tag{3.24}$$

Application of Eq. (3.20) eliminates the denominator and yields

$$\Sigma = im\sum_{\xi\neq+}\langle\psi_-|p|\psi_\xi\rangle\langle\psi_\xi|x|\psi_+\rangle\,. \tag{3.25}$$

Using the completeness of $|\psi_\xi\rangle$ we obtain

$$\Sigma = im[\langle\psi_-|px|\psi_+\rangle - \langle\psi_-|p|\psi_+\rangle\langle\psi_+|x|\psi_+\rangle]\,. \tag{3.26}$$

Finally, with the help of the above relations for matrix elements of x, p, and px we get

$$\Sigma = -m^2X_o^2(\Delta_o/\Delta)\varepsilon\,. \tag{3.27}$$

This is a mechanism of elimination of unspecified energy levels E_ξ from the problem, leading to a universal result.

3.2.3 Matrix elements - Raman process

In this section we compute the relaxation rates for two kinds of two-phonon processes - the Raman process involving a scattering of a phonon with the particle and a direct process via emission of two phonons.

We are interested in the transition rate between the eigenstates of $\mathcal{H}_o + \mathcal{H}_{ph}$

$$|\Psi_\pm\rangle = |\psi_\pm\rangle \otimes |\phi_\pm\rangle\,. \tag{3.28}$$

Here, $|\psi_\pm\rangle$ are the tunnel split states of the double well given by Eq. (3.5). The states $|\phi_+\rangle = |n_\mathbf{k}, n_\mathbf{q}\rangle$ and $|\phi_-\rangle = |n_\mathbf{k} - 1, n_\mathbf{q} + 1\rangle$ are the eigenstates of $\mathcal{H}_{ph}$ with

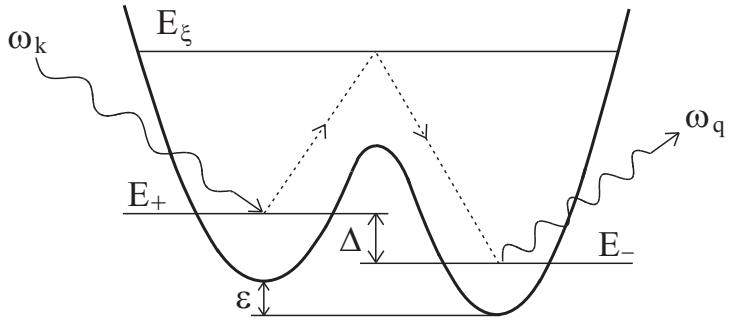

Figure 3.3: Raman process on tunnel-split levels in a double-well potential, including virtual transitions to higher levels E_ξ [the first term in Eq. (3.33) shown

energies $E_{ph,\pm}$ that correspond to phonon states before and after particle transition between $E_\pm$ states in the double well. Raman process involves absorption of a phonon of frequency $\omega_{\mathbf{k}}$ and emission of a phonon of frequency $\omega_{\mathbf{q}} = \omega_{\mathbf{k}} + \Delta$, accompanied by the transition of the particle $|\psi_+\rangle \to |\psi_-\rangle$, see Fig. 3.3. The Raman rate can be computed with the help of the Fermi golden rule in the second order in the interaction. The matrix element for this process is the sum of two matrix elements,

$$M_R = M_R^{(2)} + M_R^{(1+1)}. \tag{3.29}$$

The first term denotes the first order perturbation on

$$\mathcal{H}_{e-ph}^{(2)} = -\frac{1}{2}\,[[\mathcal{H}_o, p], p]u_x^2, \tag{3.30}$$

while the second term stands for the second order perturbation on

$$\mathcal{H}_{e-ph}^{(1)} = i[\mathcal{H}_o, p]u_x. \tag{3.31}$$

The explicit expressions for $M^{(2)}$ and $M^{(1+1)}$ are [77]

$$M_R^{(2)} = \langle\Psi_-|\,\mathcal{H}_{e-ph}^{(2)}\,|\Psi_+\rangle \tag{3.32}$$

and

$$M_R^{(1+1)} = \sum_\xi \frac{\langle\Psi_-|\,\mathcal{H}^{(1)}_{e-ph}\,|\Psi_\xi\rangle\,\langle\Psi_\xi|\,\mathcal{H}^{(1)}_{e-ph}\,|\Psi_+\rangle}{E_+ + \hbar\omega_{\mathbf{k}} - E_\xi} + \sum_\xi \frac{\langle\Psi_-|\,\mathcal{H}^{(1)}_{e-ph}\,|\Psi_\xi\rangle\,\langle\Psi_\xi|\,\mathcal{H}^{(1)}_{e-ph}\,|\Psi_+\rangle}{E_+ - \hbar\omega_{\mathbf{q}} - E_\xi}. \tag{3.33}$$

Here, $|\Psi_\xi\rangle$ is a direct product of the eigenstates of $\mathcal{H}_o$ with the phonon states $|n_{\mathbf{k}}-1, n_{\mathbf{q}}\rangle$ in the first term and $|n_{\mathbf{k}}, n_{\mathbf{q}}+1\rangle$ in the second term.

First, we calculate the phonon parts of $M^{(2)}$ and $M^{(1+1)}$ using canonical quantization of the phonon displacements [3]

$$\mathbf{u} = \sqrt{\frac{1}{2\rho V}} \sum_{\mathbf{k}\lambda} \frac{\mathbf{e}_{\mathbf{k}\lambda} e^{i\mathbf{k}\cdot\mathbf{r}}}{\sqrt{\omega_{\mathbf{k}\lambda}}} \left(a_{\mathbf{k}\lambda} + a^\dagger_{-\mathbf{k},\lambda}\right), \tag{3.34}$$

where ρ is the density of the solid, V is its volume, $\mathbf{e}_{\mathbf{k}\lambda}$ are unit polarization vectors, $\lambda = t_1, t_2, l$ denotes polarizations, and $\omega_{\mathbf{k}\lambda} = \upsilon_\lambda k$ is the phonon frequency. For brevity we will drop the polarization index. Writing $|\Psi_-\rangle = |n_{\mathbf{k}}-1, n_{\mathbf{q}}+1\rangle \otimes |\psi_-\rangle$ and $|\Psi_+\rangle = |n_{\mathbf{k}}, n_{\mathbf{q}}\rangle \otimes |\psi_+\rangle$, for the phonon matrix element in $M^{(2)}$ one obtains

$$\langle n_{\mathbf{k}}-1, n_{\mathbf{q}}+1|\,u_x^2\,|n_{\mathbf{k}}, n_{\mathbf{q}}\rangle \tag{3.35}$$

$$= \frac{1}{\rho V} e^x_{\mathbf{k}\lambda} e^x_{\mathbf{q}\epsilon} e^{i(\mathbf{k}-\mathbf{q})\cdot\mathbf{r}} \sqrt{\frac{n_{\mathbf{k}}(n_{\mathbf{q}}+1)}{\omega_{\mathbf{k}}\omega_{\mathbf{q}}}} \equiv M^R_{ph}. \tag{3.36}$$

For the phonon matrix elements in $M_R^{(1+1)}$ one obtains

$$\langle n_{\mathbf{k}}-1, n_{\mathbf{q}}+1|\,u_x\,|n_{\mathbf{k}}-1, n_{\mathbf{q}}\rangle\,\langle n_{\mathbf{k}}-1, n_{\mathbf{q}}|\,u_x\,|n_{\mathbf{k}}, n_{\mathbf{q}}\rangle \tag{3.37}$$

$$= \langle n_{\mathbf{k}}-1, n_{\mathbf{q}}+1|\,u_x\,|n_{\mathbf{k}}, n_{\mathbf{q}}+1\rangle\,\langle n_{\mathbf{k}}, n_{\mathbf{q}}+1|\,u_x\,|n_{\mathbf{k}}, n_{\mathbf{q}}\rangle \tag{3.38}$$

$$= M^R_{ph}/2, \tag{3.39}$$

(One can see from the completeness relation that the sum of these two expressions is M^R_{ph}.)

Next, we evaluate the particle parts of $M_R^{(2)}$ and $M_R^{(1+1)}$. For $\langle\psi_-|\,[[\mathcal{H}_o\,p],p]\,|\psi_+\rangle$ that enters $M^{(2)}$, writing the commutator explicitly and inserting the identity operator $\mathbb{I}=\sum_\xi |\psi_\xi\rangle\langle\psi_\xi|$ results in

$$\langle\psi_-|\,(\mathcal{H}_o p^2 - 2p\mathcal{H}_o p + p^2\mathcal{H}_o\,)\,|\psi_+\rangle \tag{3.40}$$

$$= \sum_\xi (E_+ + E_- - 2E_\xi)\,\langle\psi_-|\,p\,|\psi_\xi\rangle\,\langle\psi_\xi|\,p\,|\psi_+\rangle\,. \tag{3.41}$$

The particle part of $M^{(1+1)}$ simplifies to

$$-\langle\psi_-|\,[\mathcal{H}_o,p]\,|\psi_\xi\rangle\,\langle\psi_\xi|\,[\mathcal{H}_o,p]\,|\psi_+\rangle \tag{3.42}$$

$$= (E_\xi - E_-)(E_\xi - E_+)\,\langle\psi_-|\,p\,|\psi_\xi\rangle\,\langle\psi_\xi|\,p\,|\psi_+\rangle\,. \tag{3.43}$$

Collecting the terms, for M of Eq. (3.29) one obtains

$$M_R = \frac{1}{2}M_{ph}^R \sum_\xi \langle\psi_-|\,p\,|\psi_\xi\rangle\,\langle\psi_\xi|\,p\,|\psi_+\rangle\,Q_\xi, \tag{3.44}$$

where

$$Q_\xi \equiv E_+ + E_- - 2E_\xi + (E_\xi - E_-)(E_\xi - E_+) \tag{3.45}$$

$$\times\left[\frac{1}{E_\xi - E_+ - \omega_{\mathbf{k}}} + \frac{1}{E_\xi - E_+ + \omega_{\mathbf{q}}}\right]. \tag{3.46}$$

A common mistake that propagates through literature [78] is summation of rates due to $M_R^{(2)}$ and $M_R^{(1+1)}$, instead of adding matrix elements first and then squaring the result and computing the rate. This mistake is not innocent since $M_R^{(2)}$ and $M_R^{(1+1)}$ may cancel leading parts of each other. Taking into account conservation of energy $\omega_{\mathbf{q}} = \omega_{\mathbf{k}} + \Delta$ and the relation $E_- = E_+ - \Delta$, one can rewrite this expression as

$$Q_\xi = \frac{2\omega_{\mathbf{k}}(\omega_{\mathbf{k}} + \Delta)(E_\xi - E_+ + \Delta/2)}{(E_\xi - E_+ - \omega_{\mathbf{k}})(E_\xi - E_+ + \omega_{\mathbf{k}} + \Delta)}. \tag{3.47}$$

One has $Q_\pm = \mp\Delta$. We consider the case of $\omega_{\mathbf{k}} \sim T \ll E_\xi - E_+$ and $\Delta \ll E_\xi - E_+$, when

$$Q_\xi \cong \tilde{Q}_\xi \equiv \frac{2\omega_{\mathbf{k}}(\omega_{\mathbf{k}} + \Delta)}{E_\xi - E_+}. \tag{3.48}$$

It follows from Eq. (3.23) that the terms with $\xi = \pm$ in Eq. (3.44) disappear. Using Eq. (3.24), one obtains

$$M_R = \frac{1}{2} M_{ph}^R \sum_{\xi \neq +} \langle \psi_- | \, p \, | \psi_\xi \rangle \langle \psi_\xi | \, p \, | \psi_+ \rangle \, \tilde{Q}_\xi = M_{ph} \omega_{\mathbf{k}} (\omega_{\mathbf{k}} + \Delta) \Sigma \tag{3.49}$$

and finally, with the help of Eqs. (3.36) and (3.27),

$$M_R = -\frac{1}{\rho V} e^x_{\mathbf{k}\lambda} e^x_{\mathbf{q}\epsilon} \sqrt{\frac{n_{\mathbf{k}}(n_{\mathbf{q}} + 1)}{\omega_{\mathbf{k}} \omega_{\mathbf{q}}}} m^2 X_o^2 \varepsilon \frac{\Delta_o}{\Delta} \omega_{\mathbf{k}} \left(\omega_{\mathbf{k}} + \Delta \right). \tag{3.50}$$

Here we have suppressed an irrelevant phase factor. This result for the Raman matrix element is insensitive to the explicit form of the double-well potential $V(x)$. It would be a hopeless task to obtain it from Eq. (3.13).

3.2.4 Matrix elements - direct two-phonon process

In this section we turn attention to the relaxation due to emission of two phonons of frequencies $\omega_{\mathbf{k}}$ and $\omega_{\mathbf{q}}$. Unlike the Raman process which requires finite number of phonons in the system the transition of the particle from excited to ground state via emission of two phonons occurs even at zero temperature - spontaneous two-phonon emission. The phonon part of Eq. (3.32) yields

$$\langle n_{\mathbf{k}} + 1, n_{\mathbf{q}} + 1 | u_x^2 | n_{\mathbf{k}}, n_{\mathbf{q}} \rangle = \frac{1}{\rho V} e^x_{\mathbf{k}\lambda} e^x_{\mathbf{q}\epsilon} \sqrt{\frac{(n_{\mathbf{k}} + 1)(n_{\mathbf{q}} + 1)}{\omega_{\mathbf{k}} \omega_{\mathbf{q}}}} \equiv M_{ph}^D \tag{3.51}$$

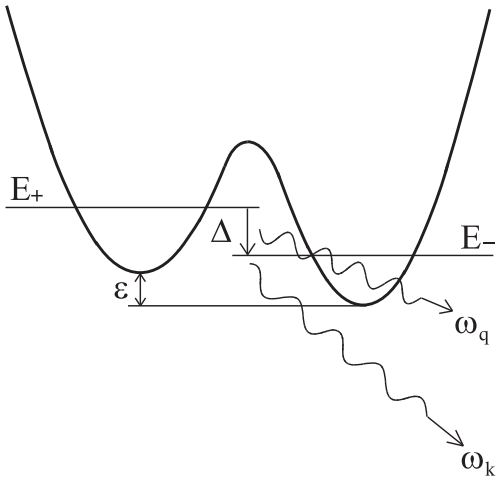

Figure 3.4: Direct process - the particle transits from the excited state to the ground state radiating two phonons of frequencies $\omega_{\mathbf{k}}$ and $\omega_{\mathbf{q}}$.

The formula for the matrix element $M_D^{(1+1)}$ becomes modified through the new relation for energy conservation $\omega_{\mathbf{k}} + \omega_{\mathbf{q}} = \Delta$:

$$M_D^{(1+1)} = \sum_{\xi} \frac{\langle \Psi_- | \mathcal{H}_{e-ph}^{(1)} | \Psi_\xi \rangle \langle \Psi_\xi | \mathcal{H}_{e-ph}^{(1)} | \Psi_+ \rangle}{E_+ - \hbar\omega_{\mathbf{k}} - E_\xi} \tag{3.52}$$

$$+ \sum_{\xi} \frac{\langle \Psi_- | \mathcal{H}_{e-ph}^{(1)} | \Psi_\xi \rangle \langle \Psi_\xi | \mathcal{H}_{e-ph}^{(1)} | \Psi_+ \rangle}{E_+ - \hbar\omega_{\mathbf{q}} - E_\xi}, \tag{3.53}$$

where $|\Psi_\xi\rangle$ corresponds to the state product $|\psi_\xi\rangle \otimes |n_{\mathbf{k}} + 1, n_{\mathbf{q}}\rangle$ in the first term and $|\psi_\xi\rangle \otimes |n_{\mathbf{k}}, n_{\mathbf{q}} + 1\rangle$ in the second. The matrix element of $M_D^{(1+1)}$ for the phonon field becomes

$$\begin{aligned} & \langle n_{\mathbf{k}} + 1, n_{\mathbf{q}} + 1 | u_x | n_{\mathbf{k}}, n_{\mathbf{q}} + 1 \rangle \langle n_{\mathbf{k}}, n_{\mathbf{q}} + 1 | u_x | n_{\mathbf{k}}, n_{\mathbf{q}} \rangle \\ = \quad & \langle n_{\mathbf{k}} + 1, n_{\mathbf{q}} + 1 | u_x | n_{\mathbf{k}} + 1, n_{\mathbf{q}} \rangle \langle n_{\mathbf{k}} + 1, n_{\mathbf{q}} | u_x | n_{\mathbf{k}}, n_{\mathbf{q}} \rangle \\ = \quad & M_{ph}^D / 2. \end{aligned} \tag{3.54}$$

The particle part of the matrix elements was worked out in the previous section. Combining $M_D^{(2)}$ and M_D^{1+1} we obtain

$$M_{ph}^D = \frac{1}{2} M_{ph}^D \sum_{\xi} \langle \psi_- | p | \psi_\xi \rangle \langle \psi_\xi | p | \psi_+ \rangle Q_\xi^D, \tag{3.55}$$

where

$$Q_\xi^D \equiv E_+ + E_- - 2E_\xi + (E_\xi - E_-)(E_\xi - E_+) \times \left[\frac{1}{E_\xi - E_+ - \omega_{\mathbf{k}}} + \frac{1}{E_\xi - E_+ - \omega_{\mathbf{q}}}\right]. \tag{3.56}$$

We can simplify this expression with the help of the energy conservation $\omega_{\mathbf{k}} + \omega_{\mathbf{q}} = \Delta$ and the relation $E_+ - E_+ = \Delta$, so that

$$Q_{ph}^D = 2\frac{\Delta(E_\xi - E_+)^2 + [\omega_{\mathbf{k}}(\Delta - \omega_{\mathbf{k}}) + \Delta^2/2](E_\xi - E_+) + \omega_{\mathbf{k}}(\Delta - \omega_{\mathbf{k}})\Delta/2}{(E_\xi - E_+ - \omega_{\mathbf{k}})(E_\xi - E_+ + \omega_{\mathbf{k}} - \Delta)}. \tag{3.57}$$

As previously mentioned we have $\Delta \ll \omega_{\mathbf{k}} \sim T \ll \omega_D$ and so,

$$Q_{ph}^D \cong 2\Delta + \frac{2\omega_{\mathbf{k}}(\Delta - \omega_{\mathbf{k}})}{E_\xi - E_+}. \tag{3.58}$$

Finally, recalling Eqs. (3.24) the total matrix element for the two-phonon direct process is

$$M^D = M_{ph}^D[\langle\psi_-|p^2|\psi_+\rangle + \omega_{\mathbf{k}}(\omega_{\mathbf{k}} - \Delta)m^2X_0^2(\Delta_0/\Delta)\varepsilon]. \tag{3.59}$$

Unlike in the case of Raman scattering we cannot obtain an analytical result for M_{ph}^D that is model independent due to the term $\langle\psi_-|p^2|\psi_+\rangle$. However, notice that the second term in Eq. (3.59) will contain a higher power of temperature than the first and will therefore dominate relaxation at elevated temperatures. At zero temperature one should expect the first term to be the leading source of two-phonon relaxation. However, this will be of no consequence since at low temperatures the one-phonon relaxation will always dominate over the higher order processes. In the next section we compute the transition rates for the Raman and the direct two-phonon processes and determine their relative importance in relaxation.

3.2.5 Transition rates

According to the Fermi golden rule [77] the Raman rate is given by (in the units where $k_B = \hbar = 1$)

$$\Gamma_2 = \sum_{\lambda\epsilon} \int \frac{d\mathbf{k}d\mathbf{q}}{(2\pi)^6} V^2 |M|^2 2\pi\delta(\omega_\mathbf{q} - \omega_\mathbf{k} - \Delta). \tag{3.60}$$

In spherical coordinates the integration variables $d\mathbf{k}d\mathbf{q} = dkdq\ k^2q^2d\Omega_\mathbf{k}d\Omega_\mathbf{q}$, and thus

$$\Gamma_2 = \frac{m^4 X_o^4 \Delta^2 \Delta_o^2 \varepsilon^2}{2\pi^3\rho^2} B^2 \int_0^{\omega_D} d\omega_\mathbf{k} d\omega_\mathbf{q} \omega_\mathbf{k}\omega_\mathbf{q} n_\mathbf{k}(n_\mathbf{q}+1) \tag{3.61}$$

$$\times \left(\frac{\omega_\mathbf{k}}{\Delta}\right)^4 \left[1 + O\left(\frac{\Delta}{\omega_\mathbf{k}}\right)\right] \delta(\omega_\mathbf{q} - \omega_\mathbf{k} - \Delta), \tag{3.62}$$

where ω_D is the Debye frequency,

$$B \equiv \int \frac{d\Omega_\mathbf{k}}{4\pi} \sum_\lambda \frac{\left(e^x_{\mathbf{k}\lambda}\right)^2}{v_\lambda^3}, \tag{3.63}$$

v_λ is the velocity of sound with polarization λ, whereas $n_\mathbf{k} = \left(e^{\omega_\mathbf{k}/T} - 1\right)^{-1}$ is the Bose occupation number of a phonon. In the limiting case of $\Delta \ll \omega_\mathbf{k} \sim T$ one obtains for the Raman rate

$$\Gamma_2 = \frac{m^4 {X_o}^4 \Delta^5 \Delta_o^2 \varepsilon^2}{2\pi^3\rho^2\hbar^{11}} B^2 \left(\frac{T}{\Delta}\right)^7 \alpha(\omega_D/T), \tag{3.64}$$

where, within the Debye model,

$$\alpha(\omega_D/T) = \int_0^{\omega_D/T} dx \frac{x^6 e^x}{(e^x-1)^2}\,. \tag{3.65}$$

At $T \lesssim \omega_D/10$, one has $\alpha \cong (16/21)\,\pi^6$.

The value of B can be calculated with the help of the transverse-phonons sum rule $\sum_{t=t_1,t_2}(\mathbf{e}_{\mathbf{k}t}\cdot\mathbf{a})(\mathbf{e}_{\mathbf{k}t}\cdot\mathbf{b}) = (\mathbf{a}\cdot\mathbf{b}) - (\mathbf{a}\cdot\hat{\mathbf{k}})(\hat{\mathbf{k}}\cdot\mathbf{b})$, where $\hat{\mathbf{k}} \equiv \mathbf{k}/k$, etc. Setting $\mathbf{a} = \mathbf{b} = \mathbf{e}_x$ and averaging over the directions of $\hat{\mathbf{k}}$ yields

$$B = \int \frac{d\Omega_\mathbf{k}}{4\pi} \left(\frac{\hat{k}_x^2}{v_l^3} + \frac{1-\hat{k}_x^2}{v_t^3}\right) = \frac{2}{3v_t^3} + \frac{1}{3v_l^3}. \tag{3.66}$$

According to theory of elasticity [48] $v_l > \sqrt{2}v_t$. Thus, the second term in this expression is a small correction and it can be neglected. Since we are interested in the region $\Delta \ll T$ we can keep only the leading order on T/Δ in Eq. (3.64). The Raman rate for $\Delta \ll T \ll \omega_D$ then becomes

$$\Gamma_2 = \frac{32\pi^3}{189}\frac{T}{\hbar}\left(\frac{\Delta_o}{\Delta}\right)^2\left(\frac{\varepsilon}{\mathcal{E}_t}\right)^2\left(\frac{T}{\mathcal{E}_t}\right)^6 , \tag{3.67}$$

where we have introduced characteristic energy and frequency scales

$$\mathcal{E}_t = \hbar\Omega_t\,, \qquad \Omega_t = \left(\frac{\hbar\rho v_t^3}{m^2 X_o^2}\right)^{1/4} \tag{3.68}$$

The Fermi golden rule for the direct two-phonon process is given by a similar integral as in Eq. (3.60)

$$\Gamma_2^D = \sum_{\lambda\epsilon}\int \frac{d\mathbf{k}d\mathbf{q}}{(2\pi)^6} V^2 |M^D_{\mathbf{kq}}|^2 2\pi\delta(\omega_{\mathbf{q}} + \omega_{\mathbf{k}} - \Delta). \tag{3.69}$$

except for the argument under the delta function which must conserve the energy according to the relation $\omega_{\mathbf{k}} + \omega_{\mathbf{q}} = \Delta$. As we mentioned earlier the first term in Eq. (3.59) will be unimportant for elevated temperatures. Employing the same simplifications that were used to calculate the Raman rate reduces Eq. (3.69) to

$$\Gamma_2^D = \frac{B^2}{4\pi^3}\frac{m^4 X_0^4 \Delta_0^2 \varepsilon^2 T^7}{\Delta^4\rho^2}\beta(\omega_D/T), \tag{3.70}$$

in which

$$\beta(\omega_D/T) = \int_0^{\omega_D/T} \frac{x^6 dx}{\cosh(x) - 1}. \tag{3.71}$$

Again we take $\Delta \ll T \ll \omega_D$ which renders the result $\beta = 32\pi^6/21$. Making the above mentioned approximation $B \approx 2/3v_t^3$ and inserting it into Eq. (3.70) gives us the final result

$$\Gamma_2^D = \frac{32\pi^3}{189}\frac{m^4 X_0^4 \Delta_0^2 \varepsilon^2 T^7}{\Delta^4\rho^2 v_t^6}. \tag{3.72}$$

If we rewrite this result in terms of the characteristic energy and frequency defined in Eq. (3.68) we discover that the Raman rate and the direct two-phonon rate are identical for elevated temperatures.

3.2.6 Double-well frame calculation

In this section we will check our result by calculating the Raman rate in the frame of reference of the double-well, as it was done for one-phonon processes in reference [64]. In the laboratory frame the Lagrangian of the particle is

$$\mathcal{L}_P = \frac{m}{2}(\dot{\mathbf{r}}' + \dot{\mathbf{u}})^2 - V(\mathbf{r}')\,, \tag{3.73}$$

where $\mathbf{r}'$ is the radius vector of the particle of mass m in the coordinate frame rigidly coupled to the double well. The linear momentum that is canonically conjugated to $\mathbf{r}'$ is given by

$$\mathbf{p}' = \frac{\partial \mathcal{L}_P}{\partial \dot{\mathbf{r}}'} = m(\dot{\mathbf{r}}' + \dot{\mathbf{u}})\,. \tag{3.74}$$

The corresponding Hamiltonian is

$$\mathcal{H}_P(\mathbf{p}', \mathbf{r}') = \mathbf{p}' \cdot \mathbf{r}' - \mathcal{L}_P = \frac{\mathbf{p}'^2}{2m} - \mathbf{p}' \cdot \dot{\mathbf{u}} + V(\mathbf{r}')\,. \tag{3.75}$$

The full Hamiltonian is $\mathcal{H}_P + \mathcal{H}_{ph}$. Contrary to the previous model described by Eq. (3.13), we now have only one interaction term, $-\mathbf{p}' \cdot \dot{\mathbf{u}}$. Similarly to Section III, one can write the matrix element for the Raman processes as

$$M_R = \sum_{\xi} \frac{\langle \psi_- | \, \mathbf{p}' \cdot \dot{\mathbf{u}} \, | \psi_\xi \rangle \langle \psi_\xi | \, \mathbf{p}' \cdot \dot{\mathbf{u}} \, | \psi_+ \rangle}{E_+ + \hbar\omega_{\mathbf{k}} - E_\xi} \tag{3.76}$$

$$+ \sum_{\xi} \frac{\langle \psi_- | \, \mathbf{p}' \cdot \dot{\mathbf{u}} \, | \psi_\xi \rangle \langle \psi_\xi | \, \mathbf{p}' \cdot \dot{\mathbf{u}} \, | \psi_+ \rangle}{E_+ - \hbar\omega_{\mathbf{q}} - E_\xi}. \tag{3.77}$$

Inserting [3]

$$\dot{\mathbf{u}} = -i\sqrt{\frac{1}{2\rho V}}\sum_{\mathbf{k}\lambda}\mathbf{e}_{\mathbf{k}\lambda}e^{i\mathbf{k}\cdot\mathbf{r}}\sqrt{\omega_{\mathbf{k}\lambda}}\left(a_{\mathbf{k}\lambda} - a^{\dagger}_{-\mathbf{k}\lambda}\right) \tag{3.78}$$

into Eq. (3.76) and evaluating the matrix elements, we obtain

$$M_R = \frac{-i}{2}M^R_{ph}\sum_{\xi}\langle\psi_-|\,p\,|\psi_\xi\rangle\,\langle\psi_\xi|\,p\,|\psi_+\rangle\,Q^R_\xi\,, \tag{3.79}$$

which coincides with Eq. (3.44) up to an insignificant phase. Same can be shown for the two-phonon process.

3.2.7 Discussion

We have demonstrated that the two-phonon relaxation of the tunnel-split states of a particle in a biased solid-state double-well potential can be expressed in terms of independently measured parameters and without any unknown constants. An interesting observation is that at a small bias the rates of Eqs. (3.67) and (3.72) are proportional to ε^2, while at a large bias it becomes independent of ε. This means that one can switch two-phonon processes on and off by controlling the bias. This result may seem strange at first, however, it is a fundamental consequence of quantum mechanics. The reason for this effect is parity. If we remove the bias, the potential well will become symmetric. Consequently, the Hamiltonian and the parity operator commute which leads to eigenstates of even or odd parity. It is easy to see that the states $|\psi_-\rangle$ and $|\psi_+\rangle$ at $\varepsilon = 0$ have even and odd parity, respectively. Therefore, the matrix elements in Eq. (3.33) will all vanish.

To find the range of parameters where two-phonon relaxation becomes important, the rate of the Raman processes should be compared with one-phonon transition rate

[64] that can be written in the form

$$\Gamma_1 = \frac{\Delta}{3\pi\hbar}\left(\frac{\Delta_o}{\mathcal{E}_t}\right)^2\left(\frac{\Delta}{\mathcal{E}_t}\right)^2 \coth\left(\frac{\Delta}{2T}\right) . \tag{3.80}$$

Notice that Eqs. (3.80) and (3.67) do not contain any unknown interaction parameters. The quantity of interest is the ratio Γ_2/Γ_1 which can tell us the importance of the second order process versus the first order process at various temperatures. In our case of $T \gg \Delta$, the $\coth(\Delta/2T)$ in Eq. (3.67) can be replaced by $2T/\Delta$. The above mentioned ratio then yields

$$\frac{\Gamma_2}{\Gamma_1} = \frac{16}{63}\pi^4\left(\frac{\varepsilon}{\Delta}\right)^2\left(\frac{\mathcal{E}_t}{\Delta}\right)^2\left(\frac{T}{\mathcal{E}_t}\right)^6 . \tag{3.81}$$

At any given temperature this ratio has a maximum at $\varepsilon = \Delta_0$. For, an electron in a double-well dot with $X_o \sim 10$ nm embedded in (or deposited on) a solid with $\rho \sim 5$ g/cm^3 and $v_t \sim 10^3$ m/s, parameter $\mathcal{E}_t$ is of order 300 K if one takes the electron effective mass, m, to be of the order of the bare mass, m_e. Then, for, e. g., $\varepsilon \sim \Delta_o \sim 1$ K, Raman processes, according to Eq. (3.81), will dominate electron-phonon relaxation above 30 K, while below that temperature the relaxation will be dominated by direct processes. The actual phonon rates for an electron are not likely to exceed 10^6 s^{-1} even at $T \sim 100$ K. Note that for $m < m_e$, which is typical in semiconductors, the rates are even smaller. For a proton in a molecular double well with $X_o \sim 0.3$ nm in a solid with $\rho \sim 5$ g/cm^3 and $v_t \sim 10^3$ m/s, one gets $\mathcal{E}_t \sim 40$ K. At $\varepsilon \sim \Delta_o \sim 1$ mK, according to Eq. (3.81), Raman processes will dominate proton-phonon relaxation above 1 K, while direct processes will dominate relaxation in the millikelvin range.

After this work was completed, we learned about a very recent paper by Stavrou and Hu [79] who also investigated two-phonon relaxation for a particle in a double dot.

Our paper and Ref. [79] bear similarities and differences. They both consider a similar system – electron in a double dot interacting with acoustic phonons. Numerical work in Ref. [79] is performed for a particular model of the double-well and is customized for GaAs elastic environment, while our approach is more general, based upon symmetry. Because of this, one cannot expect a substantial agreement between these two works. In particular, we obtain that for a spatially symmetric double well (dot) of arbitrary shape the relaxation rate is zero. The reason this is not the case in Ref. [79] is that the deformation of the dot due to the elastic environment breaks the spatial symmetry. However, the conclusions made in both works about the relative strengths of one-phonon and two-phonon processes are similar.

Finally we should note that since our model is based upon bare quantum states that are well localized in space, it is rigorous for heavy particles, like, e.g., a proton or an interstitial atom, but is less rigorous for such a light particle as an electron. Nevertheless, even for an electron our formulas should provide a good approximation in the limit of weak tunneling between the wells. Note also that at a large tunnel splitting, the actual rates for a heavy particle like proton, interstitial atom or defect, can become so large that the approximation based upon Fermi golden rule will no longer apply [80]. Even in this case, however, the matrix elements can be expressed in terms of measurable parameters of the quantum well and the solid.

3.3 Decoherence of flux qubits

3.3.1 Flux qubits as two-state systems

In 1962, Josephson [81] discovered that when a superconductor is interrupted by a thin insulating barrier the cooper pairs will flow from one side of the barrier to the

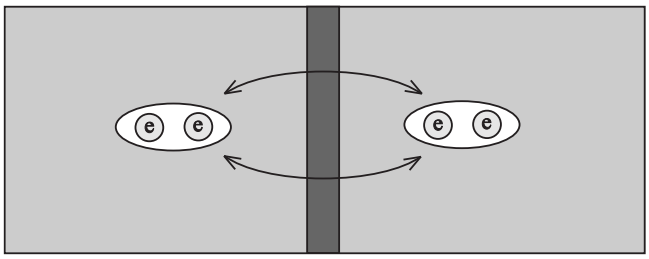

Figure 3.5: A Josephson junction consists of two superconducting electrodes separated by thin non-superconducting layer (normal metal or insulator). The cooper pairs tunnel coherently across the barrier which gives rise to the Josephson's effects.

other producing a current

$$I_s = I_c \sin \Delta\varphi, \tag{3.82}$$

where I_c is the critical current and $\Delta\varphi = \varphi_L - \varphi_R$ is the difference in phase between the left and the right superconducting electrode. Josephson also predicted that if a voltage is applied across the insulating barrier the phase difference $\Delta\varphi$ should change with time according to

$$\frac{d}{dt}\Delta\varphi = \frac{2eV}{\hbar}. \tag{3.83}$$

For constant voltage $\Delta\varphi$ will increase linearly on time which according to Eq. (3.82) generates alternating current across the insulating bridge. These type of superconductor-insulator-superconductor (SNS) junctions became known as Josephson junctions, see Fig. 3.5 and have since spawn an avalanche of research as well as numerous applications. Other types of junctions that share similar properties include the SNS and ScS, where N denotes normal metal and c stands for constriction. The common feature of all these devices is a "weak link" that couples the Cooper pair wavefunctions on the two sides of the bridge.

The above equations can be derived from general arguments that require only the assumption that cooper pairs can tunnel across the weak link separating the

two superconducting electrodes. In fact this assumption has been proven, i. e. see deGennes [9]. The argument is as follows. Let ψ_1 and ψ_2 be the wavefunctions of the superconducting electrons satisfying the Schrödinger's equation

$$i\hbar\frac{\partial\psi_\alpha}{\partial t} = E_\alpha\psi_\alpha, \tag{3.84}$$

where $\alpha = 1, 2$. Similarly, this applies to the right electrode as well. If we allow the two wavefunctions to overlap at then the total wavefunction must be a superposition of ψ_1 and ψ_2:

$$\psi = f_1 e^{i\varphi_1} + f_2 e^{i\varphi_2}, \tag{3.85}$$

where f_1 and f_2 are normalized such that $f_1^2 = N_1$ and $f_2^2 = N_2$. Provided the overlap of f_1 and f_2 at the junction is very small one can write

$$\int d^3r f_1 f_2 \approx 0, \qquad \int d^3r f_1 \hat{H} f_2 = K. \tag{3.86}$$

The second integral is nonzero because the hamiltonian involves derivatives which cannot be neglected near the insulating barrier. If a constant voltage V is applied across the device the energies of the isolated left and right electrodes are $E + e/V$ and $E - e/V$ respectively. The Schrödinger's equation then becomes a set of four equations

$$\begin{aligned}
\hbar\frac{dN_1}{dt} &= -2K\sqrt{N_1 N_2}\sin(\varphi_2 - \varphi_1) \\
\hbar\frac{dN_2}{dt} &= 2K\sqrt{N_1 N_1}\sin(\varphi_2 - \varphi_1) \\
\hbar N_L\frac{d\varphi_1}{dt} &= -eVN_1 + K\sqrt{N_1 N_2}\cos(\varphi_2 - \varphi_1) \\
\hbar N_R\frac{d\varphi_2}{dt} &= eVN_2 + K\sqrt{N_1 N_2}\cos(\varphi_2 - \varphi_1)
\end{aligned} \tag{3.87}$$

Due to conservation of current we have $N_1 + N_2 = constant$ and therefore

$$I_s = 2e\frac{dN_2}{dt} = -2e\frac{dN_1}{dt}. \tag{3.88}$$

Defining $I_c = 4eK\sqrt{N_1 N_2}/\hbar$ the first two equations give us the predicted current in Eq. (3.82) while subtraction of the last two equations yields Eq. (3.83)

One fascinating and important application of Josephson junctions, not only in technology but for fundamental understanding of quantum mechanics, is the superconducting quantum interference device (SQUID). A SQUID can by built by interrupting a superconducting loop by one or more thin insulators, see Fig. 3.6 As we are going to discuss presently SQUIDs can be used as quantum qubits which, along with their macroscopic size, makes them very useful in the field of quantum computing. For this reason, SQUIDs are often referred to as flux qubits. Flux qubits have received much attention lately due to low decoherence exhibited at a macroscopic scale. When half a flux quantum is applied to a flux qubit, the system forms a symmetric double-well potential. The two classical states associated with the minima of this potential correspond to clockwise and counterclockwise circulating currents. In terms of the total flux Φ this potential can be represented by the function

$$U(\Phi) = U_0 \left[\frac{1}{2} \left(\frac{2\pi(\Phi - \Phi_x)}{\Phi_0} \right)^2 - \beta_L \cos\left(\frac{2\pi\Phi}{\Phi_0} \right) \right], \tag{3.89}$$

where $\beta_L = 2\pi L I_c/\Phi_0$, $U_0 = \Phi_0^2/(4\pi^2 L)$, L is the inductance, and Φ_x is the external flux. For certain parameters this function behaves as a double-well potential in the vicinity of its minima. When $\Phi_x = \Phi_0/2$ the potential U is symmetric. Therefore, any deviation of Φ_x from $\Phi_0/2$ will create a bias in the minima of the two wells. The fascinating property of this system is that it exhibits quantum tunneling between the classical minima [82, 83, 84, 85], thus, providing an example of a quantum superpo-

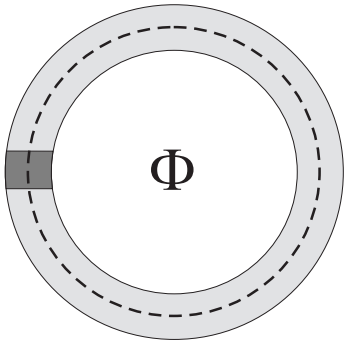

Figure 3.6: The simplest type of flux qubit with one Josephson's junction.

sition of macroscopic current states. The ground state and the first excited state of the system are symmetric and antisymmetric superpositions of clockwise and counterclockwise current states, separated by the tunnel splitting Δ. Experiments have demonstrated that the quality factor of the flux qubit, ω/Γ, can be as high as 5000 [86], thus, pushing it to the front line of promising candidates for quantum computation. Recently, this promise has been further amplified by successful experiments with coupled flux qubits [87, 88, 89].

Most of the work on decoherence of flux qubits concentrates on the effects of non-zero impedance [90], electromagnetic [82, 94, 91, 92] and $1/f$ [90, 93] noise. Decoherence due to coupling of a flux qubit to the acoustics waves has been studied to a lesser degree [94, 95].

3.3.2 Coupling of SQUID states to acoustic phonons

Tunnelling between clockwise and counterclockwise circulation is accompanied by the reversal of the angular momentum associated with the circular current. Experiments on flux qubits showed that this angular momentum can be as large as $10^{10}\hbar$, so its non-conservation would be quite dramatic. Similar problem exists for any LC circut. A freely suspended ring containing an inductor and a capacitor would have to co-wiggle

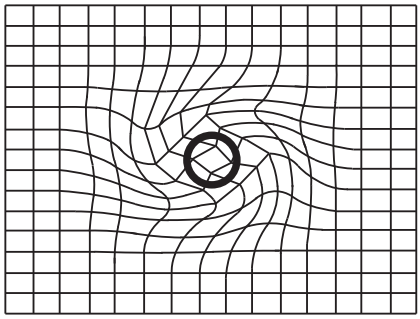

Figure 3.7: A snapshot of the elastic matrix responding to the alternating current of the flux qubit.

mechanically with the oscillating current in order to conserve the angular momentum. When such a ring is attached to a solid matrix it should produce torsional oscillations in the matrix. This immediately suggests that unless the flux qubit is in the ground state, it should have a finite probability to radiate a phonon. The latter can be viewed as a consequence of the fact that the electric current is defined with respect to the crystal lattice of ions so that quantum states of the current are inevitably entangled with the lattice states. A snapshot of this process is depicted in Fig. 3.7

We consider a loop of radius R carrying a current J oscillating with frequency $f \sim 10^9 - 10^{10}\text{s}^{-1}$ between the clockwise and counterclockwise direction of motion. The angular momentum associated with the circular current changes from L to $-L$ every half a period. As a consequence, the local environment co-wiggles with the same frequency and produces elastic distortions of the lattice in accordance with angular momentum conservation. These distortions, $\mathbf{u}(\mathbf{r}, t)$, being pure twists, satisfy $\nabla \cdot \mathbf{u} = 0$. The kinetic energy associated with the superconducting current is given in Eq. (2.60). The interaction Hamiltonian then follows:

$$\mathcal{H}_{int} = \frac{m_e}{e} \int d^3 r \mathbf{j} \cdot \dot{\mathbf{u}}. \tag{3.90}$$

This Hamiltonian satisfies all the symmetries and is free of any unknown interaction

constants.

We denote the eigenstates of the angular momentum, $L_z = L$ and $L_z = -L$, as $|\uparrow\rangle$ and $|\downarrow\rangle$, respectively. The system under consideration can be approximately modeled as a particle of spin L in a biased double well potential described by the Hamiltonian $\mathcal{H}_0$ whose lowest eigenstates are

$$|0\rangle = \frac{1}{\sqrt{2}}(C_-|\uparrow\rangle + C_+|\downarrow\rangle) \tag{3.91}$$

and

$$|1\rangle = \frac{1}{\sqrt{2}}(C_+|\uparrow\rangle - C_-|\downarrow\rangle). \tag{3.92}$$

The coefficients $C_\pm$ and the splitting energy Δ have been defined in Eqs. (3.6).

The total Hamiltonian of the system is

$$\mathcal{H} = \mathcal{H}_0 + \mathcal{H}_{ph} + \mathcal{H}_{int}. \tag{3.93}$$

The first two terms stand for the interaction-free particle and phonon Hamiltonian, respectively, and the last term is given by Eq. (3.90). Decoherence of a general superposition state $|\Psi\rangle = c_1|0\rangle + c_2|1\rangle$ will take place through relaxation of $|1\rangle$ to $|0\rangle$. The corresponding two phonon transition is determined by the matrix element of $\mathcal{H}_{int}$ that will be computed in the next Section. To shorten formulas, unless stated otherwise, we will use the units in which $k_B = \hbar = 1$.

3.3.3 Small qubit

In the case of a small flux qubit of size $R \ll \lambda_{ph}$, with λ_{ph} being the average wavelength of phonons, one can treat the local environment at the position of the qubit as a rigid matrix rotating with angular velocity $\mathbf{\Omega} = \frac{1}{2}\nabla \times \dot{\mathbf{u}}$. Equivalently, the velocity vector $\dot{\mathbf{u}}$ can be expressed in terms of the angular velocity as $\dot{\mathbf{u}} = \mathbf{\Omega} \times \mathbf{r}$, where $\mathbf{r}$ is the position

vector with its origin at the center of the qubit. The interaction Hamiltonian of Eq. (3.90) can now be simplified as

$$\mathcal{H}_{int} = \mathbf{L} \cdot \mathbf{\Omega}, \tag{3.94}$$

in which

$$\mathbf{L} = \frac{m_e}{e} \int d^3r \ \mathbf{r} \times \mathbf{j} \tag{3.95}$$

is the angular momentum of the circulating current.

The matrix element for the Raman process is obtained by inserting the interaction Hamiltonian, Eq. (3.94), into Eq. (3.29). Because the interaction Hamiltonian at hand is of the first order on $\mathbf{u}$ only the second term of Eq. (3.29) will contribute. Hence, the matrix element for the Raman process is

$$\begin{aligned} M_{ph}^R &= \langle n_{\mathbf{q}} + 1 | \, \Omega_z \, | n_{\mathbf{q}} \rangle \, \langle n_{\mathbf{k}} - 1 | \, \Omega_z \, | n_{\mathbf{k}} \rangle \\ &= \langle n_{\mathbf{k}} - 1 | \, \Omega_z \, | n_{\mathbf{k}} \rangle \, \langle n_{\mathbf{q}} + 1 | \, \Omega_z \, | n_{\mathbf{q}} \rangle \\ &= \frac{1}{8\rho V} [\mathbf{k} \times \mathbf{e}_\lambda]_z [\mathbf{q} \times \mathbf{e}_\sigma]_z \sqrt{\omega_{\mathbf{k}\lambda} \omega_{\mathbf{q}\sigma} (n_{\mathbf{q}} + 1) n_{\mathbf{k}}}. \end{aligned} \tag{3.96}$$

The action of the angular momentum operator on $|0\rangle$ and $|1\rangle$ produces the following states:

$$\begin{aligned} L_z|0\rangle &= \frac{L\Delta_0}{\Delta} \left[|1\rangle - \frac{\varepsilon}{\Delta_0} |0\rangle \right] \\ L_z|1\rangle &= \frac{L\Delta_0}{\Delta} \left[|0\rangle + \frac{\varepsilon}{\Delta_0} |1\rangle \right]. \end{aligned} \tag{3.97}$$

Inserting these results into Eq. (3.33) one can immediately see that $|\psi_\xi\rangle$ must be either $|0\rangle$ or $|1\rangle$. Thus, we only need to consider

$$\begin{aligned} -\langle 0 | \, L_z \, | 0 \rangle &= \langle 1 | \, L_z \, | 1 \rangle = \frac{L\varepsilon}{\Delta} \\ \langle 0 | \, L_z \, | 1 \rangle &= \langle 1 | \, L_z \, | 0 \rangle = \frac{L\Delta_0}{\Delta}. \end{aligned} \tag{3.98}$$

Taking into account the conservation of energy, $\omega_{\mathbf{q}} - \omega_{\mathbf{k}} = \Delta$, the Raman matrix element reduces to

$$M_R = M_{ph}^R \frac{2L^2\varepsilon\Delta_0}{\Delta^2} \frac{1}{\omega_{\mathbf{k}}(\omega_{\mathbf{k}} + \Delta)}. \tag{3.99}$$

Substitution of Eq. (3.99) into Eq. (3.60) yields

$$\begin{aligned} \Gamma_2 &= \frac{L^4\varepsilon^2\Delta_0^2}{16\rho^2\Delta^2(2\pi)^5} \sum_{\lambda,\sigma} \int d\mathbf{k}d\mathbf{q}[(\mathbf{k}\times\mathbf{e}_\lambda)_z(\mathbf{q}\times\mathbf{e}_\sigma)_z]^2 \\ &\quad \times \frac{\omega_{\mathbf{q}}(n_{\mathbf{q}}+1)n_{\mathbf{k}}}{\omega_{\mathbf{k}}(\omega_{\mathbf{k}}+\Delta)^2} \delta(\omega_{\mathbf{q}} - \omega_{\mathbf{k}} - \Delta). \end{aligned} \tag{3.100}$$

Replacing the integration variable $d\mathbf{k}$ with $\omega_{\mathbf{k}}^2 d\omega_{\mathbf{k}} d\Omega_{\hat{\mathbf{k}}}/v_i^2$ and the vector $\mathbf{k}$ with $\hat{\mathbf{k}}\omega_{\mathbf{k}}/v_i$, one obtains

$$\begin{aligned} \Gamma_2 &= \frac{L^4\varepsilon^2\Delta_0^2 D^2}{16\rho^2\Delta^2(2\pi)^5} \\ &\quad \times \int_0^{\omega_D} \frac{d\omega\omega^3(\omega+\Delta)^3}{(e^\omega - 1)(1 - e^{-(\omega+\Delta)/T})}, \end{aligned} \tag{3.101}$$

where

$$D = \sum_\lambda \int \frac{d\Omega_{\hat{\mathbf{k}}}}{v_\lambda^5} (\hat{\mathbf{k}}\times\mathbf{e}_\lambda)_z^2. \tag{3.102}$$

The sum in Eq. (3.102) runs over the two transverse polarizations. Making the change of variable $x = \omega/T$ yields

$$\Gamma_2 = \frac{L^4\varepsilon^2\Delta_0^2 D^2 T^7}{16(2\pi)^5\rho^2\Delta^2} g(\Delta/T), \tag{3.103}$$

where

$$g(\Delta/T) = \int_0^\infty \frac{dx x^3(x+\Delta/T)^3}{(e^x - 1)(1 - e^{-x-\Delta/T})}. \tag{3.104}$$

For completeness, we insert k_B and $\hbar$ into our result which in the limit $k_BT \ll \Delta$ reduces to

$$\Gamma_2 \cong \frac{\pi}{270} \frac{L^4\varepsilon^2\Delta_0^2\Delta k_B^4 T^4}{\rho^2 v_t^{10}\hbar^7}, \tag{3.105}$$

where v_t is the speed of the transverse sound. In the opposite limit $k_BT \gg \Delta$ one obtains for the rate

$$\Gamma_2 \cong \frac{15\pi}{36}\frac{L^4\varepsilon^2\Delta_0^2 k_B^7 T^7}{\rho^2\Delta^2 v_t^{10}\hbar^7}. \tag{3.106}$$

3.3.4 Large qubit

For a large qubit, $R \gg \lambda_{ph}$, one must integrate the interaction of the superconducting current with phonons along the entire loop as expressed by Eq. (3.90). When this is done the interaction hamiltonian takes the form

$$\mathcal{H}_{int} = \frac{im_e}{e}\sum_{\mathbf{k}\lambda}\sqrt{\frac{\omega_{\mathbf{k}}}{2V\rho}}(\mathbf{j}_{\mathbf{k}}\cdot\mathbf{e}_i)(a_{\mathbf{k}\lambda} - a^{\dagger}_{\mathbf{k}\lambda}), \tag{3.107}$$

where $\mathbf{j}_{\mathbf{k}} = \int dr^3\mathbf{j}e^{i\mathbf{k}\cdot\mathbf{r}}$ is the Fourier transform of $\mathbf{j}$. We can obtain j in real space from Eq. (2.18) with the superconducting phase $\varphi = (\Phi/\Phi_0)\theta$ and $f \approx 1$. In cylindrical coordinates Eq. (2.18) becomes

$$-\frac{\partial}{\partial r}\left[\frac{1}{r}\frac{\partial}{\partial r}(rA)\right] - \frac{\partial^2 A}{\partial r^2} + \lambda^{-2}A = \frac{\Phi}{2\pi\lambda^2}\frac{1}{r} \tag{3.108}$$

inside the ring, and

$$-\frac{\partial}{\partial r}\left[\frac{1}{r}\frac{\partial}{\partial r}(rA)\right] - \frac{\partial^2 A}{\partial r^2} = 0 \tag{3.109}$$

on the outside of the ring. These equations must be supplemented by the boundary conditions

$$H_r = -\frac{\partial A}{\partial z}, \qquad H_z = \frac{1}{r}\frac{\partial(rA)}{\partial r}. \tag{3.110}$$

For the case of a flux qubit made up of a ring with the cross-sectional area b much smaller than R and λ the solution to the current becomes particularly simple: $j_\phi(r,z) = J/b$. We should point out that this solution is correct only in the zeroth order on $\dot{u}$. In other words we are ignoring the corrections to the spatial and temporal structure

of the current in the ring of the flux qubit. The solution to $\mathbf{j_k}$ in this approximation is

$$\mathbf{j_k} = -i2\pi R J_1(k_\perp, R) J \mathbf{n_k}, \tag{3.111}$$

where $\mathbf{n_k}$ is a unit vector in the plane of the ring, $k_\perp$ is the z-component of $\mathbf{k}$, and $J_1(k_\perp, R)$ stands for the Bessel function of the first order. The interaction Hamiltonian can now be written as

$$\mathcal{H}_{int} = \mathbf{L} \cdot \mathbf{\Omega}_{eff}, \tag{3.112}$$

where

$$\mathbf{\Omega}_{eff} = -\frac{i}{R} \sum_{\mathbf{k}} \sqrt{\frac{\omega_{\mathbf{k}}}{2V\rho}} J_1(k_\perp, R)(a_{\mathbf{k}t} - a\dagger_{\mathbf{k}t}) \mathbf{e}_z. \tag{3.113}$$

The scalar product $\mathbf{n_k} \cdot \mathbf{e}_\lambda = \delta_{t\lambda}$ as $\mathbf{n_k}$ is in the plane of the ring. To obtain the two phonon matrix element one needs only to replace $(\mathbf{k} \times \mathbf{e}_\lambda)_z (\mathbf{q} \times \mathbf{e}_\sigma)_z$ in Eq. (3.96) with

$$-\left(\frac{2}{R}\right)^2 J_1(k_\perp R) J_1(q_\perp R). \tag{3.114}$$

Then, the rate for a large qubit becomes

$$\Gamma_2 = \frac{L^4 \varepsilon^2 \Delta_0^2}{\pi^3 8 \rho^2 \Delta^2 R^4 v_t^6} \int_0^{\omega_D} d\omega f(\omega, \Delta, T) \Theta(\omega, R, v_t, \Delta), \tag{3.115}$$

where

$$f(\omega, \Delta, T) = \frac{\omega(\omega + \Delta)}{(e^{\omega/T} - 1)(1 - e^{-(\omega+\Delta)/T})}, \tag{3.116}$$

and

$$\Theta(\omega, R, v_t, \Delta) = \int_0^\pi d\theta_1 \int_0^\pi d\theta_2 \sin\theta_2 \sin\theta_1 J_1^2 \left(\frac{\omega R}{v_t} \sin\theta_1\right) J_1^2 \left(\frac{[\omega + \Delta]R}{v_t} \sin\theta_2\right).$$

Due to its large argument, $J_1([\omega + \Delta]R/v_t \sin\theta_2)$ can be approximated by its asymptotic form. The integral over θ_2 in Eq. (3.117) then yields approximately $v_t/(\omega+\Delta)R$.

The integral over θ_1 equals

$$\frac{1}{3}\left(\frac{\omega R}{v_t}\right)^2 {}_1F_2\left(\frac{3}{2},\frac{5}{2},3,-\left(\frac{\omega R}{v_t}\right)^2\right), \tag{3.117}$$

where ${}_1F_2$ is the generalized hypergeometric function. Inserting the results just obtained into Eq. (3.115) gives

$$\Gamma_2 \cong \frac{L^4\varepsilon^2\Delta_0^2R^5}{24\pi^3\rho^2\Delta^2R^3v_t^7}\int_0^{\omega_D} d\omega \frac{\omega^3(e^{\omega/T}-1)^{-1}{}_1F_2}{(1-e^{-(\omega+\Delta)/T})}, \tag{3.118}$$

or, making the change of variable $x=\omega/T$, one can write

$$\Gamma_2 \cong \frac{L^4\varepsilon^2\Delta_0^2T^4}{24\pi^3\rho^2\Delta^2R^3v_t^7}\int_0^{\omega_D/T} dx \frac{x^3(e^x-1)^{-1}{}_1F_2(-\beta^2x^2)}{(1-e^{-x-\Delta/T})}, \tag{3.119}$$

where $\beta = RT/v_t$. In the limit $T \gg \Delta$, the integral in Eq. (3.119) simplifies to

$$\int_0^\infty dx \frac{x^3e^x{}_1F_2(-\beta^2x^2)}{(e^x-1)^2}, \tag{3.120}$$

or, after integrating by parts

$$\int_0^\infty dx \frac{x^3e^x{}_1F_2(-\beta^2x^2)}{(e^x-1)^2} = \frac{6}{\beta^2}\int_0^\infty dx \frac{J_2(2\beta x)}{e^x-1}. \tag{3.121}$$

For $\beta \gg 1$, Eq. (3.121) reduces to $3\beta^{-2}$. The rate then becomes

$$\Gamma_2 \cong \frac{L^4\varepsilon^2\Delta_0^2k_B^2T^2}{8\pi^3\rho^2\Delta^2R^5v_t^5\hbar^2}, \tag{3.122}$$

where we again inserted k_B and $\hbar$ into our result. In the limit $k_BT \ll \Delta$, one obtains

$$\Gamma_2 \cong \frac{L^4\varepsilon^2\Delta_0^2k_B^4T^4}{24\pi^3\rho^2\Delta^2R^3v_t^7\hbar^4}\ K\left(\frac{Rk_BT}{\hbar v_t}\right), \tag{3.123}$$

where

$$K(y) = \int_0^\infty \frac{x^3{}_1F_2(-y^2x^2)}{e^x-1}dx. \tag{3.124}$$

We are interested in the transition temperature between the rate due to a direct process and the Raman process. The former was calculated in Ref. [94]. It was shown that

$$\Gamma_1 = \frac{L^2\Delta^5}{12\pi\rho v_t^5\hbar^4}\coth\left(\frac{\Delta}{2k_BT}\right) \tag{3.125}$$

for a small qubit and

$$\Gamma_1 = \frac{L^2\Delta^2}{4\pi R^3\rho v_t^2\hbar}\coth\left(\frac{\Delta}{2k_BT}\right) \tag{3.126}$$

for a large qubit.

In the limit $k_BT \ll \Delta$, equations (3.105) and (3.125) yield for a small qubit

$$\frac{\Gamma_2}{\Gamma_1} = \frac{12\pi^2L^2\varepsilon^2\Delta_0^2k_B^4T^4}{270\rho\Delta^4v_t^5\hbar^3}. \tag{3.127}$$

For, e.g., $L \sim 10^2$, $\rho \sim$5g/cm^3, $v_t \sim 5\times10^3$m/s, and $f_0 \sim 5\times10^9$s^{-1}, the ratio in Eq. (3.127) yields $10^{-8}T$. Clearly, for $k_BT \ll \Delta$ ($T \sim 10^{-2}$K), the two phonon process is utterly insignificant. In the opposite limit $k_BT \gg \Delta$, equations (3.106) and (3.125) give

$$\frac{\Gamma_2}{\Gamma_1} = \frac{90\pi^2L^2\varepsilon^2\Delta_0^2k_B^6T^6}{\rho\Delta^6v_t^5\hbar^3}. \tag{3.128}$$

For the same parameters as considered above, Eq. (3.128) yields $10^{-2}T^6$. The two phonon process thus dominates over a one phonon process above $T \sim$ 2K. At $T \sim$ 20K the decoherence rate due to two phonon processes is of order 10^6s^{-1} and, therefore, its contribution to the quality factor of the qubit cannot be ignored.

For a large qubit in the small temperature limit one obtains with the help of equations (3.123) and (3.126)

$$\frac{\Gamma_2}{\Gamma_1} = \frac{L^2\varepsilon^2\Delta_0^2k_B^4T^4}{6\pi^2\rho\Delta^4v_t^5\hbar^3}K\left(\frac{Rk_BT}{\hbar v_t}\right). \tag{3.129}$$

For a large qubit parameters: $L = 10^{10}$, $R \sim 10^{-4}$m and $T \sim 10^{-2}$K, Eq. (3.129) yields 10^{-5}. As in the case of a small qubit, the two phonon rate is negligible compared to the one phonon rate. In the large temperature limit equations (3.122) and (3.126) give

$$\frac{\Gamma_2}{\Gamma_1} = \frac{L^2\varepsilon^2\Delta_0^2 k_B T}{4\pi^2 R^2 \rho \Delta^3 v_t^3 \hbar}, \tag{3.130}$$

which yields $10^{-6}T$. Evidently, for a large qubit, one phonon processes are the dominant source of decoherence at any temperature. For the numbers used above the one phonon rate is of order $10^6 \mathrm{s}^{-1}$.

A few important observations for flux qubits follow from the above results. Firstly, acoustic decoherence should definitely be taken into account when the quality factor as large as 10^4 is desired. Secondly, for small biased qubits the inelastic scattering of thermal phonons by the qubit can become a dominant mechanism of decoherence above 20K. Finally, the proportionality of this mechanism to the bias provides an additional way to control the flux qubit.

3.4 Conclusion of Part II

We have considered decoherence due to the two-phonon channel of two different systems: a particle in a double-well potential and a flux qubit. Although these two systems are completely different, especially in size and complexity, we showed, based upon symmetry arguments, that the decoherence rate for the two-phonon process at elevated temperatures is obtainable, in the long-wavelength limit, exclusively in terms of measurable parameters. For a particle in a double well potential the direct two-phonon and Raman processes become equally important at higher temperatures and consequently double the relaxation rate. We checked our results by taking a

different approach to obtaining the Raman matrix elements, namely also considering the problem in the reference frame of the double well potential. This approach simplified the interaction Hamiltonian by making it linear on the quantized velocity field $\dot{\mathbf{u}}$. We found that the Raman matrix elements calculated by these two approaches were identical. For typical values of the energy splitting, the bias, and the parameters of the solid we found that the temperature at which two-phonon processes begin to dominate over one-phonon processes is of order 30K.

Our analysis of the decoherence time of a flux qubit showed that only small flux qubits with angular momentum $\sim 10^2\hbar$ are sensitive to processes involving phonon scattering. Decoherence of large flux qubits is dominated exclusively by direct one-phonon channel. In both cases, we found the rate to be proportional to the square of the bias which, besides temperature, allows for additional control of the system. The novelty of our approach to computing relaxation rates lies in the fact that all our results are free of unknown interaction constants. This presents a great advantage to experimental verification of our findings. As a concluding remark we would like to point out that the above mentioned methods, which were based on symmetry and conservation of linear and angular momenta, have been successfully applied to spins and spin clusters in various magnetic systems [96, 97] that have yielded universal results in terms of measurable parameters as well.

Papers by J. Albert

Published and submitted works

Articles

1. C. C. Gerry, A. Benmoussa, E. E. Hach, III, and J. Albert. *Maximal violation of a Bell inequality by entangled spin coherent states*, accepted to Phys. Rev. A. (2008).

2. J. Albert and E. M. Chudnovsky. *Voltage from mechanical stress in type-II superconductors: Depinning of the magnetic flux by moving dislocations*, Appl. Phys. Lett. **93**, 042503 (2008).

3. J. Albert, E. M. Chudnovsky, and D. A. Garanin. *Symmetry implications for decoherence in solid state quantum dots*, Proceedings of the 26th International Conference On Group Theoretical Methods in Physics, Springer-Verlag (Physics Series), to appear (2008).

4. J. Albert and E. M. Chudnovsky. *Nucleation of superconducting vortices by exciting acoustic standing waves in type-II superconductors*, Phys. Rev. B **77**, 092506 (2008).

5. J. Albert and E. M. Chudnovsky. *Decoherence of flux qubits due to scattering of thermal phonons*, Phys. Rev. B **75**, 144502 (2007).

6. J. Albert, E. M. Chudnovsky, and D. A. Garanin. *Phonon-induced relaxation of a two-state system in solids*, Phys. Rev. B **74**, 115102 (2006).

7. C. C. Gerry and J. Albert. *Finite violations of a Bell inequality for high spin: An optical realization*, Phys. Rev. A 72, 043822 (2005).

8. C. C. Gerry, J. Albert, and A. Benmoussa. *Dark states of two-mode quantized fields in two-channel model: competing k- and l-photon processes*, J. Phys. A: Math. Gen. **38**, 1333-1344 (2005).

Bibliography

[1] H. K. Onnes, Liiden Comm. **120b**, **122b**, **124c** (1911)

[2] W. Meissner and R. Ochsenfeld, Naturwissenschaften **21**, 787 (1933)

[3] C. Kittel, *Quantum Theory of Solids* (Wiley, NY - London, 1963)

[4] F. and H. London, Prog. Roy. Soc. (London) **A149**, 71 (1935)

[5] A. Fetter and J. D. Walecka, *Quantum Theory of Many-Particle Systems* (Dover, 2003)

[6] V. L. Ginzburg and L. D. Landau, Zh. Experim. i Teor. Fiz. **20**, 1064 (1950)

[7] J. Bardeen, L. N. Cooper, and J. R. Schrieffer, Phys. Rev. **108**, 1175 (1957)

[8] L. P. Gor'kov, Soviet Phys.-JETP **9** 1364 (1959)

[9] P. G. deGennes, *Superconductivity of Metals and alloys* (W. A. Benjamin, New York 1966)

[10] M. Tinkham, *Introduction to Superconductivity* (Dover, NY 2004)

[11] A. A. Abrikosov, Sov. Phys. JETP **5**, 1174 (1957)

[12] N. Kopnin, *Theory of Nonequilibrium Superconductivity* (Oxford 2001)

[13] J. D. Livingston, International Conference on Science of Superconductivity, Colgate University, Hamilton, NY, (1963)

[14] C. P. Bean and J. D. Livingston, Phys. Rev. Lett. **12**, 1 (1964).

[15] Fröhlich, Phys. Rev. **79**, 845 (1950)

[16] E. Maxwell, Phys. Rev. **78** 477 (1950)

[17] J. Bardeen and D. Pines, Phys. Rev. **99**, 1140 (1955)

[18] V. L. Safonov, arXiv:quant-ph/0202095v2 (2002)

[19] F. Wagner, Ann. Physik **3**, 77 (1994)

[20] F. Wagner, J. Phys. A: Math. Gen. **39**, 8221-8230 (2006)

[21] L. N. Cooper, Phys. Rev. **104**, 1187 (1956)

[22] A. I. Larkin, Soviet Phys.-JETP **31**, 4 (1970)

[23] A. I. Larkin and Yu. N. Ovchinnikov, J. Low Temp. Phys. bf 34, 409 (1970)

[24] Feiglman, *et. al*, Phys. Rev. Lett. **63**, 20 (1989)

[25] T. Natterman, Phys. Rev. Lett. **64**, 2454 (1990)

[26] E. H. Brandt, J. Low Temp. Phys. **26**, 709 (1977)

[27] E. M. Chudnovsky, Phys. Rev. B **40**, 11355 (1989)

[28] E. M. Chudnovsky, Phys. Rev. B **43**, 7831 (1990)

[29] E. M. Chudnovsky, Europhys. Lett. **43**, 445 (1998)

[30] B. I. Ivlev and R. S. Thompson, Phys. Rev. B **44**, 22 (1991)

[31] B. I. Ivlev and R. S. Thompson, Phys. Rev. B **45**, 2 (1992)

[32] E. M. Chudnovsky, Phys. Rev. B **64**, 212503 (2001)

[33] J. Bardeen and M. J. Stephen, Phys. rev. **140**, A1197 (1965)

[34] C. Caroli and K. Maki, Phys. Rev. **159** 306, 316 (1967)

[35] R. W. Morse and H. V. Bohm, Bull. A. Phys. Soc. **3**, 225 (1958)

[36] T. Tsuneto, Phys. Rev. **121**, 402 (1961)

[37] R. W. Morse, *Ultrasonic Attenuation in Metals at Low Temperatures*, in K. Mendelssohn (ed.) Progress in Cryogenics, vol. I, Heywood, London (1959), pg. 219.

[38] K. Fossheim, Phys. Rev. Lett. **19**, 81 (1967)

[39] J. Pankert, *et. al*, Phys. Rev. Lett. **62**, 3052 (1990)

[40] D. Domingez, *et. al*, Phys. Rev. Lett. **74**, 2579 (1995)

[41] D. Domingez, *et. al*, Phys. Rev. B **51**, 15649 (1995)

[42] P. Nozières and W. F. Winen, Philos. Mag. **14**, 667 (1966)

[43] H. Suhl,Phys. Rev. Lett. **14**, 226 (1965)

[44] E. M. Chudovsky and A. P. Kuklov, Phys. Rev. Lett. **91**, 6 (2003)

[45] Domingez, *et. al*, Phys. Rev. B **53**, 10 (1996)

[46] E. B. Sonin *et. al.*, Phys. rev. B **57**, 575 (1998)

[47] E. M. Chudnovsky and L. N. Bulaevsky, Phys. rev. B **72**, 094518 (2005)

[48] L. D. Landau and E. M. Lifshitz, *Theory of Elasticity* (Pergamon, New York, 1959)

[49] J. Albert and E. M. Chudnovsky, Appl. Phys. Lett. **93**, 042503 (2008)

[50] V. A. Al'shitz and V. L. Indenbom, Sov. Phys. Usp. **18**, 1 (1975).

[51] D. Mordehai and I. Kelson, Phys. Rev. B **74**, 184115 (2006) and references therein.

[52] E. Nadgornyi, *Dislocation dynamics and Mechanical properties of crystals, Progress in Material Science*, Vol. 31 (Pergamon Press, london, 1988)

[53] J. P. Hirth and J. Lothe, *Theory of dislocations* (Wiley, New York, 1982).

[54] P. Rosakis, Phys. Rev. Lett. **86**, 1 (2000).

[55] P. Gumbsch and H. Gao, Science **283**, 968 (1999).

[56] L. P. Grotelueschen, PhD. thesis, Brown University, 1992; Y. W. Zang, T. C. Wang, and Q. H. Tang. Acta Mech. Sin. **11**, 76 (1995).

[57] F. London, *Superfluids* (Wiley, New York, 1950), Vol. 1.

[58] S. J. Barnett, Phys. Rev. **6**, 239 (1915).

[59] J. Larmor, Lond. Math. Soc. Proc. **1**, 1 (1903).

[60] J. Albert and E. M. Chudnovsky, Phys. Rev. B **77**, 092506 (2008)

[61] M. M. de Lima, Jr. and P. V. Santos, Rep. Prog. Phys. **68**, 1639 (2005).

[62] C. P. Bean anf J. D. Livingston, Phys. Rev. Lett. **12**, 1 (1964)

[63] A. J. Leggett, S. Chakravarty, A. T. Dorsey, M. P. Fisher, A. Garg, W. Zwerger, Rev. Mod. Phys. **59**, 1 (1987)

[64] E. M. Chudnovsky, Phys. Rev. Lett. **92**, 120405 (2004)

[65] T. Fujisawa *et al.*, Science **282**, 932 (1998)

[66] T. Fujisawa, W. G. van der Wiel, and L. P. Kouwenhowen, Physica (Amsterdam) **7E**, 413 (2000)

[67] W. G. van der Wiel et al., Rev. Mod. Phys. **75**, 1 (2003)

[68] G. Ortner et al., Phys. Rev. **B72**, 165353 (2005)

[69] W. J. M. Naber, T. Fujisawa, H. W. Liu, and W. G. van der Wiel, Phys. Rev. Lett. **96**, 136807 (2006)

[70] M. R. Gräber, M. Weiss, and C. Schönenberg, arXiv:cond-mat/0605220

[71] R. Orbach, Proc. R. Soc. A **264**, 458 (1961)

[72] T. H. Stoof and Yu. V. Nazarov, Phys. Rev. **B53**, 1050 (1996)

[73] T. Brandes and B. Kramer, Phys. Rev. Lett. **83**, 3021 (1999)

[74] J. Albert, E. M. Chudnovsky, and D. A. Garanin, Phys. Rev. B **74**, 115102 (2006)

[75] J. Albert, E. M. Chudnovsky, and D. A. Garanin, Proceedings of 26th International Colloquium on Group Theory Methods in Physics, Springer-Verlag (Physics Series), to appear (2007).

[76] R. L. Mössbauer, Zeitschrift fr Physik A Hadrons and Nuclei **151**, 124143 (1958)

[77] E. Merzbacher, *Quantum Mechanics* (John Wiley and Sons, 1998)

[78] A. Abragam and B. Bleaney, *Electron Paramagnetic Resonance of Transition Ions* (Clarendon Press, Oxford, 1970)

[79] V. N. Stavrou and X. Hu, Phys. Rev. **B73**, 205313 (2006).

[80] L. A. Openov, Phys. Rev. Lett. **93**, 158901 (2004); E. M. Chudnovsky, Phys. Rev. Lett. **93**, 208901 (2004)

[81] B. D. Josephson, Phys. Lett. **1**, 251 (1962)

[82] J. R. Friedman, V. Patel, W. Chen, S. K. Tolpygo, and J. E. Lukens, Nature **406**, 43 (2000)

[83] C. H. van der Wal, A. C. J. ter Haar, F. K. Wilhelm, R. N. Schouten, C. J. P. M. Harmans, T. P. Orlando, S. Lloyd, and J. E. Mooij, Science **290**, 773 (2000)

[84] D. Vion, A. Aassime, A. Cottet, P. Joyez, H. Pothier, C. Urbina, D. Esteve, M. Devoret, Science **296**, 886 (2002)

[85] Y. Yu, S. Han, X. Chu, S. Chu, Z. Wang, Science **296**, 889 (2002)

[86] D. P. DiVincenzo, F. Brito, and Roger H. Koch, Phys. Rev. B **74**, 014514 (2006)

[87] R. McDermott, R. W. Simmonds, M. Steffen, K. B. Cooper, K. Cicak, K. D. Osborn, S. Oh, D. P. Pappas, and J. M. Martinis, Science **307**, 1299 (2005)

[88] J. B. Majer, F. G. Paauw, A. C. J. ter Haar, C. J. P. M. Harmans, and J. E. Mooij, Phys. Rev. Lett. **94**, 090501 (2005)

[89] T. Hime, P. A. Reichardt, B. L. T. Plourde, T. L. Robertson, C.-E. Wu, A. V. Ustinov, J. Clarke, Science 314, 1427 (2006)

[90] J. Martinis, S. Nam, J. Aumentado, and K. M. Lang, Phys. Rev. B **67**, 094510 (2003)

[91] R. Migliore and A. Messina, Phys. Rev B **72**, 214508 (2005)

[92] P. Bertet, I. Chiorescu, G. Burkard, K. Semba, C. J. P. M. Harmans, D. P. DiVincenzo, and J. E. Mooij, Phys. Rev. Lett. **95**, 257002 (2005)

[93] Y. Yoshihara, K. Harrabi, A. O. Niskanen, Y. Nakamura, and J. S. Tsai, Phys. Rev. Lett. **97**, 167 (2006)

[94] E. M. Chudnovsky and A. B. Kuklov, Phys. Rev. B **67**, 064515 (2003)

[95] J. Albert and E. M. Chudnovsky, Phys. Rev. B **75**, 144502 (2007)

[96] E. M. Chudnovsky, D. A. Garanin, and R. Schilling , Phys. Rev. B **72**, 094426 (2005)

[97] C. Calero, E. M. Chudnovsky, and D. A. Garanin, Phys. Rev. B **74**, 094428 (2006)